Hypoxia Activated Prodrugs of DNA-PK Inhibitors as Radiosensitisers.

By

Prarthita Dasgupta

Auckland Cancer Society Research Centre

Faculty of Medical and Health Sciences

The University of Auckland

Auckland

New Zealand

July 2022

Abstract

Radiation therapy is a widely used treatment for many different cancer types. However, efficacy is often limited by tumour regrowth due to radioresistant hypoxic tumour cells and DNA DSB repair, and also by normal tissue toxicity. DNA-dependent Protein Kinase (DNA-PK), is a key repair protein in the Non Homologous End Joining (NHEJ) pathway which is responsible for most of the repair of radiation-induced DSBs. Inhibition of DNA-PK has been identified as a useful way to radiosensitise tumour cells, but concerns about sensitisation of normal tissues within the radiation field have been raised. One approach to selectively target DNA-PK inhibitors to tumour tissue is to use Hypoxia Activated Prodrugs (HAP). The HAP is designed to be activated under hypoxic conditions, therefore providing tumour-selective delivery of the DNA-PK inhibitor, and enhance radiation therapy. This thesis investigates the *in vitro* behaviour of a newly developed inhibitor of DNA-PK, SN39536, and a corresponding HAP, SN39884.

In Chapter 3 we investigated the metabolic activation of SN39884 and its ability to release the effector, SN39536, under oxic and anoxic conditions. We explored the dependence of metabolic activation upon a common one-electron reductase, cytochrome P450 oxidoreductase (POR), using three HCT116 human colorectal carcinoma variants that either, did not express POR (PORko-R), overexpressed POR (POR-G), or constitutively expressed POR (HCT116-G). We investigated cellular uptake of SN39536 and SN39884 by analysing both intracellular and extracellular concentrations under oxic and anoxic conditions. SN39884 was found to be stable under oxic conditions and released the DNA-PK inhibitor, SN39536, selectively under anoxic conditions in all three cell lines. Concentrations of SN39536 were 2-3 fold higher in POR-G cells than PORko-R and HCT116-G, indicating that POR contributed to SN39884 metabolism. However, both PORko-R and HCT116-G metabolised SN39884 to a similar extent, indicating that other reductases contributed to SN39884 metabolism under anoxia. Intracellular concentrations were ~10 fold higher than extracellular concentrations for both prodrug, SN39884, and effector, SN39536, under oxic and anoxic conditions. This suggested the extravascular diffusion of the compounds would not be limited by avid cellular uptake.

In Chapter 4 we used regrowth inhibition assays to investigate the growth of cells after exposure to SN39884 and SN39535, in combination with radiation, to evaluate radiosensitisation of the three HCT116 POR variants. The effector SN39536 alone, had little effect on cell growth, except at the highest concentration (10 μM), but demonstrated effective radiosensitisation under oxic conditions in all three cell lines. Prodrug SN39884 was stable under oxic conditions, but at the highest concentration (10 μM), demonstrated some toxicity in cells exposed to radiation and treated with drug alone. Under anoxia, SN39884 demonstrated radiosensitisation of all three cell lines, with POR expression not differentiated in this assay.

In Chapter 5 we used clonogenic survival assays to evaluate radiosensitisation of the HCT116 POR variant cells by SN39536 and SN39884 under oxic and anoxic conditions. We determined Sensitiser Enhancement Ratios for 10% survival (SER_{10}) values for comparison. The effector SN39536 radiosensitised all three cell lines at 1 μM (SER_{10} 2.19 – 2.29). SN39884 (1 μM) did not result in radiosensitisation in all cell lines under oxic conditions (SER_{10} 1.01 – 1.12). However, under anoxia, SN39884 radiosensitised all cell lines, but gave a higher SER_{10} for high POR expressing POR-G cells (SER_{10} 1.55) compared to PORko-R and HCT-116-G cells (SER_{10}

1.34 and 1.36, respectively). The clonogenic survival assay provided a more accurate reflection of the metabolic activation of the prodrug under anoxia and could discriminate the activity of the prodrug more precisely than the growth inhibition assay.

Overall, we were able to demonstrate that HAP, SN39884, was stable under oxic conditions, and the corresponding DNA-PK inhibitor, SN39536, was able to robustly radiosensitise the cell lines, regardless of POR expression. SN39884 was shown to be able to release SN39536 under anoxic conditions and this produced radiosensitisation, especially in POR overexpressing cells. Further research into these DNA-PK inhibitors is warranted, with the next steps involving 3-D cellular models to evaluate (pro)drug metabolism and diffusion, and *in vivo* work to further investigate efficacy and tumour selectivity.

1. Chapter 1. Literature Review

1.1 Overview

Developing drugs that target the DNA Damage Response (DDR) to exploit a DDR dependency in cancer cells is a topical theme in cancer research. Radiation therapy is widely used to treat cancer and causes cytotoxic double stand breaks (DSBs). Resistance to radiotherapy is mediated by tumour hypoxia, which reduces the number of cytotoxic lesions formed, and by efficient DNA DSB repair. Much of the repair of DNA DSBs is mediated by DNA-dependent Protein Kinase (DNA-PK), which is a key repair protein in the Non Homologous End Joining (NHEJ) pathway. This thesis explores the activity of a newly developed inhibitor of DNA-PK (DNA-PKi), SN39536, and a related a Hypoxia Activated Prodrug (HAP), SN39884. The HAP has been designed to be activated under hypoxic conditions, therefore providing tumour-selective delivery of the DNA-PKi, and enhancing radiation therapy.

1.2 Cancer; a malignant cell phenotype

Cancer is a disease in which alterations to the genome result in mutations that produce dominant gain of function oncogenes and recessive loss of function tumour suppressor genes to elicit the six cancer phenotypes (Table 1.1), as described by (Hanahan & Weinberg, 2000), (Figure 1.1). These original hallmarks were supplemented with two new characteristic traits: deregulating cellular metabolism and avoiding immune destruction (Hanahan & Weinberg, 2011) and a recent update considers several more enabling properties such as phenotypic plasticity, disrupted differentiation, non-mutational epigenetic reprogramming and polymorphic microbiomes (Hanahan, 2022).

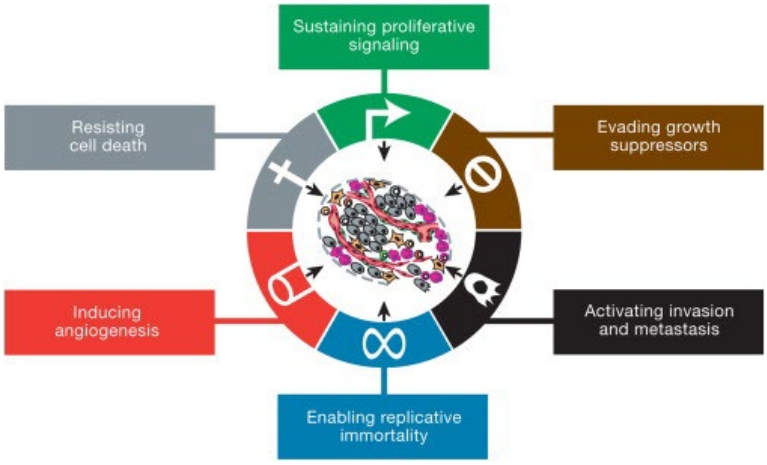

***Figure 1.1: The Hallmarks of Cancer**. Characteristics acquired during the development of human tumour cells. (Hanahan & Robert, 2011).*

Table 1.1 The Six Basic Hallmarks of Cancer. *Description of the six basic cancer phenotypes suggested by Hanahan & Weinberg.*

Hallmark of Cancer	Description
Evading apoptosis	Apoptosis is a cell death pathway that is triggered due to abnormalities and this pathway is evaded by cancer cells in most cancers. Sensors and effectors of this pathway can be targeted and inactivated, and anti-apoptotic factors can be upregulated for cancer cell survival.
Self-sufficiency in growth signals	Cancer cells have been observed to overexpress growth factor receptors on their surface, enabling them increase their response to the normal levels of growth factor ligands that are present. Cancer cells can also synthesise high levels of growth factors which increase autocrine stimulation.
Insensitivity to anti-growth signals	Mechanisms that enable responses to the various antigrowth signals are mostly present during the cell's growth phase. But these signalling checkpoints can be disrupted by mutations in tumour suppressive genes so the receptors are no longer functional. This results in uncontrolled cell proliferation.
Sustained angiogenesis	For cells to be able to function they need to be within 100 μM from a capillary blood vessel. Tumours need to recruit new blood vessels to promote tumour growth. A number of angiogenic inducers are upregulated and inhibitors are downregulated in tumours.
Limitless replicative potential	Cells have a finite replicative potential, called the Hayflick limit. This is due to the progressive loss of telomere length at the ends of chromosomes, during replication cycles. Eventually when the chromosome end is unprotected, chromosome damage leads to cell death. However, tumour cells can maintain their telomeres by upregulating the expression of telomerases, allowing unlimited multiplication.
Tissue invasion and metastasis	Cells from the primary tumour can break away, and travel through the blood vessels or the lymphatic system to colonise different tissues. This metastasis is the cause of 90% of mortalities due to cancer in humans.

Cancer is a disease that is increasing in incidence and mortality rates globally with a predicted 22 million new cancer cases and 13 million deaths due to cancer occurring annually by 2030 (Fidler, Bray, & Soerjomataram, 2018). This has been attributed to an increasingly ageing population and to the risk factors associated with socio-economic development (Bray et al., 2018). Currently, cancer is the second leading contributor to mortality worldwide (8.97 million deaths annually), and malignant disease is expected to remain a significant clinical burden for a long time (Mattiuzzi & Lippi, 2019). Therefore, there is a lot of effort being put in to make cancer care more efficient through new technologies to improve diagnosis, screening and treatment, and through the development of personalised medicine – which will provide more targeted approaches to cancer treatment (Mattiuzzi & Lippi, 2019).

1.3 Radiation Therapy to kill cancer cells and spare normal cells

Currently, approximately 60% of all patients diagnosed with cancer get treated with radiotherapy as a frontline treatment (Jarosz-Biej, Smolarczyk & Cichoń, & Kułach, 2019) and it is estimated to contribute 40% towards curative treatment (Baskar, Lee, Yeo, & Yeoh, 2012). Radiotherapy has better local tumour control and fewer side effects compared to chemotherapy (Jarosz-Biej et al., 2019). This makes radiotherapy good as a combination therapy; as it is commonly used in combination with chemotherapy, surgery or immunotherapy (Jarosz-Biej et al., 2019). For example, radiotherapy is used in combination with surgery to shrink tumours before surgery or eradicate microscopic tumour cells that were not able to be removed by surgery (Baskar et al., 2012). Radiotherapy, depending on where the tumour is in the body, is administered by either external beam therapy or internal radiation therapy. External beam radiotherapy (EBRT) involves aiming the radiation beam from outside the body to the location of the tumour and is the more common method of delivery. Internal radiation therapy (brachytherapy) involves inserting a sealed radioactive source into, or adjacent to, the tumour. This is used particularly in prostrate and gynaecological malignancies (Baskar et al., 2012). The key objective of radiotherapy is to maximise the dose to the tumour while minimising the dose to the surrounding healthy normal cells (Baskar et al., 2012).

Radiotherapy usually involves using electromagnetic ionizing radiation such as X-rays and γ-rays to kill cancer cells (Kim et al., 2015). X-rays and γ-rays are electromagnetic radiation, which differ in how they originate and their wavelengths (Trojanowicz, Bobrowski, Szreder, & Bojanowska-Czajka, 2018). X-rays have slightly lower energy than γ-rays and are therefore less penetrative (Trojanowicz et al., 2018).

X-rays are produced by accelerating electrons outside of the nucleus and stopping them in a device to convert the kinetic energy into electromagnetic energy (Hall, 2006). In contrast, γ-rays are produced from the decay of an unstable nucleus of radioactive isotopes (Hall, 2006). Otherwise they share similar properties.

Individual photons of γ-rays with energies higher than 10eV can interact with matter and cause displacement of an electron from its orbit around an atom, resulting in an atom that is positively charged (ionised). Interactions with tissue cause deposition of energy in the cells the radiation passes through (Baskar et al., 2012). Therefore electromagnetic radiation is indirectly ionising; damage is caused by the charged particles.

Radiation can also come from other sources, such as protons which are positively charged and weigh 2000 times more than an electron – this makes it difficult and expensive to accelerate these to generate radiation at relevant energies. There are also alpha particles which are positively charged helium nuclei of 2 protons and 2 neutrons. These can be emitted by the decay of radionucleotides such as radium undergoing alpha decay to radon and emitting an alpha particle. These particles are also expensive to accelerate because of their mass.

Neutrons have a similar mass to protons and are neutral, thus they cannot be accelerated like other particles. They are produced as by-products from charged particles accelerating or fission reactions.

Heavy charged particles are positively charged ions of elements such as carbon, neon and argon. Since they must be accelerated to very high energies to be relevant to radiotherapy, these are also difficult and expensive particles to use for therapy (Hall, 2006).

The main mechanism of energy deposition (within the 100 keV to 25 MeV energy range) is the Compton Effect. The γ- or X-ray photons displace an outer shell electron which loses energy as it is scattered in a new direction to become a photon with a longer wavelength – because the energy is imparted to accelerating the displaced electron. This photon goes on to conduct more ionising events until the energy is dissipated, resulting in more atoms with unpaired electrons and free electrons (Hall, 2006). The other main mechanism of energy deposition is the photoelectric effect which occurs at a lower energy range (around 10-50 keV). In this case, the γ- or X-ray photons displace an inner shell electron and the resulting vacancy is filled by an outer shell electron. This transition causes emission of a characteristic low-energy X-ray. The photoelectric effect is useful for diagnostic radiology because the atomic number greatly affects the mass absorption coefficient; therefore bone attenuation is very high because of the high atomic number of calcium (Hall, 2006).

The density of ionisation events affects the biological effectiveness of radiotherapy (Tannock, Hill, Bristow, Harrington, & Amir, 2013). Linear Energy Transfer (LET) refers to the tracks of ionising radiation along which energy is deposited non-uniformly (Hall, 2006).

The X-rays and γ-rays used for clinical radiotherapy, are categorised as low LET radiation. This means that the charged particles travel further and deposit energy over a larger distance (sparsely ionising) due to being smaller and easier to accelerate. Conversely, high LET radiation from alpha and beta particles, neutrons, protons and heavy charged particles deposit greater energy over shorter distances. This dense concentration of energy in a smaller area causes more damage to tissues than low LET radiation (Niemantsverdriet et al., 2012). However, for this reason high LET radiation is more precise and has greater relative biological effectiveness (RBE), because most of the dose is absorbed by the target and not by surrounding normal tissue. The greater mass of high LET particles, such as protons, means that their ionising tracks are straighter and less random than low LET particles such as electrons (Tannock et al., 2013). This is demonstrated by measuring radiation dose over depth of tissue, where it can be seen (Figure 1.2) that the dose deposition from electromagnetic radiation photons decreases exponentially over the depth in water. Water phantoms are commonly used as a model for soft tissues to measure dose distribution because it has been shown to have similar spread to soft tissues, due to its similar mass attenuation and absorption (Cameron et al., 2017). In contrast, radiation depositions from protons and carbon particles have a sharp maximum at the far end of their range that is known as the Bragg peak and very little energy is deposited outside this peak – leading to more precise dose distribution (Schulz-Ertner & Tsujii, 2007).

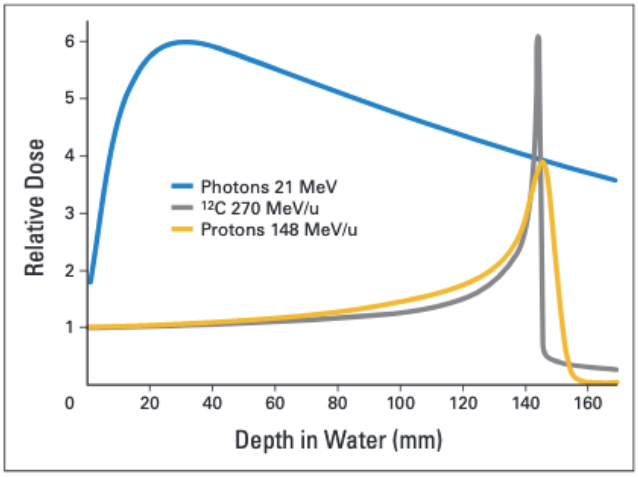

Figure 1.2: Penetration Depths of Doses of Photons, Protons and Carbon Ions in Water. *Particle beams have a sharp increase (Bragg Peak) in energy deposition at the high end of their range, as opposed to photon beams which peak early in its range and exponentially decreases from there. (Schulz-Ertner & Tsujii, 2007).*

1.3.1 Fractionation of Radiation Doses to Spare Normal Tissue

It was apparent from early treatments of patients that radiation had harmful effects on normal tissue as well as killing cancer cells, and a need to increase the therapeutic ratio was identified. In 1927 a research group in France led by Claude Regaud found that sterilising a ram's testes using a single dose of radiation also caused normal tissue damage of the scrotum, but if the radiation treatment was spread out over a few weeks using a lower doses, then sterilisation occurred without necrosis of the scrotum (Bernier, Hall, & Giaccia, 2004). This eventually led to the conventional multi-fraction regimen used today, where splitting the radiation dose into smaller fractions with sufficiently long breaks in between increases the therapeutic ratio. The biological factors that influence the response of normal and tumour cells to radiotherapy and account for the efficacy of fractionated therapy are summarised as the 5 R's (Tannock et al., 2013) (Table 1.2).

Table 1.2: The 5 R's of Radiation Biology. *The Five Biological Factors that Influence Response to Radiation Therapy.*

5 R's	**Description**
Repair	Sub-lethal damage repair.
Repopulation	Regeneration and proliferation of surviving cells.
Redistribution	Cycling of cells into a more radiosensitive phase (G2 and M).
Reoxygenation	Radioresistant hypoxic tumour cells can gain access to oxygen which enhances cell killing in subsequent treatments.
Radiosensitivity	Tissues have different proliferation rates and cells in different phases of the cell cycle will have different radiosensitivities.

Fractionation allows time for normal cells to repair sub-lethal damage. This spares more normal cells from dying and also gives the surviving cells a chance to repopulate. Cell death from radiotherapy can trigger the tissue to increase cell proliferation (Hall, 2006). Fractionation also increases radiation damage to more tumour cells by allowing reoxygenation of previously hypoxic tumour cells which are resistant to radiotherapy (Table 1.2). It also allows for the redistribution of cells that were initially in the radioresistant G1 and S phases to move into the more radiosensitive G2 and M phases of the cell cycle (Tannock et

al., 2013), (Hall, 2006). Different cell types display different radiosensitivity and this is an important factor for their responses to fractionation. For example, in normal tissue there are cells that divide more frequently than others.

Fractionation can also allow repopulation of cancer stem cells to occur in the tumour. This could also possibly result in a faster rate of proliferation than before, this is known as accelerated repopulation (Hall, 2006).

According to the law of Bergonie and Tribondeau (1906), immature, undifferentiated and actively dividing cells are more radiosensitive than mature, well differentiated cells (Bolus, 2017). Tissues such as bone marrow, skin and gastrointestinal mucosa have high cell renewal rates and are therefore early responding tissues, where radiation causes early cell death (within three months of treatment). This is an acute response that does not normally limit therapy as the stem cells in the tissue are able to repopulate and regenerate quickly (Tannock et al., 2013). Damage to early responding tissues results in common acute side effects that are seen soon after radiation treatment, such as xerostomia (dry mouth) damage), vomiting and erythema (skin inflammation) which are caused by cell death in the salivary glands, intestine, and skin, respectively. These side effects can be mitigated by using a fractionated therapy regimen to allow regeneration of the early responding tissues in between the fractions (Tannock et al., 2013), while also increasing damage to the tumour through reoxygenation and redistribution (Figure 1.1).

In late responding tissues such as the central nervous system, liver and the kidney, where cells divide less frequently, responses occur more than three months after treatment and damage can take years to develop. Irradiation damage in these slow proliferating tissues can cause development of fibrosis through inflammatory responses. Another common late response is telangiectasia which is the appearance of 'spider veins' from vascular damage. Loss of microvasculature can lead to atrophy of muscles and organs. This late toxicity is dose limiting for radiation therapy, as large doses can leave fewer stem cells which will increase the time of proliferation even more (Tannock et al., 2013). In the 1980's Withers found that late tissue responses were determined mostly by fraction size, whereas acute tissue and cancer cells responses were determined by both fraction size and overall radiotherapy treatment time (Withers, 1985).

Hyper-fractionation is a strategy to the reduce damage caused to late responding tissues by delivering radiotherapy in more fractions of lower doses. This prevents high doses to late responding tissues – which leaves more cells for proliferation (Hall, 2006). Another strategy utilised is accelerated hyper-fractionation where multiple fractions of small doses are given in 6-8 hour intervals (which is the amount of time that allows for repair for most normal tissues) and therefore the overall treatment time is reduced. Thus, the time for repopulation of cancer stem cells is reduced, and late responding tissues will not be affected due to their slow cell proliferation (Tannock et al., 2013).

Conversely, strategies for delivering high doses of radiotherapy in a single dose or few doses are being explored. Hypo-fractionation reduces overall treatment time and results in good tumour control (Siva, MacManus, & Ball, 2010). This approach poses a risk to both early and late responding normal tissues, but improved technology gives more accurate radiation delivery and spares normal tissues, reducing the need for fractionation (Hall, 2006).

Stereotactic Body Radiation Therapy (SBRT) or Stereotactic Ablative Radiotherapy (SABR) is a treatment modality that delivers radiation that is precisely targeted to the tumour in a large

single dose or in a small number of fractions (Folkert & Timmerman, 2017). This method spares normal tissue due to its precise radiation beam and was initially used for small targets in metastatic brain tumours that are difficult to reach with conventional surgery (Siva et al., 2010).

A single high dose of radiation may be more effective in treating hypoxic tumours, as it has been observed that the difference of radiosensitivity between hypoxic tumours and well oxygenated ones decreased with increasing LET (Tinganelli et al., 2013). The benefit would be most significant for late responding tissues compared to early responding tissues; in which fractionation and reoxygenation would overcome resistance more effectively (J. M. Brown, Carlson, & Brenner, 2014). Vascular damage and antitumour immunity stimulation are also thought to contribute to the effectiveness of hypo-fractionation (Telarovic, Wenger, & Pruschy, 2021). There is some debate on whether the loss of reoxygenation from fractionation and the vascular damage would only increase hypoxia, and therefore lead to radioresistance (Telarovic et al., 2021). Currently, highly hypoxic cancers such as head and neck cancers are treated with hyper-fractionation, except in advanced cases where hypofractionation is becoming popular (Van Beek et al., 2016). It has also been suggested that hypo-fractionation might also reduce the differential radiosensitivity in tumours, due to some cells being in a more radioresistant phase of the cell cycle. Hypo-fractionation would reduce the frequency and time of treatment and this would reduce tumour cell repopulation (Sia, Szmyd, Hau, & Gee, 2020).

Today SBRT/SABR is also used for tumours that are very close to important organs such as the spinal cord and lungs (Bernier et al., 2004). SBRT is now the recommended standard treatment modality for patients with stage I Non-Small Cell Lung Cancer (NSCLC) where surgery is not possible (Nyman et al., 2016), (Bernier et al., 2004). Local control rates are around 74-100%, and patients have a relatively good quality of life after treatment with few cases of grade 3-5 toxicities reported (Nyman et al., 2016).

1.3.2 Technology Innovation of Radiation Delivery

Precision in targeting EBRT to tumours and sparing the surrounding normal tissues has improved over the years, with increasing technical innovation and advancements (Thariat, Hannoun-Levi, Sun Myint, Vuong, & Gérard, 2013). Wilhelm Conrad Röntgen discovered X-rays in 1895 in Germany. He found that X-rays were formed by producing photon energy from the kinetic energy of the fast moving electrons that were accelerated from the negative cathode and stopped at the positive anode inside a gas discharge tube, connected to a high voltage source (Bernier et al., 2004). The rays emitted (Bremsstrahlung – braking radiation) could be filtered to use as a beam and blacken photographic film to produce an X-ray image of the structure it passed through.

Treatment of patients with tumours using radiation by both EBRT and brachytherapy began shortly after, when Becquerel discovered natural radioactivity in 1896 and the Curies isolated polonium and radium in 1898 (Thariat et al., 2013). Control of the electrons, and therefore the radiation dose, was difficult using gas discharge tubes for EBRT. Improvements were made by William Coolidge in the U.S.A. in 1913, who developed the Coolidge X ray tube which had tungsten filaments at the electrodes; the cathode could be heated to determine intensity and the voltage applied determined wavelength of the X-ray (Bernier et al., 2004; Thariat et al., 2013). This technology was used until the 1950s. However, this technology only allowed production of low energy photons in the 10-50 keV range. This meant that the photoelectric

effect dominated over the Compton effect. Consequently, a higher proportion of the radiation dose was attenuated in the bone and, due to low penetration power, mostly absorbed in the skin. These factors resulted in a heterogeneous dose distribution and reduced the dose to the tumour (Bernier et al., 2004).

The first linear accelerator (LINAC) machine was developed and installed by Fry and colleagues in 1948. An electromagnetic wave carried electrons down a long tube, therefore accelerating them to much greater energies than X-ray tubes (Bernier et al., 2004). This higher energy ensured that the Compton effect dominated, thus reducing bone attenuation and skin surface energy deposition - sparing the skin (Hall, 2006). The LINAC machine is still used today, with improvements having been made over the decades, particularly in the development of multi-leaf collimators. These collimators are lead shields that shape the radiation beams to the contours of the tumour to spare the surrounding normal tissues (Bernier et al., 2004).

Electron beams are the most commonly used radiotherapy treatment because they are cost-effective and are useful for treating tumours close to the body's surface (Baskar et al., 2012). But proton, neutron and heavy particle radiation produced by cyclotrons and synchrotrons are gaining more use because of their favourable dose localisations. This localisation, defined as the Bragg peak (Figure 1.2) delivers maximum energy to the tumour and spares normal tissue more than electron beams do (Schulz-Ertner & Tsujii, 2007). The high LET dose depositions had a sharp peak at the end of their range with low dose deposition outside of this peak, in contrast to low LET dose distributions that decreased exponentially. The Bragg peak can be spread out; Spread Out Bragg Peak (SOBP) if the peak is too narrow to cover a large tumour. This is achieved by varying the energy of the beam through deflection using magnetic fields to conform to the shape of the tumour. However, the complexity and expense of the machines required to deliver protons and heavy ions means that less than 1% of radiotherapy patients get treated with this technology currently (Mohan & Grosshans, 2017). The radiation beams are narrow and can go up to 230 MeV, and are useful when tumour is surrounded by radiosensitive normal tissue (Mohan & Grosshans, 2017).

1.3.3 Treatment Planning Systems to Increase Delivery Accuracy

A key development occurred with advances in computer technology that enabled improved treatment planning systems (TPS) to better determine dose distribution and identify the organs at risk (OAR) (Thariat et al., 2013). This involves defining the planning target volume (PTV); that is, the area that will be treated by radiotherapy (Figure 1.3). The PTV includes the target volume (gross tumour volume; GTV), the volume surrounding tissue that is suspected of subclinical tumour extension (clinical target volume; CTV), as every organ in the human body moves, the movement of the target is also accounted for (internal target volume (ITV) (Figure 1.3), (Ikushima, 2010).

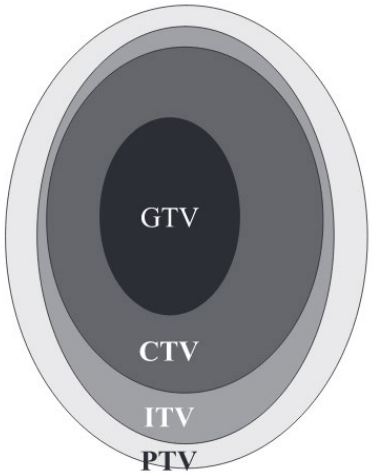

Figure 1.3: Target Volume Definition in Treatment Planning. *Gross Tumour Volume (GTV), Clinical Target Volume (CTV), Internal Target Volume (ITV), Planning Target Volume (PTV). ((Ikushima, 2010)*

Initially, 2D rectangular images from X-ray radiographs of the tumour were used to define the irradiation field (Ikushima, 2010). This has been replaced by a 3D modality; 3D Conformal Radiotherapy (3DCRT), which uses Computed Tomography (CT) imaging to produce a 3D image by resolution of multiple 2D images. This 3D image can be used to plan a treatment schedule that uses multi-leaf collimators to limit radiation to within the 3D shape of the tumour for more accurate dose delivery (Eschwège, 2000).

Improvement to the 3DCRT method came in the form of Intensity Modulated Radiation Therapy (IMRT), where the tumour volume defined in the 3D CT image is assigned particular dose levels and an inverse treatment planning system is utilised where multiple photon beams are modulated to generate specific doses of radiation to different parts of the PTV. This improves dose distribution by allowing an increase in the dose to the tumour while reducing normal tissue exposure (Eschwège, 2000).

In order to increase the precision and decrease the error in the PTV, a 4D method called Image Guided Radiation Therapy (IGRT) was developed which accounts for tumour and organ movement. For example, the respiratory motion of the lungs have the largest internal movement and result in variable exposure of both tumour and normal tissue over time. This method uses 3D CT/MRI images taken during the target's motion over time, and this is sorted into phases which increases the precision of targeting and thus the therapeutic ratio as well (Ikushima, 2010).

The SBRT/SABR modalities utilise a radiation beam that is narrow and delivers a large dose, therefore the treatment planning needs to be very accurate. In addition to utilising techniques, such as using markers to track tumours and 4D IGRT imaging to account for any organ motion, this technique also commonly utilises methods to restrict organ movement. For example, to inhibit lung movement, methods such as abdominal compression are employed (Folkert & Timmerman, 2017).

Radiotherapy has undergone dramatic changes over the century with major improvements in the precision of tumour targeting and more innovation is underway with reductions in the costs of high LET radiation machines (Baskar et al., 2012). This has been accompanied by increased understanding that the radiosensitivity of cells is influenced by many factors, including the phase of the cell cycle, DNA damage response, cell death pathways activation and oxygen concentrations within the tumour (Bernier et al., 2004). There is now considerable

interest in manipulating these factors by identifying key molecules that can be pharmacologically targeted to enhance radiotherapy efficacy (Bernier et al., 2004).

1.3.4 Ionising Radiation Chemistry

Cellular damage is mediated by free radicals produced by ionising radiation (Desouky, Ding, & Zhou, 2015). These free radicals interact with molecules within cells and result in damage to cellular structures either directly or indirectly (Minniti, Goldsmith, & Brada, 2012). The most important cellular structure targeted by radiotherapy is nuclear DNA (Holley, Miao, St. Clair, & St. Clair, 2014). Direct interactions with photons (which contain energy equal to *hv* where *h* is Planck's constant and *v* is the frequency) of ionising radiation involve ionisation of a DNA molecule (Equation 1 and Figure 1.4). This generates an unstable radical ion which decays to form a neutral radical by losing a proton (Equation 2). The electron released from the ionisation event can also go on to damage the DNA via indirect interactions (Equation 3) (J. M. Brown & Wilson, 2004).

$$DNA\text{-}H + hv \rightarrow \quad DNA\text{-}H^{\cdot +} + e^{-} \qquad \textit{Equation 1}$$

$$DNA\text{-}H^{\cdot +} \rightarrow \quad DNA^{\cdot} + H^{+} \qquad \textit{Equation 2}$$

Indirect interactions involving the radiolysis of water (Equation 3) are more common because cells are ca. 80% water (Azzam, Jay-Gerin, & Pain, 2012). This reaction forms an ionised water molecule ($H_2O^{\cdot +}$) which decays to form the hydroxyl radical and a proton (Equation 4). The hydroxyl radical is very reactive and is the major DNA damaging species generated by ionising radiation (Figure 1.4), causing direct damage to the DNA (Juan, Pérez De La Lastra, Plou, & Pérez-Lebeña, 2021). It causes 75% of X-ray damage to DNA (Hall, 2006).

$$H_2O + hv \rightarrow \quad H_2O^{\cdot +} + e^{-} \qquad \textit{Equation 3}$$

$$H_2O^{\cdot +} \rightarrow \quad OH^{\cdot} + H^{+} \qquad \textit{Equation 4}$$

The hydroxyl radical can abstract H atoms from unsaturated carbon atoms leading to oxidation of pyrimidine and purine bases and can also abstract H atoms from saturated carbon atoms, such as deoxyribose sugars (Equation 5), eventually leading to strand breaks. (Juan et al., 2021).

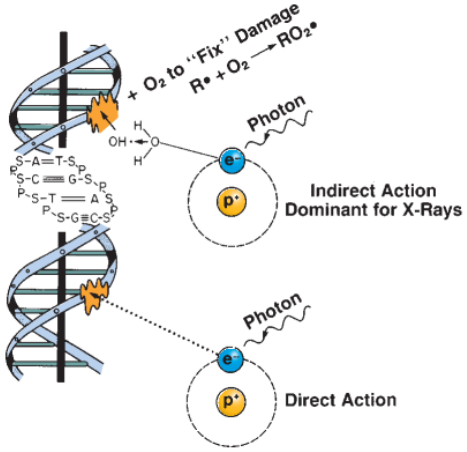

Figure 1.4: Direct and Indirect Damage to the DNA: *X-ray photon interacts with the electron (e^-) orbiting the atom of the absorbing material (p^+ is the proton). Direct interactions form a DNA radical from direct ionisation. Indirect interactions from water radiolysis result in the formation of the hydroxyl radical which causes damage to the DNA through hydrogen abstraction. Under aerobic conditions the DNA radical is oxidised, forming a radical species that degrades DNA structure and eventually causes strand breaks. (Hall, 2006).*

$$RH_2 + OH^{\cdot} \rightarrow \quad RH^{\cdot} + H_2O \qquad \textit{Equation 5}$$

Other Reactive Oxygen Species (ROS) are also formed by ionising radiation, such as the free radical superoxide ($O_2^{\cdot -}$) and hydrogen peroxide (H_2O_2) and these species are not as reactive or damaging to biological molecules. Superoxide is formed by the addition of a single electron; reducing O_2 to $O_2^{\cdot -}$ (Equation 6).

$$O_2 + e^- \rightarrow \quad O_2^{\cdot -} \qquad \textit{Equation 6}$$

Detoxification of superoxide ($O_2^{\cdot -}$) can occur through the enzyme superoxide dismutase (SOD) reducing it to H_2O_2 (Equation 7). Hydrogen peroxide can participate in the Haber Weiss (Equation 8) and Fenton Reaction pathways (Equation 9) producing hydroxyl radicals, or can be detoxified through the enzymes; catalase, glutathione peroxidases and thioredoxin reductase producing H_2O and O_2 (Equation 10), (Juan et al., 2021).

$$\xrightarrow{\text{SOD}}$$

$$O_2^{\cdot -} + 2H^+ \rightarrow \quad H_2O_2 \qquad \textit{Equation 7}$$

$$\textit{Haber Weiss Reaction:} \quad O_2^{\cdot -} + H_2O_2 \rightarrow \quad OH^- + OH^{\cdot} + O_2 \qquad \textit{Equation 8}$$

$$\textit{Fenton Reaction:} \quad Fe^{2+} + H_2O_2 \rightarrow \quad Fe^{3+} + HO^{\cdot} + OH^- \qquad \textit{Equation 9}$$

$$\xrightarrow{\text{Catalase/Glutathione peroxidases/thioredoxin}}$$

$$H_2O_2 \rightarrow \quad H_2O + O_2 \qquad \textit{Equation 10}$$

The DNA radical (DNA·) that is formed by direct or indirect ionisation (Equation 2 and Equation 5) can either be repaired by reduction (Equation 11) or the damage

can be 'fixed' by oxidation (Equation 12) through which the damage is made permanent. (J. M. Brown & Wilson, 2004), (Figure 1.4).

Reduction of the DNA radical occurs through reaction with thiols (R-SH) such as glutathione which donate a hydrogen atom from the sulfhydryl group (SH), to restore the DNA to its original undamaged form (Equation 11), (Robert Grimes & Partridge, 2015).

$$DNA^{\cdot} + R\text{-}SH \rightarrow DNA\text{-}H + RS^{\cdot} \qquad \textit{Equation 11}$$

Oxidation of the DNA radical occurs favourably over restoration by a sulfhydryl group under aerobic conditions through reaction with oxygen to form the organic peroxyl radical (DNA-OO·), Equation 12), (Robert Grimes & Partridge, 2015), (Figure 1.4).

$$DNA^{\cdot} + O_2 \rightarrow DNA\text{-}OO^{\cdot} \qquad \textit{Equation 12}$$

When the peroxyl radical is formed on a sugar unity of the DNA creating further reaction leads to strand breaks. Damage can also occur to the DNA base due to the reactivity of the peroxyl radical (Bryant-Friedrich, 2010). This can occur on multiple bases on the strand through hydrogen atom abstraction. This leads to clustered lesions on the DNA strand (Bryant-Friedrich, 2010). These are difficult to chemically repair due to the resulting electrophilic nature of the base modifications (Equation 11), which impair repair polymerases involved in Base Excision Repair (BER) (Bryant-Friedrich, 2010). Eventually, the clustered lesions lead to DNA strand breaks.

There is competition between oxidation of the damage from the DNA damaging hydroxyl radicals being produced and the fast chemical repair by thiols (glutathione and cysteine) which reverse DNA damage by reducing the DNA radical (J. M. Brown & Wilson, 2004). Hence, in hypoxic conditions, fast chemical repair by thiols is favoured. But in the presence of oxygen; oxidation is favoured, resulting in DNA strand breaks and 'fixing' the damage to the DNA. (Robert Grimes & Partridge, 2015), (Hall, 2006). This means that the effectiveness of radiation therapy is impaired under hypoxic conditions. Hypoxic tumour cells are more likely to result in survival and tumour regrowth after radiation therapy (J. M. Brown & Wilson, 2004). The oxygen enhancement ratio (OER) describes the ratio of the radiation doses under hypoxic and aerobic conditions required for the same biologic effect. The OER varies according to ionising density. For low LET X- and γ-ray radiation the OER is large and ranges from 2.5 to 3.5, whereas high LET alpha radiation is not as affected by a differential oxygen effect and therefore is much lower and closer to unity. The OER for neutron radiation is approximately 1.6 (Hall, 2006).

1.4 The DNA Damage Response

Damage fixation can result in either DNA-DNA or DNA-protein crosslinks, base damage, single strand breaks (SSBs) or double strand breaks (DSBs) in the DNA (Holley et al., 2014), (Minniti et al., 2012). For every 1 Gy of radiation about 10^5 ionisation events occur per cell which result in around 1000-3000 crosslinks, 2000 single strand breaks and 40 double strand breaks (Tannock et al., 2013). Most lesions are repaired successfully, through various enzymes that work through specific repair mechanisms, to protect the DNA (Tubbs & Nussenzweig, 2017). It is estimated that normally each human cell in the body suffers 70,000 lesions per day (Tubbs & Nussenzweig, 2017) due to the ROS produced by aerobic metabolism, and 75% of these are SSBs (Lomax, Folkes, & O'Neill, 2013).

1.4.1 The Cell Cycle and Checkpoints

Cells go through a cycle of proliferation and growth in order to divide. The cell cycle has four phases; G_1, S, G_2, and M phases (Figure 1.5). G_1, S and G_2 phases make up the interphase where the cells increase in size and prepare for DNA duplication. These phases consist of the first growth phase (G_1), the synthesis phase, where DNA is replicated (S) and G_2 phase is where the cellular content is reorganised for cell division in the mitotic phase (M) (Sia et al., 2020). Cells in the mitotic phase are most radiosensitive, whereas cells in the S phase are the most radioresistant (Pawlik & Keyomarsi, 2004).

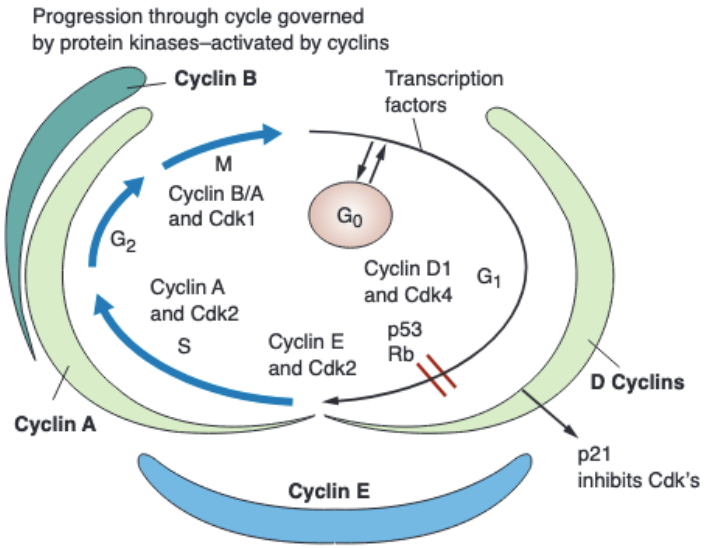

Figure 1.5: Phases of the Cell Cycle and its checkpoints. *G_1 Phase is associated with the cyclin D-CDK 4 complex, the S phase is associated with the cyclin E-CDK 2 complex, G_2 is associated with the cyclin B-CDK1 complex (Hall, 2006).*

Cell cycle checkpoints are present to ensure that the progression of a damaged cell through the cell cycle is delayed until repair can be completed (S. P. Jackson & Bartek, 2009). There are key delays in the second growth phase (G_2), just before starting mitosis, and in the first growth phase (G_1) just before the synthesis phase (S) (Lomax et al., 2013). The damage is detected at the checkpoints and is repaired before the cell can go on to divide, preventing mutations being passed down to the progeny or mitotic catastrophic cell death (Begg, Stewart, & Vens, 2011).

Progression through the cell cycle is driven by cyclin-dependent kinases (CDKs) (Figure 1.5). CDKs can become activated only by forming complexes with cyclins, once active they can begin phosphorylating proteins required for a cell's progress into the next phase (Joiner & van der Kogel, 2018). Each CDK-cyclin complex is specific for different phases of the cycle, and are all activated in different ways.

G_1 arrest is initiated by inhibition of the Mouse Double Minute 2 homolog (MDM2) protein, which lifts inhibition of the tumour suppressor p53 and this leads to activation of p21 which is an inhibitor of cyclin D–CDK 4. Inhibition of cyclin D-CDK 4 renders it unable to phosphorylate the tumour suppressor protein Rb which therefore doesn't release E2F which is the transcription factor needed to drive cell cycle progression through G_1 phase (R.-X. Huang & Zhou, 2020), (Joiner & van der Kogel, 2018).

S phase arrest is initiated by phosphorylation of checkpoint kinases Chk1 and Chk2 which activates them to phosphorylate the phosphatases Cell Division Cycle 25A (CDC25A) and Cell Division Cycle 25C (CDC25C), respectively, thus inactivating them. CDK2 needs to be dephosphorylated to be active and bind cyclin E. Therefore inactivation of CDC25A and CDC25C inhibits CDK2 activation and blocks progression (Joiner & van der Kogel, 2018).

G_2 arrest also is initiated by phosphorylation of Chk1 and Chk2. Phosphorylation of Chk1 leads to late G_2 phase arrest whereas Chk2 leads to early G_2 arrest. Phosphorylation of both Chk1 and Chk2 lead to CDC25A and CDC25C inhibition and therefore this blocks the cyclin B-CDK1 complex activation (Joiner & van der Kogel, 2018).

Activation of these checkpoints occurs through the DNA damage response (DDR) signalling pathway, which in response to DNA damage, can activate the cell cycle arrest checkpoints, repair pathways and cell death pathways (Marechal & Zou, 2013).

1.4.2 DNA Damage Repair

The DDR starts with the recognition of DNA damage by various sensors which send signals to transducers to activate effectors which initiates cell cycle arrest and repair or cell death (Marechal & Zou, 2013).

1.4.2.1 *Base Excision Repair*

Mutations derived from base damage can often be benign (Holley et al., 2014) due to the degeneracy of the genetic code (Gonzalez, Giannerini, & Rosa, 2019) and they would be unlikely to impede transcription. Therefore to prevent miscoded mutations from becoming permanent, these mutations can be detected and repaired through the Base Excision Repair (BER) pathway by the action of specific DNA glycosylase enzymes which recognise and remove the damaged bases. Examples include the 8-Oxoguanine Glycosylase (OGG1) which recognises 8-oxoguanine (O) opposite cytosine (C) and removes it, and the glycosylase, mutY homologue (MUTYH), which recognises adenine (A) opposite O and removes it. The endonuclease; Apurinic/Apyrimidinic Endonuclease (APE-1) cleaves the sugar backbone (creating an intermediate SSB), allowing DNA polymerase β to incorporate the correct base, and DNA ligase III, complexed to the scaffold protein, X-ray Repair Cross Complementing 1 (XRCC1), completes the repair by annealing the strand (Giglia-Mari, Zotter, & Vermeulen, 2011). This is known as the Short patch BER for repairing a single nucleotide errors. The repair of 2 – 12 nucleotides is achieved by the long patch BER pathway. In this case, the glycosylases that recognise the damaged bases leave the DNA sugar backbone intact, and APE1 catalyses the formation of an overhang flap on the 5' side of the damage. A complex of proteins; Replication Factor C (RFC), Proliferating Nuclear Cell Antigen (PCNA) and DNA polymerase δ/ε synthesise the correct 2 – 12 bases. Flap Structure-specific Endonuclease (FEN1) is recruited by PCNA to cleave the overhanging flap and Ligase I seals the strand break (Tannock et al., 2013). This pathway is involved in the repair of most of the endogenous mutations that occur spontaneously (Hoeijmakers, 2001).

1.4.2.2 *Nucleotide Excision Repair*

Larger lesions, such as DNA crosslinks, can be repaired by Nucleotide Excision Repair (NER) which is similar to BER except that dual incisions are made on either side of the damage by the endonucleases; Xeroderma Pigmentosum complementation group F - Excision Repair Cross Complementation 1 (XPF-ERCC1) and Xeroderma Pigmentosum complementation group G (XPG) before being filled in by DNA polymerases δ/α and sealed by ligase I (Hoeijmakers, 2001), (S. P. Jackson & Bartek, 2009). There are two ways in which lesions are

recognised in the NER repair pathway; global genome repair (GG-NER) and transcription coupled repair (TC-NER). GG-NER surveys the whole genome independently of transcription and large distortions to the DNA, such as the production of 6-4 photoproducts (6-4PPs) from the absorption of photons, can be recognised and removed by the complex; Xeroderma Pigmentosum complementation group C/human Homolog RAD 23 B (XPC/hHR23B). The TC-NER pathway relies on RNA polymerase for recognition as it is stalled during replication due to DNA damage and requires Cockayne syndrome factors A and B (CSA and CSB) to displace the stalled RNA polymerase to allow access for repair, thus this pathway can sense smaller distortions such as cyclobutane pyrimidine dimers (Hoeijmakers, 2001).

Both BER and NER pathways rely on an undamaged complementary strand and are therefore repair lesions quite faithfully (Giglia-Mari et al., 2011); hence mutations in both BER and NER enzymes do not lead to cellular radiosensitivity, with the exception of XRCC1 which is involved in the repair of SSBs (Hall, 2006), (Giglia-Mari et al., 2011).

1.4.2.3 *Single Strand Break Repair*

SSBs generated either as an intermediate in the BER pathway, or due to damage from various sources (Figure 1.6) (Caldecott, 2014), do not contribute significantly to cell cytotoxicity either, due to being repaired using the opposite strand as a template.

SSBs generated as an intermediate do not need to be recognised due to being part of a scheduled repair process, but SSBs generated due to direct damage have to be first detected by a sensor. This sensor is Poly [ADP-ribose] polymerase 1 (PARP1), which recruits the scaffold protein XRCC1, and this results in the repair of the phosphodiester backbone with Polymerase β and Ligase III as in BER (Giglia-Mari et al., 2011), (Abbotts & Wilson, 2017), (Figure 1.6). SSBs, despite not having many consequences in terms of cell cytotoxicity, are still important to repair as they can potentially go on to generate DSBs if left unrepaired (Hoeijmakers, 2001). Also SSBs that occur directly opposite each other in both strands, or many SSBs in close proximity to each other (clustered lesions/locally multiply damaged site) - by energy deposition in the radiation tracks, would cause DSBs to occur through the collapse of replication forks during replication (Hall, 2006), (Joiner & van der Kogel, 2018).

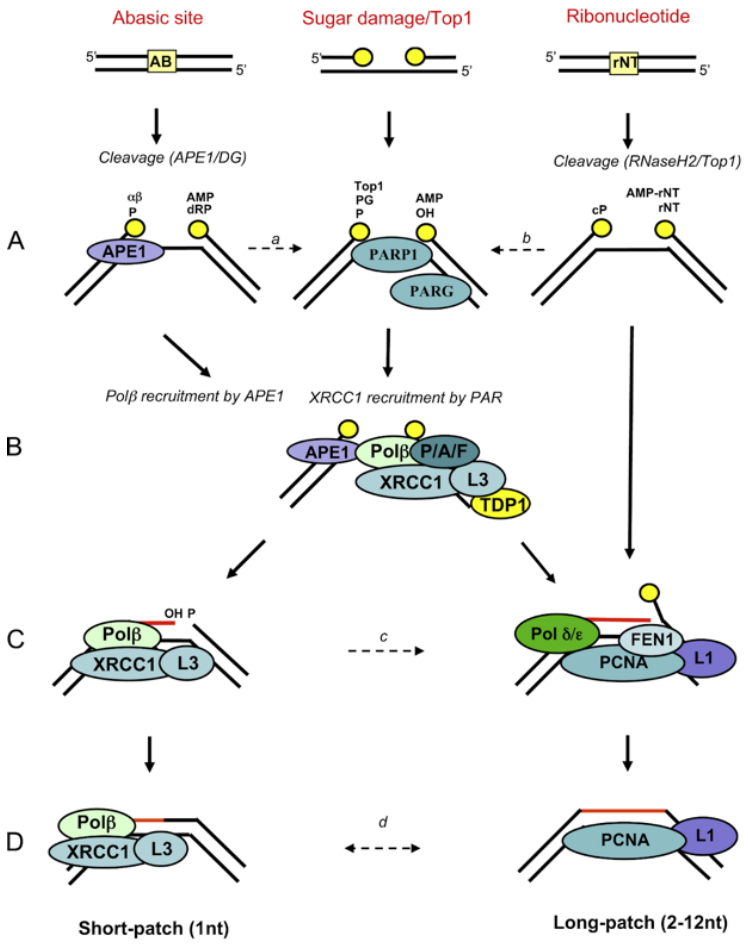

Figure 1.6: Single Strand Break Repair. *SSBs can be generated in different ways; (left;) during BER at abasic sites, (middle); from oxidised deoxyribose degradation or generated from the TOP1-DNA cleavage complex that cannot complete religation, (right); during BER at ribonucleotides by RNaseH2 in Ribonucleotide Exision Repair or by Top1 cleavage. (Caldecott, 2014).*

1.4.2.4 *Double Strand Break Repair*

DSBs are considered the most important lesion generated by ionising radiation because they contribute most significantly to radiation-induced cell killing. Since both strands are damaged, this particular lesion is difficult to repair (Giglia-Mari et al., 2011).

There are two main repair pathways involved in the repair of DSBs; Non-homologous End Joining (NHEJ) and Homologous Recombination Repair (HRR) (**Figure 1.7**), (Joiner & van der Kogel, 2018). Approximately 85% of DSBs are repaired by the NHEJ pathway, which is a fast, but low fidelity process, as it involves directly joining the two ends of the DNA together. NHEJ can operate in any phase of the cell cycle, although it is more predominant in the G1 phase (Han & Huang, 2020). HRR repairs fewer DSBs than NHEJ and is slower, but is more accurate because it uses homologous sequences as a template for repair. This dependence limits HRR to only operate in the S and G2 phase (Han & Huang, 2020).

The onset of DSBs is followed by the recruitment of many proteins to the site of damage. The histone variant H2AX that is present around the DSB in the DNA is phosphorylated at the Ser139 residue (Mah, El-Osta, & Karagiannis, 2010). Phosphorylated H2AX (γH2AX) acts as a signal to recruit the proteins required for repair of DSBs.

H2AX can be phosphorylated by three different protein kinases that are all members of the phosphatidylinositol 3-kinase-related kinase (PIKK) family; Ataxia Telangiectasia mutated

(ATM), Ataxia Telangiectasia and Rad3-related (ATR), and DNA-dependent protein kinase catalytic subunit (DNA-PKcs) (Burger, Ketley, & Gullerova, 2019). These protein kinases work to phosphorylate many substrates that are involved in DDR and can therefore have overlapping functions (Tannock et al., 2013).

ATM is the major protein kinase involved in phosphorylating H2AX and other substrates involved in DDR, and is known as the master regulator of DDR due to its importance in signal transmission in response to DSBs (Joiner & van der Kogel, 2018). The protein complex MRN is comprised of three proteins; Mre11 (Meiotic Recombination 11), Rad50 and NBS1 (Nijmegen Breakage Syndrome 1), and MRN binds to ATM through NBS1 and guides ATM to the site of damage (Joiner & van der Kogel, 2018). The MRN complex is known to be one of the fastest sensors of DSBs. Once ATM becomes associated with the DSB it is activated and phosphorylates H2AX at the Ser139 residue. H2AX phosphorylation spreads over the surrounding area through regulation by the protein Mediator of DNA-damage Checkpoint 1 (MDC1) (Mah et al., 2010), which binds to γH2AX after phosphorylation by ATM. This amplifies the signal, creating a molecular beacon for repair proteins (Chapman, Taylor, & Boulton, 2012), forming the irradiation induced foci (IRIF) (Goodarzi & Jeggo, 2012).

Two proteins accumulate at the IRIF after H2AX phosphorylation; p53-Binding Protein 1 (53BP1) and Breast Cancer 1 (BRCA1), which are both in competition with each other (Han & Huang, 2020). The protein 53BP1 blocks DNA end resection through the recruitment of further proteins, and therefore promotes NHEJ over HRR. But in the G_2/S phase BRCA1 can overcome the inhibition by 53BP1 to promote HRR by removing the inhibition on end resection (Nakada, 2016). This restriction based on cell cycle phase is known to be partly regulated by cell cycle specific CDKs, but the exact mechanisms have not yet been elucidated (Chapman et al., 2012).

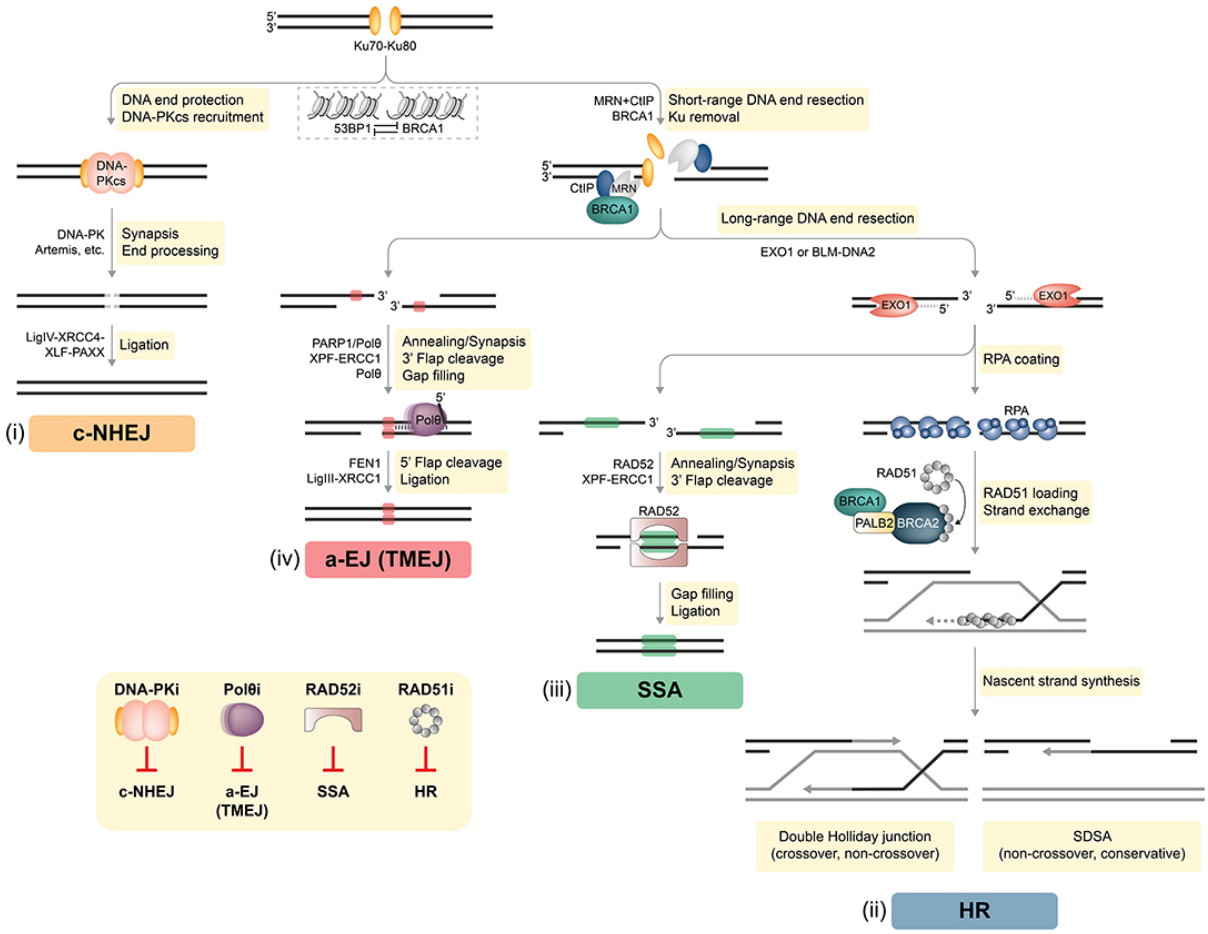

Figure 1.7: Summary of the four DSB repair pathways*. NHEJ, AEJ, SSA and HRR. 53BP1 drives NHEJ and BRCA1 inhibits 53BP1 to drive HRR. NHEJ is sensed by Ku70/80 and is activated by the recruited DNA-PKcs complex. AEJ is an alternative to NHEJ using HRR processes. SSA is a faster alternative to HRR and does not require sister strand invasion. HRR is initiated by the MRN complex and is the most high fidelity process utilising the undamaged strand as a template. (Trenner & Sartori, 2019)*

1.4.2.5 *Homologous Recombination Repair*

HRR requires an undamaged homologous sister chromatid to utilise as a template for the repair of the damaged strand and so can only operate in the S and G2 phase (Han & Huang, 2020). BRCA1 promotes HRR by heterodimerising with BARD1 to ubiquitylate CtBP-1 interacting protein (CtIP) and this increases the CtIP levels at the IRIF site (Chapman et al., 2012), (Figure 1.7). The first step of HRR is end resection which is initiated by CtIP binding to MRN and this enhances the endonuclease activity of Mre11; creating a strand break on the 5' side of the break and the exonuclease activity of Mre11 resects the DNA in a 3' – 5' direction, resulting in a 3' overhang of ssDNA (Scully, Panday, Elango, & Willis, 2019). To extend the resection to create long 3' ssDNA tail the endonuclease, DNA replication helicase/Nuclease 2 (DNA2) and Exonuclease 1 (EXO1) resect the DNA in a 5'-3' direction while the helicases, Bloom syndrome helicase (BLM) and Werner syndrome helicase (WRN), unwind the DNA (Figure 1.7). The ssDNA is rapidly coated in Replication Protein A (RPA), which protects the ssDNA from protein interactions (Scully et al., 2019), (Figure 1.7). To facilitate strand invasion RPA must be displaced. RAD51 by binds to ssDNA which forms a nucleoprotein filament that can begin the search for homologous DNA (Joiner & van der Kogel, 2018). To overcome the inhibition of RAD51, loading the protein Breast Cancer 2 (BRCA2) with the help of BRCA1-BRCA1-Associated Ring Domain (BARD-1) complex, competes with RPA to allow RAD51

nucleation on ssDNA (Scully et al., 2019). Many proteins aid RAD51 in the search for homologous DNA and strand invasion such as XRCC2, XRCC3, RAD52, RAD51B, C and D.

Once the homologous sister chromatid is found, helicases such as BLM unwind the DNA and the nascent strand invades the homologous sister chromatid forming a displacement loop, "D-loop", in order to access the bases of the template for correct DNA synthesis (Joiner & van der Kogel, 2018). This crossover structure allows base pairing between the two strands forms, and is known as the Holliday Junction. Synthesis occurs from the 3' end with Polymerase δ. To resolve the Holliday Junction, BLM helicase forms a complex with Topoisomerase IIIa and the proteins, RecQ-Mediated genome Instability 1 and 2 (RMI1 and RMI2), which separates the two sister chromatids and ligase 1 ligates the DNA ends (Scully et al., 2019). The RPA coating of ssDNA in HRR is significant for not just for protecting the ssDNA from interfering protein interactions, but also because it leads to the recruitment of ATR and ATR interacting protein (ATRIP) (Marechal & Zou, 2013). As the ssDNA is extended during resection there is a switch from activating ATM to ATR; this is known as the ATM-ATR switch (Marechal & Zou, 2013). ATR-ATRIP goes on to phosphorylate H2AX at the ssDNA, and this leads to phosphorylation of Chk1 which is known to localise Rad51 to ssDNA thus promoting HRR (Bahassi et al., 2008). Phosphorylation of Chk1 also leads to phosphorylation of the phosphatase CDC25A. This phosphorylation inactivates CDC25A making it unable to remove the inhibitory phosphate group on the cyclin B-CDK1 complex, which needs to be in its dephosphorylated form to be active (Joiner & van der Kogel, 2018). Cyclin B-CDK1 inhibition leads to cell cycle arrest at the G_2 – S checkpoint (Joiner & van der Kogel, 2018).

1.4.2.6 *Non-Homologous End Joining*

The third protein kinase that can phosphorylate H2AX, DNA-PKcs, is recruited to the site of damage by the Ku70/Ku80 heterodimer which binds with high affinity to the broken DNA ends on either side of the breaks, bridging and aligning them closer (Figure 1.7).

The phosphorylation of H2AX creates the IRIF that causes rapid localisation of 53BP1, which in turn recruits PTIP and RIF1 to inhibit end resection. Localisation of 53BP1 can also supress BRCA1 if BRCA1 is not stimulated by cell cycle specific CDKs. If BRCA1 is stimulated to overcome 53BP1 suppression, then the CtIP will be upregulated to enhance Mre11 endonuclease activity, thus promoting end resection in HRR, and its exonuclease activity will displace Ku70/80 (Scully et al., 2019).

The NHEJ repair pathway is active throughout interphase (Han & Huang, 2020) and is initiated when DNA-PKcs is activated by binding to the Ku complex forming the DNA-PK active protein kinase complex (Fell & Schild-Poulter, 2012). This leads to autophosphorylation of DNA-PKcs on Ser2056 and recruiting the endonuclease Artemis. Artemis prepares both strands of the DNA for ligation by trimming damaged ends and creating 3' and 5' overhangs that can be base paired for ligation. This causes gaps which can be filled in by Polymerase μ and Polymerase λ (Scully et al., 2019). This results in blunt ends that can be ligated by the XRCC4, XRCC-4 Like Factor (XLF) and DNA ligase 4 complex (Figure 1.7). DNA ligase is enhanced by the other two components of the complex to carry out the actual ligation reaction (Tannock et al., 2013). The Polynucleotide Kinase (PNK) removes any sugar groups that hinder the ligation process (Joiner & van der Kogel, 2018).

HRR and NHEJ are the two main pathways involved in DSB repair. There are other minor pathways that serve as alternative pathways to HRR and NHEJ and which use different proteins.

1.4.2.7 *Single Strand Annealing*

Single strand annealing (SSA) is an alternative to HRR. SSA is an error prone homology directed repair pathway that does not require a sister strand to invade and use as a complementary sequence (Scully et al., 2019). It is also fast, making this pathway useful for when there is not enough time for HRR (Blasiak, 2021). This pathway relies on two DSB flanking homologous repeats that are annealed together. When the 3' ssDNA overhang that is generated by resection is coated in RPA, this triggers ATR-ATRIP which, if RAD51 is not functionally available to direct strand invasion in HRR, phosphorylates the Abelson tyrosine-protein kinase 1 (ABL1) which activates RAD52 (Sotiriou et al., 2016), (Al-Minawi, Saleh-Gohari, & Helleday, 2007). RAD52 can bind to RPA heterotrimers on the 3' ssDNA which promotes annealing of the homologous repeats adjacent to each other. Then the 3' overhangs are displaced by the endonuclease XPF-ERCC1 complex, which is recruited by RAD52 (Figure 1.7). The gaps are filled in by a polymerase and the strands are ligated (Figure 1.7). The identity of the polymerases and ligases involved are not yet known (Blasiak, 2021). The deletion of the original sequence between the homologous regions represent a loss of genetic information (Bhargava, Onyango, & Stark, 2016).

1.4.2.8 *Alternate End Joining*

Alternate End Joining (altEJ) which is sometimes called Microhomology-Mediated End Joining (MMEJ) is an alternative to NHEJ that doesn't use NHEJ factors (Scully et al., 2019). AltEJ also relies on flanking microhomologies around the DSB like SSA, but unlike SSA, altEJ can utilise smaller regions of microhomology (around 10-19 nucleotides) (S. Sharma et al., 2015). PARP1 binds to the ends at the site of DSB damage in a process that is not well understood yet, and recruits the MRN complex with CtIP to resect the strands back to the microhomology regions in a similar process to that found in HRR. If the microhomology regions are far from the DSB site then further resection will need to be carried out by endonuclease DNA2 and the exonuclease EXO1 with the helicase BLM (Seol, Shim, & Lee, 2018) (Figure 1.7). Once the microhomology regions are exposed they are annealed by a mechanism not yet identified (Seol et al., 2018). The 3' non-homologous overhangs are processed by XPF-ERRC1 complex and Polymerase θ can fill in the gaps and Ligase III seals (Scully et al., 2019). The presence of RPA coating on the generated ssDNA will inhibit altEJ, and will encourage repair via HRR (Deng, Gibb, De Almeida, Greene, & Symington, 2014). This pathway is also obligatorily error prone and results in loss of genetic information, but has the benefit of effecting very fast repair.

1.4.3 Cell Death

Despite the complex repair mechanisms that exist, many cells with DSB cannot be repaired, or are misrepaired, which can lead to cell killing or the development of mutations in the DNA (Prise, Schettino, Folkard, & Held, 2005). DSBs in the DNA cause breaks in the chromosome. The broken ends of the chromosome are said to be 'sticky' due to the unpaired bases which can join to other 'sticky' ends (Hall, 2006). This results in rearrangements of the chromatid or the chromosome – depending on when during the cell cycle the radiation induces damage in the genome of the cell. Cells irradiated during early interphase (G_1 / early S phase), before the duplication, results in chromosome aberrations as the damaged strand is replicated in the S phase. If the damage is induced in late interphase (G_2 / late S phase), then chromatid aberrations result as the sister chromatids are duplicated (Tannock et al., 2013). The gross chromosomal aberrations induced by radiation that commonly lead to cell lethality (loss of

replicative potential) include the formation of dicentric and acentric fragments and anaphase bridges, due to a failure to complete mitosis.

Dicentric fragments are formed due to the presence of a break in each of the two separate chromosomes in early interphase (G_1). The sticky ends can join incorrectly during exchange, which after replication in the S phase, will produce a chromosome with two centromeres; a dicentric fragment and two acentric fragments. The acentric fragments will not be able to undergo mitosis because the centromeres will fail to engage and separate to the poles during anaphase (Hall, 2006). Acentric fragments form micronuclei and represent a loss of genetic information from the daughter cells (J. M. Brown & Attardi, 2005). Large deletions which result in a large amount of genetic information loss can also be lethal to the cell.

With dicentric fragments, there is equal chance that the centromeres on the same sister chromatid can either be pulled to the same pole or the opposite pole (Cook et al., 2021). If the chromatid is pulled to the same pole then segregation can occur without breakage, but if pulled to the opposite poles, the chromatid is stretched between the poles. This event is known as an anaphase bridge and this eventually leads to breakage (Cook et al., 2021). Anaphase bridges can be produced in many ways, such as by breaks in late interphase (G_2), in the chromatids of the same chromosome which can join together and therefore result in anaphase bridges as they are stretched to the opposite poles (Hall, 2006).

Non-lethal aberrations such as symmetric translocations, where breaks in two different G_1 chromosomes are exchanged with each other, or small deletions, have an equal chance of occurring as lethal aberrations. They are known as stable aberrations because the cells survive through mitosis and the aberration is passed on to the progeny (Hall, 2006).

The frequency of lethal chromosomal aberrations (E) can be determined by a linear-quadratic relationship with radiation dose (D):

$$E = \alpha D + \beta D^2 \qquad \textit{Equation 13}$$

Where α represents the cell killing by a single track event causing both breaks which is proportional to the dose and is therefore a linear relationship (Equation 13). β represents the cell killing by a two track event from two separate electrons each causing a single break, which is proportional to the square of the dose and is therefore a quadratic relationship. The α/β ratio is where cell killing by linear and quadratic components is equal and this value is used to determine response of tissues to radiation. Generally, a lower α/β ratio indicates a late responding tissue (typically around 3 Gy) and a higher ratio indicates an early responding tissue (typically around 10 Gy) (J. M. Brown et al., 2014).

This is important when determining which dose delivery strategy to utilise, as it allows comparison between the surrounding normal tissue response and the tumour response. For example, if the tumour has a lower α/β ratio than the surrounding normal tissue; this suggests that the tumour is more late-responding than the surrounding normal tissue and therefore hypo-fractionation with large doses would be more effective than hyper-fractionation with small doses, as that would spare the tumour more than the surrounding normal tissue (Folkert & Timmerman, 2017).

The inability to complete mitosis due to aberrant division is known as mitotic catastrophe (Joiner & van der Kogel, 2018). Mitotic catastrophe serves as a trigger for initiating cell death pathways such as apoptosis, autophagy, necrosis and senescence (Sia et al., 2020). The major cause of cell death from irradiation is mitotic catastrophe (Joiner & van der Kogel, 2018).

Some cells do die before entering mitosis, and this early cell death is caused by the direct activation of cell death pathways (most commonly the intrinsic apoptosis pathway) from the DNA damage. In contrast, cell death triggered by mitotic catastrophe is known as late cell death. Many factors converge to influence which cell death pathway is taken to remove the cell. These include radiation dose, oxygen levels and activity of key regulators in the cell cycle like p53 (J. M. Brown & Attardi, 2005). Mitotic catastrophe can trigger multiple pathways in one cell, therefore it can be that the most rapid pathway ends up being the mechanism of death (Joiner & van der Kogel, 2018).

1.4.3.1 *Apoptosis*

Apoptosis is a programmed cell death pathway that involves condensation of the chromatin and nuclear fragmentation which causes the cell to shrink and start fragmenting (membrane blebbing) into apoptotic bodies. There are three distinct pathways that initiate apoptosis (Sia et al., 2020). The intrinsic pathway involves p53 activation leading to activation of pro-apoptotic factors and the family of caspases to initiate apoptosis (Eriksson & Stigbrand, 2010). The extrinsic pathway involves activation of various death receptors present on the cell membrane that are activated upon binding with extracellular ligands such as TNF binding to its cognate receptor, which is triggered by inflammatory stimuli.
The ceramide pathway involves hydrolysis of acid sphingomyelinase in the plasma membrane which generates the second messenger ceramide to activate apoptosis (Kolesnick & Fuks, 2003).

1.4.3.2 *Autophagy*

Autophagy is also a programmed cell death pathway that involves the sequestration of cytoplasmic content in double membrane vesicles called autophagosomes that fuse with lysosomes to degrade and reprocess organelles. This pathway is regulated by autophagy-related genes and can be activated under cellular stress (Type II cell death) by the mTOR pathway and endoplasmic reticulum stress (Tam, Wu, & Law, 2017).

1.4.3.3 *Senescence*

Senescence is another programmed cell death pathway that leads to permanent cell cycle arrest, and therefore loss of the ability to divide, rendering it reproductively dead. This can occur in a number of ways, but the most common is activation of p53 which leads to strong prolonged inhibition of cyclin D-CDK4 and permanent cell cycle arrest at G_1. Cells in this kind of quiescence are known as G_0 cells (Tannock et al., 2013).

1.4.3.4 *Necrosis*

Necrosis is an unregulated cell death pathway which involves cell swelling, membrane rupture and release of lysosomal enzymes. These enzymes are not contained in a vesicle and causes damage in an uncontrolled manner (Joiner & van der Kogel, 2018). This cell death pathway is activated by severe changes to the cell, such as extreme pH and ion imbalances. A similar programmed cell death pathway called necroptosis can occur through inhibition of Cas8 signalling, allowing Receptor Interacting Proteins RIPK1 and RIPK2 to trigger necroptosis (Tannock et al., 2013).

1.4.4 Variable (Diversity) Joining (V(D)J); an Essential Process that Relies on Error Prone Repair Pathways

Although the inability to correctly repair DSBs can lead to cell death, the error prone nature of the NHEJ repair pathway that produces deletions and rearrangements, is useful for generating antibody diversity in V(D)J recombination (Hall, 2006). V(D)J recombination is the

rearrangement of Variable, Diversity and Joining gene segments that generate novel antigen binding sequences for antibody diversity (Figure 1.8). The endonucleases Recombination Activating Genes 1 and 2 (RAG1 and RAG2) cleave the double strand between V, D or J segments by recognising and binding the flanking Recombination Signalling Sequences (RSS) creating a DSB that produces a pair of hairpin coding ends (CE) and a pair of blunt signal ends (SE) (Menolfi & Zha, 2020), (Figure 1.8). The blunt signal ends are ligated together to form a circular DNA by the XRCC4, XLF and DNA ligase 4 complex as occurs in NHEJ (Menolfi & Zha, 2020). The hairpin coding ends have to be processed before ligation. DNA-PK binds to the broken DNA and recruits Artemis which trims damaged ends, creating 3' and 5' overhangs that can be base paired for ligation by the XRCC4, XLF and DNA ligase 4 complex as in NHEJ (Menolfi & Zha, 2020).
This process is important in the adaptive immune system which allows recognition of antigens from a wide range of pathogens.

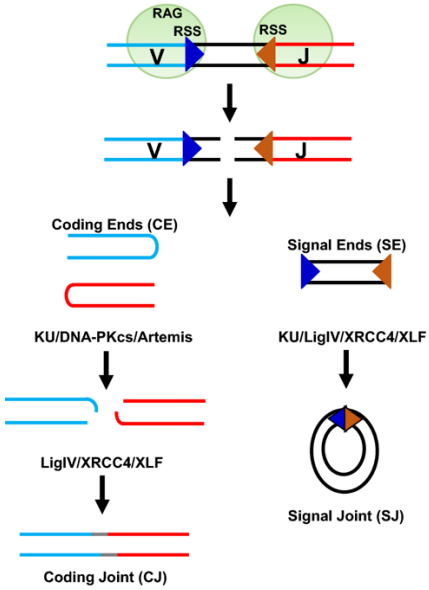

Figure 1.8: *V(D)J Recombination process*. *Error prone pathways such as NHEJ are important for random rearrangements of V(D)J segments to generate diverse antibodies. (Menolfi & Zha, 2020).*

1.4.5 Mutations in DNA Repair

It has long been known that deficiencies in DDR pathways can predispose individuals to cancer, and germline mutations can be passed down (Y. Liang, Lin, Brunicardi, Goss, & Li, 2009). For example, mutation of the MUTYH DNA glycosylase in BER causes MUTYH-associated polyposis which is a form of colorectal cancer (Siva et al., 2010) and mutations in the Cockayne Syndrome (CS) factors A and B in NER cause Cockayne Syndrome which is a form of dwarfism (Taghdiri et al., 2017). Mutations in the DSB sensors such as ATM lead to ataxia-telangiectasia which involves progressive neurological issues, mutation of NBS1 in the MRN complex leads to Nijmegen Syndrome which involves microcephaly and intellectual disability among others (R. Sharma, Lewis, & Wlodarski, 2020) and mutations in DNA-PKcs lead to Severe Combined Immunodeficiency (SCID) (Collis, Deweese, Jeggo, & Parker, 2005).

Although deficiencies in the DDR pathway can lead to cell death or initiate malignant transformation they can also be exploited for cancer therapy (Y. Liang et al., 2009). This approach relies on the concept of Synthetic Lethality. Synthetic lethality was first described

in *Drosophila melanogaster*, and occurs when the loss of two individual genes separately is non-toxic, but loss of both at the same time is a lethal combination (Bridges, 1922), (Dobzhansky, 1946).

The concept of Synthetic Lethality can be applied to inhibit the repair pathways specifically in cancer cells (O'Connor, 2015). The first molecular targeted therapeutic agent to utilise this concept involved treating breast and ovarian cancer patients with BRCA-deficient cancer cells with the Poly [ADP-ribose] polymerase (PARP) inhibitor Olaparib. PARP1 is important in BER and inhibition of PARP1 with olaparib results in an increase in SSB. These SSB lead to the formation of DSBs during the replication process. This was effective because in the absence of BRCA the HRR pathway is defective. Reliance on the error prone NHEJ pathway increases genetic instability which eventually leads to cell death through mitotic catastrophe in these cells (O'Connor, 2015).

Cancer cells can be targeted by two different targeted therapies to induce contextual synthetic lethality, for example by using radiation therapy to induce DSBs in the DNA in combination with a DDR specific inhibitor to block repair in cancer cells, which increases the radiosensitivity of cells (O'Connor, 2015). DSB sensors such as ATM, ATR and DNA-PKcs are key factors in DDR and are therefore attractive as targets for inhibiting repair in cancer cells during anti-tumour treatment to increase cancer cell susceptibility and therefore treatment sensitivity (Y. Liang et al., 2009).

1.5 The PIKK Family

The Phosphatidylinositol-3 Kinase-related Kinases (PIKK) is a family of serine/threonine protein kinases, and in addition to ATM, ATR and DNA-PKcs, also includes Mammalian Target Of Rapamycin (mTOR), Transcription Domain Associated Protein (TTRAP) and Suppressor of Morphogenesis in Genetalia-1 (SMG-1) (Rivera-Calzada et al., 2015). mTOR has various roles in cell proliferation, cell growth and protein synthesis (Rivera-Calzada et al., 2015). SMG-1 is known to phosphorylate key proteins involved in the mRNA surveillance pathway such as Nonsense mediated mRNA decay (NMD) to remove transcripts with premature stop codons (Chang, Imam, & Wilkinson, 2007). TTRAP is the only member to not possess kinase activity, and forms complexes with Histone Acetyl-Transferase (HAT) on chromatin to activate transcription. TTRAP has been shown to be involved in cell cycle checkpoints (Murr, Vaissière, Sawan, Shukla, & Herceg, 2007).

Members of the PIKK family all share common structural motifs. The C terminal ends with the highly conserved FATC (FRAP, ATM and TRRAP C-terminal) domain (Figure 1.9), which is always preceded by the Kinase Domain, except in the case of SMG-1 which has an insert with unknown function (Rivera-Calzada et al., 2015). The FATC domain is made up of 30 amino acids, and are highly conserved. Replacement of the FATC domain of ATM with the FATC domain of ATR, TRRAP or DNA-PKcs does not alter its function (Lempiäinen & Halazonetis, 2009). Nonetheless, this domain is important for kinase function as it has been seen that deletion of even one residue can abolish function. One mutation occurring in the disease ataxia-telangiectasia targets the FATC domain, mutating a critical cysteine residue important for disulphide bond formation, and prevents activation of ATM (Guo, Deshpande, & Paull, 2010).

The kinase domain is the structural motif that defines the PIKKs as a family, and is where the signal transduction by phosphorylation of proteins on serine and threonine residues occurs (Abraham, 2004).

The 100 residue FRB (FKBP12-rapamycin-binding) domain present next to the PIKK domain in all members except ATM and ATR, is less conserved and small deletions do not appear to interfere significantly with activity (Lempiäinen & Halazonetis, 2009). The FRB domain in mTOR is where rapamycin and FKBP12 bind as the name suggests.

In all members the N-terminal region is composed of HEAT (Huntington Elongation factor 2, A subunit of PP2A and TOR1) repeats of different lengths which form helical scaffolds that are involved in protein-protein interactions, followed by a FAT domain (Rivera-Calzada et al., 2015). The FAT domain and FATC domain is where Ku70/80 induce conformational change in DNA-PKcs (Spagnolo, Rivera-Calzada, Pearl, & Llorca, 2006).

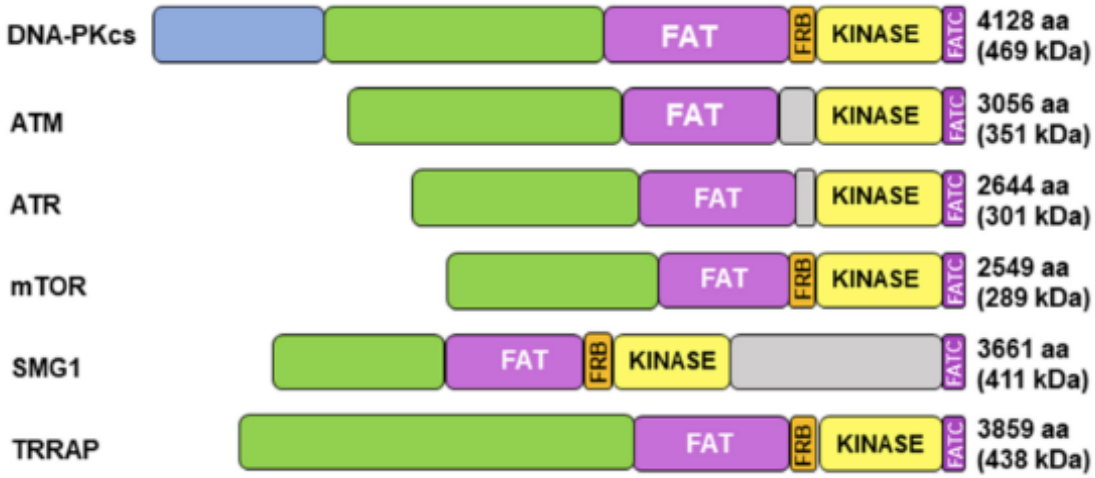

Figure 1.9: Sequence Homology Between Members of the PIKK Family. *The highly conserved 30 amino acid FATC domain (purple) is present in all members at the C-terminal. Followed by the kinase domain (yellow) in all but the SMG-1 where it an unknown insert is present in between the kinase domain and the FATC domain. The 100 residue variable FRB domain (orange) is present in only DNA-PKCs mTOR, SMG-1 and TRRAP after the kinase domain. The FAT domain is present in all members followed by the HEAT repeats (green and blue) important for protein-protein interactions. (Mohiuddin & Kang, 2019).*

PIKKs are considered atypical protein kinases because they are unusually large (T. Hunter, 1995) (Abraham, 2004), they do not have all of the conserved sequences found in the catalytic domain of classical protein kinases, such as the GXGXXG ATP binding motif, and they are structurally different (Pospisilova, Seifrtova, & Rezacova, 2017). The ATP binding site in the catalytic subunit has high sequence homology to the ATP binding site in the kinase domain of members of the phosphatidylinositol 3-kinase (PI3K) family (Abraham, 2004) (Lempiäinen & Halazonetis, 2009) (Figure 1.10). The PI3K family are lipid kinases that have roles in cell survival, motility, proliferation and differentiation and these kinases are often associated with cancer. The PI3K pathway is one of the most frequently activated signalling pathways (Knight & Shokat, 2007). PI3K activation causes the generation of the second messenger phosphatidylinositol (3,4,5)-triphospate (PIP_3) from phosphatidylinositol (3,4) bisphosphate (PIP_2) in the membrane activating many various downstream effectors (Andrs et al., 2015). There are three different classes of PI3Ks; Class I, Class II and Class III.

Class I is the most well characterised, which is further divided into two subgroups; Class Ia includes catalytic subunits p110α, p110β and p110δ which all link PI3K activity to growth factor tyrosine kinase receptors. Class Ib includes the p110γ catalytic subunit that links PI3K activity to G-protein coupled receptors (Knight & Shokat, 2007). Class I PI3Ks have very conserved ATP binding sites (Knight & Shokat, 2007).

Class II and III are not well understood, but it is known that Class II includes a p110-like catalytic subunit that exists in three different isoforms and Class III includes vacuolar protein sorting 34 (Vps34) (Andrs et al., 2015).

The PIKK family are considered to be Class IV PI3Ks due to the homology of their kinase domains motifs (Figure 1.10) to those of a PI3K family member (Andrs et al., 2015), (Hartley et al., 1995). This similarity in ATP binding sites within the PIKK and PI3K families presents a major challenge in the design of selective inhibitors (Menolfi & Zha, 2020).

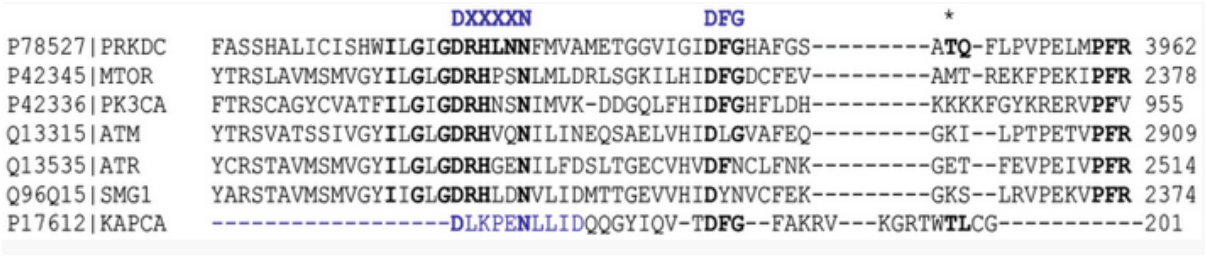

Figure 1.10: Catalytic Site Homology in Catalytically Active PIKK Members and PI3K (PK3CA) and Protein Kinase A Family (KAPCA). *The conserved aspartic acid sequence (DXXXXN) and the magnesium binding motif (DFG) that are important for catalysis and is present in both typical protein kinases and PIKKs are shown in blue. (Bartlett & Lees-Miller, 2018)*

1.5.1 DNA-PKcs

The development of inhibitors against DNA-PKcs that are selective and potent is a challenge due to selectivity issues, but developing DNA-PKcs inhibitors is of great interest because of the potential of these inhibitors to act as radiosensitisers. As noted above, DNA-PKcs is required for the NHEJ repair pathway which is active throughout interphase and repairs 85% of radiation-induced DSBs. DNA-PKcs expression has also been implicated in chemoresistance and poor clinical outcomes in patients with ovarian cancer and hepatocellular cancer (C. Cano, Harnor, Willmore, & Wedge, 2018).

The role of DNA-PK in V(D)J recombination is vital for processing of the hairpin coding ends to allow ligation into coding joints. Mice that are homozygous for a nonsense mutation at the amino acid 4046, which results in a truncated protein lacking the highly conserved FATC domain were found to suffer from Severe Combined Immuno-Deficiency (SCID) (Beamish, 2000). This causes impaired activity of DNA-PKcs, even though the kinase domain is still intact (Beamish, 2000). These mice have impaired V(D)J recombination, and tissues from SCID mice have been observed to be more three-fold more radiosensitive than tissues from normal mice (Shinohara et al., 2005), (Biedermann, Sun, Giaccia, Tosto, & Brown, 1991).

Therefore targeting DNA-PK in tumour cells presents an efficient mechanism of inhibiting DSB repair and increasing sensitivity to radiation therapy (Shinohara et al., 2005).

However, a number of studies have identified that DNA-PK is upregulated in tumour cells (Collis et al., 2005). Other studies have identified further interactions for DNA-PK. Various cancer associated survival factors can regulate DNA-PKcs activity including the threonine/serine kinase Akt1. Akt1 is involved in phosphorylating Bcl-2 Associated Death promoter (BAD) causing dissociation from Bcl-2/Bcl-X and therefore is anti-apoptotic. Akt1 is known to promote DNA-PKcs autophosphorylation (Goodwin & Knudsen, 2014). The Epidermal Growth Factor Receptor (EGFR) has been observed to be able to enhance the activity of DNA-PKcs (Goodwin & Knudsen, 2014).

DNA-PK has also been found to have roles that contribute to the some of the Six Hallmarks of Cancer. Genomic instability is caused by an interaction with Snail1, an E-box binding transcription factor, which promotes the Epithelial to Mesenchymal Transition (EMT) (Goodwin & Knudsen, 2014). DNA-PK has also been implicated in the survival of cells under hypoxia where it was seen that DNA-PK phosphorylates the tumour suppressor P53, which causes the release of RPA70, which in turn is anti-apoptotic and contributes to hypoxia resistance (Goodwin & Knudsen, 2014).

DNA-PK has been a challenging target to design inhibitors for, as structure based drug binding studies were limited, and therefore screening methods have been the main approach to discovering new inhibitors, utilising medicinal chemistry to optimise promising compounds (C. Cano et al., 2018). As most DNA-PK inhibitors are designed to bind to the ATP-binding site, good selectivity and potency is essential for progression onto clinical development. It is only recently that cryo-electron microscopy has been used to define the three dimensional structure of the DNA-PK holoenzyme to 6.6 Å (Yin, Liu, Tian, Wang, & Xu, 2017) and 5.8 Å resolution (Sharif et al., 2017). Two recent publications have described higher resolution cryo-EM structures of DNA-PKcs at 2.8 Å (Chaplin et al., 2021) and several recent inhibitors bound in the kinase domain (S. Liang et al., 2022). These structures will catalyse even more drug discovery activity against this target. With increasing knowledge of the DNA-PK structure, in the future drugs could be designed to target allosteric sites to increase specificity (S. Liang et al., 2022).

1.6 DNA-PK inhibitors

There have been considerable efforts over the last thirty years to identify novel, selective inhibitors of DNA-PK. Much of the early work was based on compounds that were know inhibitors of related kinases such as PI3K and ATM. As such these compounds tend to have low selectivity for DNA-PK and demonstrated *in vivo* toxicities thought to be associated with inhibition of these other kinases. This discussion covers examples of the main classes developed and focusses on recent compounds which have advanced to the clinic.

1.6.1 *Wortmannin*

The first identified molecule, wortmannin (Figure 1.11) was discovered in 1957 (Wipf & Halter, 2005) and later was found to be capable of inhibiting PI3K family and the structurally similar PIKK family members (Andrs et al., 2015). Wortmannin is a furanosteroid metabolite of *Penicillium funiculosum* and *Taloromyces (Penicillium) wortmannii* (Karve et al., 2012). Wortmannin forms covalent adducts by alkylation at the amino acid lysine 802 in the kinase domain region of DNA-PKcs (Pospisilova et al., 2017), (Davidson, Amrein, Panasci, & Aloyz, 2013). This results in formation of an irreversible bond between Wortmannin and the protein which causes non-competitive potent inhibition of kinase activity, with an IC_{50} of around 5 nM for DNA-PK (Davidson et al., 2013). Inhibition of DSB repair and G_2/M phase arrest in cells was found to increase in a dose dependent manner (Pospisilova et al., 2017) and wortmannin was also found to be an effective radiosensitiser in *in vitro* studies (Collis et al., 2005).

Despite its merits, Wortmannin lacks the needed selectivity to differentiate between members of the PI3K and PIKK family and did not proceed onto clinical trials due to observed poor solubility in aqueous solutions (Collis et al., 2005),high *in vivo* toxicity and its low stability (Andrs et al., 2015), (Davidson et al., 2013).

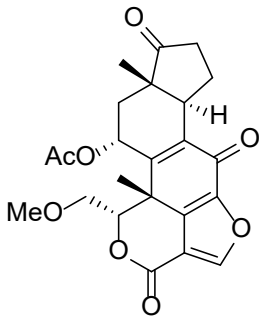

Figure 1.11. *Chemical Structure of Wortmannin*

Semisynthetic analogues of Wortmannin were developed to improve Wortmannin's limiting properties.

1.6.2 *PX-866*

In 2004, PX-866 (Figure 1.12) , also known as Sonolisib, was developed by Oncothyreon. PX-866 is a furanosteroid viridin formed by opening the furan ring at the C-20 position of Wortmannin (Ihle et al., 2004). PX-866 is a potent, irreversible broad spectrum inhibitor of the PI3K family (Ihle et al., 2004). It was shown to have improved solubility, stability and activity with reduced toxicity (Ihle et al., 2004), (D. S. Hong et al., 2012). PX-866 was active as a monotherapy against ovarian, colon and non-small cell lung cancer mouse xenografts (Ihle et al., 2004). It was also found to increase the growth inhibition by radiotherapy of human ovarian cancer tumour xenografts and had an additive effect with cisplatin in non-small cell lung cancer xenografts (Ihle et al., 2004). PX-866 also demonstrated anti-tumour efficacy in patient-derived head and neck squamous cell carcinoma (HNSCC) xenografts, with additive effects found with docetaxel (Jimeno et al., 2015). On the basis of this evidence it proceeded onto Phase I clinical trials where it was observed to be well tolerated in patients with advanced solid tumours and displayed a favourable toxicity profile and potent anti-tumour activity (D. S. Hong et al., 2012). It then proceeded onto Phase II clinical trials where PX-866 failed to improve clinical outcomes in combination with docetaxel compared to docetaxel alone in patients with relapsed/metastatic HNSCC, although it was found to have manageable toxicity. Due to the failure to improve clinical outcomes it did not proceed to Phase III clinical trials.

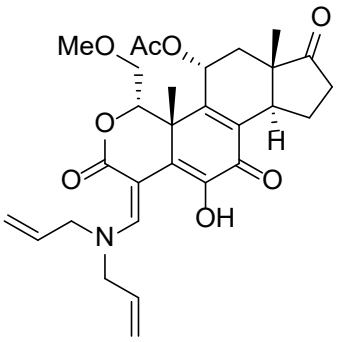

Figure 1.12. *Chemical structure of PX-866 (Sonolisib)*

1.6.3 *PWT-458*

PWT-458 (pegylated 17-hydroxywortmannin, Figure 1.13) was developed in 2005 by Pfizer and is a polyethylene glycol (PEG)-ylated derivative (Zhu, Hou, & Mao, 2015). PWT-458 is a prodrug that upon cleavage of the polyethylglycol polymer, releases the active 17-hydroxy-wortmannin (17-HWT), which has been found to be a potent inhibitor of PI3K in several

animal models (Zhu et al., 2015). PWT-458 has shown single agent activity against PTEN-negative U87MG glioma, NSCLC A549 tumour and VHL-negative A498 RCC xenograft models (Yu et al., 2005). PWT-458 was also seen to have an additive effect in combination with paclitaxel in glioma and non-Small Cell Lung Cancer (NSCLC), with observed complete arrest of tumour growth in the NSCLC model (Yu et al., 2005). A synergising effect was also seen with PWT-458 in combination with Interferon-A in RCCA498 tumours which resulted in reduced tumour vasculature causing significant tumour regression (Yu et al., 2005). Although this compound shows promising anti-tumour activity as a consequence of its activity against PI3K family members, it has not entered into human clinical trials yet (Cleary & Shapiro, 2010).

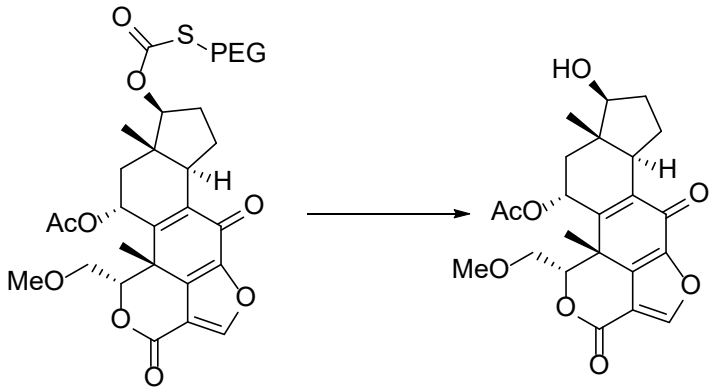

Figure 1.13. *Prodrug PWT-458 undergoes, cleavage of the PEG chain to release 17-hydroxy-wortmanin.*

1.6.4 *LY2094002*

LY2094002 (Figure 1.14) is another early PI3K inhibitor that was developed (Vlahos, Matter, Hui, & Brown, 1994), (Cleary & Shapiro, 2010). It was identified in 1994 by Eli Lilly through screening compounds derived from the polyphenol quercetin (Vlahos et al., 1994), (C. Cano et al., 2018), a bioflavenoid that was previously shown to have inhibitory activity against PI3K (Matter, Brown, & Vlahos, 1992), (Andrs et al., 2015). LY2094002 is a chromen-4-one structure that has lower potency than Wortmannin, with an IC_{50} of 1.4 µM for DNA-PK (Davidson et al., 2013). LY2094002 was further shown to have equipotent inhibitory activity against PI3K, DNA-PK and mTOR *in vitro* (Andrs et al., 2015; Roger J. Griffin et al., 2005). Therefore, like wortmannin, LY2094002 is a non-specific inhibitor of PI3K and PIKK family members. However, unlike wortmannin, it is a competitive inhibitor that binds reversibly at the Val-882 residue in the ATP binding site of the kinase domain through hydrogen bonding with the oxygen in the morpholine ring structure (Walker et al., 2000), (C. Cano et al., 2018). This morpholine ring moiety has been proven by X-ray crystallography (Figure 1.15) to have a crucial role in inhibitory activity (Walker et al., 2000), (Andrs et al., 2015), (Harnor, Brennan, & Cano, 2017).

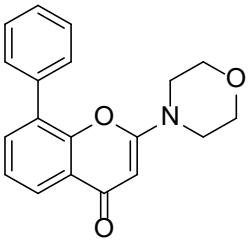

Figure 1.14. *Chemical Structure of LY2094002*

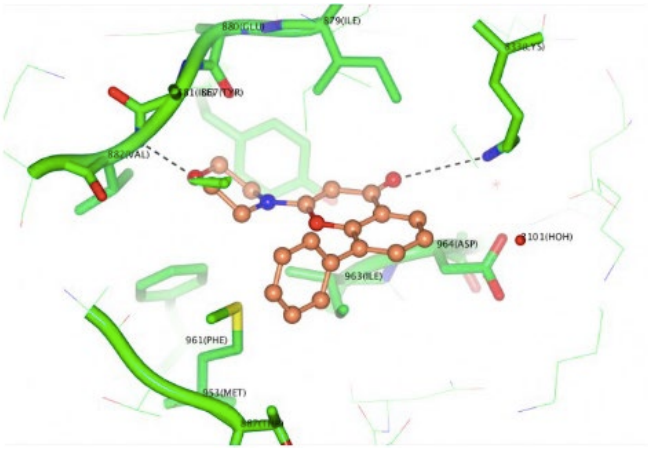

Figure 1.15. *X-ray crystallography structure of LY2094002 in complex with PI3K at the ATP-binding domain. (Harnor et al., 2017).*

Studies conducted *in vitro* and *in vivo* have demonstrated that LY2094002 induces cell growth inhibition in combination with cisplatin in human pancreatic xenograft models, has antiangiogenic activity through the inhibition of K channels (Eisenreich & Rauch, 2011), (Kamili, Kandoti, Radhakrishnan, Konde, & Vattikutti, 2020), induces G1 phase cell cycle arrest in melanoma cells (Casagrande et al., 1998) and increased radiosensitivity in the T24 human bladder cancer cell xenografts in mice (Gupta et al., 2003).

As well as its lack of specificity, LY2094002 had several issues, such as rapid metabolic clearance, low bioavailability, poor solubility and *in vivo* toxicity, that limited its clinical potential (Collis et al., 2005). Nonetheless, LY2094002 has proved to be a useful lead compound, with modifications of the structure to create compounds with more favourable properties (Pospisilova et al., 2017), (Andrs et al., 2015).

1.6.5 *NU7026*

Researchers at the University of Newcastle upon Tyne and KuDOS Pharmaceuticals developed benzopyranone and pyrimidoisoquinolinone derivatives of LY2094002 (Roger J Griffin et al., 2005), (C. Cano et al., 2018). They identified a chromen-4-one derivative with a fused ring, NU7026 (Figure 1.16) (Veuger, Curtin, Richardson, Smith, & Durkacz, 2003). This compound had 5-fold increased potency against DNA-PK, compared to LY2094002, with an IC_{50} of 0.23 μM (Harnor et al., 2017), and was also 70-fold more selective for DNA-PK than PI3K (p110α) (Hollick et al., 2003). It was inactive against ATM and ATR (Veuger et al., 2003). NU7026 was shown to potentiate the growth inhibitory effect of six different topoisomerase II poisons (which are known to induced DSBs) by 2-19 fold in K562 and ML-1 human leukemia cells through inhibition of DSB repair and induction of G2/M arrest (Willmore et al., 2004). Sensitisation to the topoisomerase poison mitoxantrone was also observed in HL-60 and HL-60MX leukemia cells (Mikusová, Tichý, Rezáčová, & Vávrová, 2011). NU7026 was also shown to achieve 2-fold greater radiosensitisation in mouse embryonic fibroblast cells (Veuger et al., 2003).

Despite these promising *in vitro* results, NU7026 did not proceed onto clinical trials as *in vivo* experiments in mice demonstrated that NU7026 underwent rapid clearance due to extensive metabolism especially hydroxylation of the morpholine ring (Nutley et al., 2005).

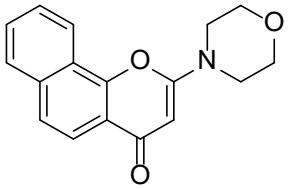

Figure 1.16. *Chemical Structure of NU7026*

1.6.6 *NU7441*

Further work by the University of Newcastle upon Tyne and KuDOS Pharmaceuticals group screened 8-aryl substituted chromen-4-ones revealing inhibitors with comparable activity to NU7026 (Leahy et al., 2004). Addition of a dibenzothiophenyl group on the chromen-4-one (2-*N*-morpholino-8-dibenzothiophenyl-chromen-4-one, NU7441) (Figure 1.17) increased potency by 100-fold compared to LY294002, with an IC_{50} of 14 nM (Leahy et al., 2004), (Zhao et al., 2006). Modest concentrations of NU7441 (1 μM) increased sensitivity to radiation (2-4-fold) and the topoisomerase II inhibitors etoposide (2-12-fold) and doxorubicin (2-10-fold) in LoVo and SW620 human colon cancer cell lines (Zhao et al., 2006). This sensitisation was mediated by DNA-PK inhibition because DNA-PKcs-deficient V3 cells, although more sensitive to ionising radiation and etoposide alone, were not sensitised by NU7441. In contrast, NU7441 did sensitise DNA-PKcs-complemented V3-YAC cells. The ATM inhibitor KU55933 further potentiated cytotoxicity in the DNA-PKcs deficient V3 cells, demonstrating that the lack of enhancement by NU7441 was not due to saturating cytotoxicity (Zhao et al., 2006). Radiosensitisation by NU7441 was seen in MCF7 breast carcinoma cells (Cowell, Durkacz, & Tilby, 2005). NU7441 was shown to increase G_2-M arrest in combination with etoposide (92%), doxorubicin (21%) and ionising radiation (61%) in SW620 cells, with slightly less pronounced effects observed in LoVo cells compared to treatment alone (Zhao et al., 2006). NU7441 was seen to also prolong γH2AX foci after ionising radiation or etoposide induced DNA damage, which are known to resolve as repair proceeds, showing NU7441's radiosensitisation and chemosensitisation ability (Zhao et al., 2006).

NU7441 enhanced etoposide phosphate efficiency by 100% in SW620 colorectal carcinoma xenografts in mice and the combination did not cause additional toxicity (Zhao et al., 2006). The ability of NU7441 to inhibit DNA-PK was also demonstrated in hepatocellular carcinoma cells (HCC) and the combination of NU7441 with doxorubicin supressed tumour growth in HCC tumour xenografts in mice (Cornell et al., 2015).

NU7441 had limited aqueous solubility and oral bioavailability, which prevented using higher dosages *in vivo*, although the promising effects of NU7441 encouraged further development of this class for the purpose of clinical utilisation (Zhao et al., 2006).

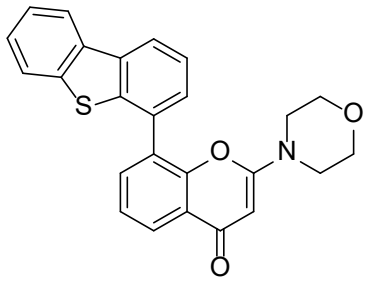

Figure 1.17. *Chemical Structure of NU7441.*

1.6.7 *KU-0060648*

To overcome the limitations of NU7441, the University of Newcastle upon Tyne and KuDOS group utilised a homology model of the ATP-binding domain of DNA-PK derived from the PI3Kγ crystal structure (C. l. Cano et al., 2013). This model showed that when NU7441 is bound to the ATP binding site, the dibenzothiophene 1-position of NU7441 is directed into the solvent, away from the binding pocket and therefore was predicted to be able to accommodate polar side chains that would increase the solubility of the compound (C. l. Cano et al., 2013). Exploration of a library of analogues led to the identification of KU0060648 (Figure 1.18).

KU0060648 was a potent inhibitor of DNA-PK, with an IC_{50} of 5 nM, and was a potent radiosensitiser *in vitro* (C. l. Cano et al., 2013). Unexpectedly, KU0060648 was also found to be a potent inhibitor of the PI3K family members, with an IC_{50} of 4 nM against PI3K p110α. Screening of the other library members revealed that they were also dual inhibitors of DNA-PK and PI3K enzymes. *In silico* docking studies indicated that there is a common binding pocket for both kinases, where the dibenzothiophene 1-substituent is located (Andrs et al., 2015).

The effect of KU0060648 on the chemosensitivity of the topoisomerase II poisons; doxorubicin and etoposide was investigated in isogenically paired DNA-PK proficient and deficient cell lines (V3-YAC and V3, respectively) and (M059-Fus-1 and M059J cells, respectively). All lines had similar PI3K activity (Munck et al., 2012). KU0060648 potentiated the cytotoxicity of both doxorubicin and etoposide in the DNA-PK proficient cells more than in the deficient cells, which were intrinsically more sensitive to drug alone, thus showing that chemosensitisation by KU0060648 was mostly due to DNA-PK inhibition (Munck et al., 2012).

KU0060648 was well tolerated in mice and was found to have good oral bioavailability (Munck et al., 2012). It provided significant single agent activity in SW620 colorectal cancer tumour xenografts in mice, but not in MCF7 breast cancer tumour xenografts suggesting a potential role for PI3-K inhibition in its activity (Munck et al., 2012). When KU0060648 was combined with etoposide phosphate, significant additional tumour growth delay in both MCF7 and SW620 models was observed (Munck et al., 2012).

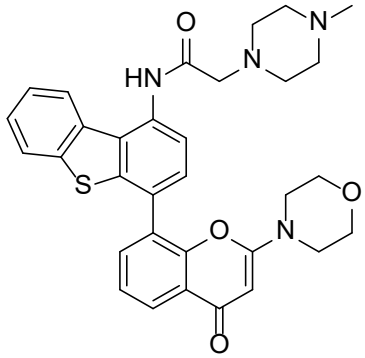

Figure 1.18. *Chemical Structure of KU0060648.*

1.6.8 *ICOS series*

Another series of DNA-PK inhibitors was reported by the ICOS Corporation (now Eli Lilly and Company) and Array BioPharma which are derived from the LY294002 compound (Kashishian et al., 2003). These compounds also contained the morpholine ring moiety on a hydroxybenzalaldehyde motif (Andrs et al., 2015). The first representative of this new series; 2-hydroxy-4-morpholin-4-yl-benzaldehyde, which was called IC60211 (Figure 1.19) and had

moderate potency with an IC_{50} of 400 nM against DNA-PK (Kashishian et al., 2003). Optimisation of IC60211 led to the generation of compounds that are more potent and they all contained the arylmorpholine substructure. Although these derivatives were potent DNA-PK inhibitors (e.g., IC86621 IC_{50} 120 nM, IC87361 34 nM) they were also found to be active against members of the PI3K family as well. A more advanced morpholino-flavonoid compound IC87361 had improved (50-fold) selectivity for DNA-PK compared to p110β.

IC86621 was found to significantly enhance the cytotoxicity of DSB inducing agents; etoposide and bleomycin *in vitro*, and was also shown to block religation of radiation induced DNA DSBs (Kashishian et al., 2003). IC86621 had limited bioavailability due to poor solubility and rapid clearance; nonetheless, IC86621 demonstrated a 4-fold increase in radiosensitisation of HCT116 human colon carcinoma tumour xenografts in nude mice (Kashishian et al., 2003).

IC87361 was demonstrated to significantly radiosensitise B16F0 melanoma and Lewis Lung Carcinoma tumour xenografts in a variety of different mouse backgrounds mice with no toxicity observed during the 4 week study period (Shinohara et al., 2005).

IC486241 was developed later, with the compound consisting of the morpholine ring attached to an acridone core (Davidson, Grenier, et al., 2012). This was found to be a potent chemosensitiser of 3 breast cancer cell lines (MCF7, BT-20 and MDA-MB-436) in combination with topoisomerase II inhibitor doxorubicin (Davidson, Coulombe, et al., 2012). IC486241 decreased doxorubicin-induced γH2AX foci, and this was suggested to be due to IC486241 binding reversibly to the ATP-binding pocket of DNA-PKcs therefore blocking autophosphorylation of Ser2056 and phosphorylation of H2AX. Again, the pharmacokinetic properties of IC486241 were not optimal because of low aqueous solubility and a low plasma half-life, which limited its clinical potential.

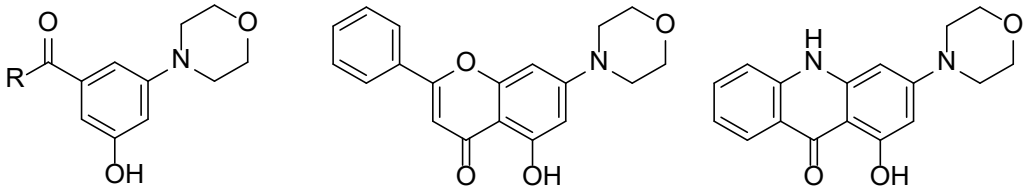

IC60211 R = H
IC86621 R = Me

IC87361

IC486241

Figure 1.19. *Chemical Structures of ICOS compounds.*

1.6.9 *SU11752*

With the interest in developing selective DNA-PK inhibitors, without PI3K inhibition, Sugen Incorporated conducted a library screen of three-substituted indolin-2-ones (Ismail et al., 2004). This class of compounds have been used as lead compounds in the development of selective protein kinase inhibitors (L. Sun et al., 1999), that have proceeded onto clinical trials (Ismail et al., 2004). SU11752 (Figure 1.20), an ATP competitive DNA-PK inhibitor, with an IC_{50} of 0.13 μM (Ismail et al., 2004) was identified as the best candidate. SU11752 was a poor inhibitor of PI3K with an IC_{50} of 1.10 μM against p110γ and was found to inhibit DSB repair in human glioblastoma cells treated with DSB-inducing drug calicheamicin γ1 at 12 μM. Inhibition of ATM was not found at the same concentration. A five-fold increase in radiosensitisation was observed compared to radiation alone in the human glioblastoma cells (Ismail et al., 2004).

Despite these promising *in vitro* results, the low potency of SU11752 made it unsuitable for clinical development. It was noted that SU11752 would make a good starting point for the

development of specific inhibitors against DNA-PK, as all previous DNA-PK inhibitors were originally identified as PI3K inhibitors resulting in additional inhibition activity against PI3K and leading to toxicity issues (Ismail et al., 2004).

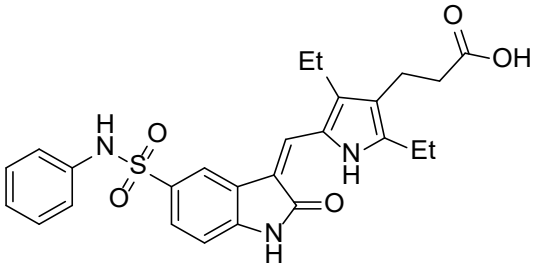

Figure 1.20. *Chemical Structure of SU11572.*

1.6.10 *CC-115*

Celgene Corporation identified a dual inhibitor of mTOR and DNA-PK with an IC_{50} of 21 nM against mTOR and 13 nM against DNA-PK (Mortensen et al., 2015). PK/PD studies looking at mTOR inhibition in tumour bearing mice resulted in CC-115 (Figure 1.21) being chosen as the representative for clinical development, due to its good potency and demonstrated safety *in vitro* and *in vivo* (Mortensen et al., 2015). CC-115 was found to have radiosensitising potential in 7 different melanoma cell lines (Bürkel et al., 2020).

A Phase I trial (NCT01353625) of CC-115 was conducted in patients with advanced solid tumours or hematologic malignancies (Munster et al., 2019). Part A of the trial found that the optimal dose was 10 mg, twice a day. In Part B CC-115 was found to have good tolerability, with few grade 3 adverse events and no grade 4 toxicities reported in any of the 74 patients given the optimal dose in 28-day cycles (Munster et al., 2019). Efficacy was promising with at least 50% biomarker inhibition occurring with CC-115 in concentrated plasma in a 24 hour period (Munster et al., 2019). It was also found to be able to cross the blood-brain barrier prompting further investigation in Phase II trials. A Phase II trial (NCT02977780) evaluated CC-115 in patients with newly diagnosed glioblastoma in the Individualised Screening Trial of Innovative Glioblastoma Therapy (INSIGhT) trial, which allowed for more efficient testing by decreasing the number of patients required (Rahman et al., 2020), (Rahman et al., 2021). There was no difference in progression free survival or overall survival in the 12 patients randomised to the treatment group (10 mg CC-115, twice daily, in combination with radiation) compared to the 50 patients in the control group (Rahman et al., 2020). In the 12 patients in the treatment group, seven had possible treatment-related toxicities greater than grade 3. Therefore CC-115 was discontinued due to toxicity concerns and an unfavourable risk-to-benefit ratio (Rahman et al., 2020).

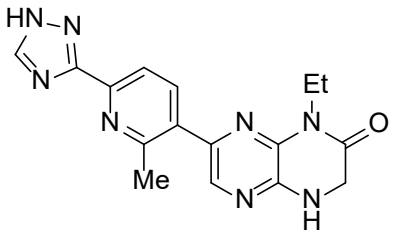

Figure 1.21. *Chemical Structure of CC-115.*

1.6.11 *VX-984*

Vertex Pharmaceuticals developed the deuterated ATP-competitive DNA-PK inhibitor called VX-984 (also known as M9831) (Figure 1.22) for clinical development. VX-984 has potent

cytotoxic activity in combination with doxorubicin and etoposide in established cancer cell lines. It was also active with doxorubicin in endometrial primary tumour explants and with etoposide in small cell lung cancer primary tumour explants (D Boucher et al., 2016). VX-984 enhanced the cytotoxicity of ionising radiation in a NSCLC cell line by 3-fold (Diane Boucher et al., 2016). VX-984 was reported to have an IC_{50} of 88 $\pm$ 64 nM against DNA-PK autophosphorylation of Ser2056 in A549 lung cancer cells, and was found to be 80-fold more selective for DNA-PK than for PI3Kα (C. Cano et al., 2018).

VX-984 was found to inhibit radiation-induced DNA-PKcs phosphorylation in orthotopic brain tumour xenografts in mice, and survival was increased with the combination therapy by 32 days compared to treatment with vehicle (Timme, Rath, O'Neill, Camphausen, & Tofilon, 2018). This also showed that VX-984 was capable of crossing the blood brain barrier, and because no toxicities relating to VX-984 were detected in these experiments, it was thought that VX-984 could have the potential to improve glioblastoma treatment response (Timme et al., 2018).

VX-984 was evaluated in a Phase I clinical trial (NCT02644278) in combination with pegylated liposomal doxorubicin in patients with advanced solid tumours. However, the study was discontinued during the dose escalation phase for business reasons decided by the sponsor.

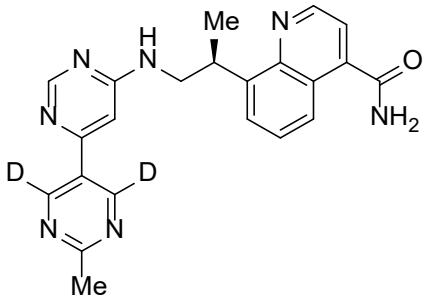

Figure 1.22. *Chemical Structure of VX-984.*

1.6.12 *M3814*

Merck have developed a potent and selective, orally administered DNA-PK inhibitor called M3814 (also called nedisertib or peposertib) (Figure 1.23). M3814 has good radiosensitising ability *in vitro* and *in vivo* through inhibition of DNA-PK (Zenke et al., 2016), (Fuchss et al., 2017). Oral administration of M3814, in combination with a fractionated radiation schedule (5 x 2 Gy daily doses for 6 weeks), resulted in the complete regressions in tumour xenograft models (colon, head and neck, lung and pancreas), with only minor toxicity symptoms that were fully reversible (Zenke et al., 2020).

The first clinical study of M3814 involved patients with advanced solid tumours (NCT02316197) and explored the safety, tolerability and the pharmacokinetics and pharmacodynamics in dose escalation studies (Van Bussel et al., 2021). It was found that there were no Dose Limiting Toxicities (DLTs) at the 400 mg twice a day dose, and this was taken as the Recommended Phase II dose (RP2D). Grade 3 M3814-related serious adverse events commonly included maculopapular rash and nausea at the highest dose level (Van Bussel et al., 2021). The occurrence of maculopapular rash was considered notable as this symptom is associated with inhibition of PI3K (Van Bussel et al., 2021). However, M3814 displayed >100-fold selectivity for DNA-PK (IC_{50} 0.6 nM) over PI3-K isoforms *in vitro* (Zenke et al., 2020), undermining this assertion. But as these Grade 3 toxicities only occurred in 23% of patients,

with no reported Grade 4 toxicities, M3814 was therefore concluded to be well tolerated as a single agent (Van Bussel et al., 2021).

The next clinical trials involve M3814 in a combination therapy setting with chemotherapy, radiotherapy and immunotherapy. A phase Ia/1b trial is currently in progress with M3814 in combination with radiotherapy and in combination with cisplatin and radiation therapy in patients with locally advanced solid tumours (NCT02516813). So far it has been found that M3814 at the 100 mg and 200 mg doses are tolerable and 2 DLTs (grade 3 mucositis and odynophagia) were found at the 400 mg dose (Van Triest et al., 2018). Currently, a once a day 300 mg dose is being investigated since the last update (Van Triest et al., 2018). A phase 1b/2 trial is also currently in progress with M3814 in combination with radiotherapy and the antimetabolite capecitabine in patients with locally advanced rectal cancer (NCT03770689). A phase I dose escalation trial involving M3814 in combination with the anti-PD-L1 agent Avelumab, with and without radiotherapy, in patients with advanced solid tumours is also underway (NCT03724890). M3814 is a leading DNA-PK inhibitor candidate for clinical use.

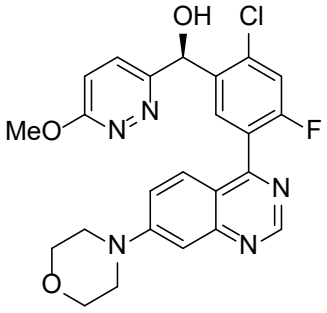

Figure 1.23. *Chemical Structure of M3814.*

1.6.13 *AZD7648*

AstraZeneca have developed a potent and selective DNA-PK inhibitor called AZD7648 (Figure 1.24), through screening their kinase inhibitor collection and optimising pharmacokinetics and potency against DNA-PK (Fok et al., 2019). AZD7648 was found to inhibit DNA-PK with an IC_{50} of 0.6 nM. AZD7648 was shown to have greater than 90-fold selectivity over ATM, ATR and mTOR and three different PI3K isoforms (Fok et al., 2019). AZD7648, in combination with ionising radiation, was shown to decrease *in vitro* clonogenic survival of A549 and NCI-H1299 NSCLC cells in a dose-dependent manner. Oral administration of 100 mg/kg AZD7648 (once daily for 5 days), in combination with daily (5 x 2 Gy) radiation, resulted in 90% tumour regression in the mice A549 tumour xenografts compared to 50% with ionising radiation alone (Fok et al., 2019).

Treatment with AZD7648, in combination with the topoisomerase II inhibitor doxorubicin, in the ovarian cancer cell line OAW42 led to dose dependent reduction in cell viability in 5 days treatment. *In vivo* studies with 37.5 mg/kg AZD748 twice a day for 28 days in combination with 2.5 mg kg^{-1} doxorubicin every week for 4 weeks showed dose dependent tumour growth inhibition by 77% in BT474 breast cancer cell xenografts (Fok et al., 2019).

The combination of AZD7648 with the PARP inhibitor olaparib was synergistic and inhibited cell growth in the ATM-deficient hypopharyngeal carcinoma cell line FaDu and in the A549 NSCLC cell line. Combination of AZD7648 (75 mg/kg twice daily) with olaparib (100 mg/kg one daily) for 70 days AZD7648 induced complete tumour regression of FaDu ATM KO xenografts in all 11 mice (Fok et al., 2019).

AZD7648 has advanced onto Phase I/IIa clinical trials (NCT03907969) where it will be studied alone as monotherapy, or in combination with doxorubicin or olaparib, in dose escalation studies to evaluate safety and tolerability in patients with advanced solid tumours and to establish a Recommended Phase 2 Dose (RP2D) (Yap et al., 2020).

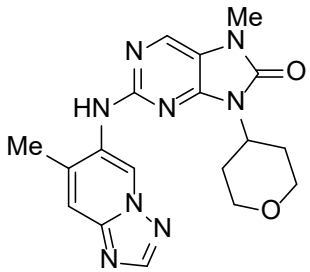

Figure 1.24. *Chemical Structure of AZD-7648.*

1.6.14 *BR101801*

A new agent, BR101801, was recently described by Boryung Pharmaceuticals. BR101801 (structure not disclosed) is an inhibitor of PI3K and DNA-PK and was found to radiosensitise MDA-MB-231 breast cancer cells, inhibiting autophosphorylation of Ser2056 on DNA-PK and stabilising γH2AX foci. BR10181 was found to radiosensitise MDA-MB-231 breast cancer tumour xenografts when given at 50 mg/kg orally for the entire experiment (70 days) in combination with radiation (5 x 2 Gy for 5 days) (J. H. Lee et al., 2021). Interestingly, BR101801 seems to also be able to increase CD8+ T-cells and decrease immune suppressive Tregs cells, potentially stimulating anti-cancer immunity (Wang et al., 2021).

A Phase I/II clinical trial (NCT04018248) is currently underway conducting dose escalation studies to evaluate the safety and tolerability and to find the RP2D in patients with advanced hematologic malignancies.

1.6.15 *BAY-8400*

Bayer Pharmaceuticals recently disclosed a DNA-PK inhibitor, BAY-8400 (Figure 1.25), that was found through screening of the Bayer library for ATR inhibitors. A triazoloquinoxaline compound that had 10-fold selectivity for DNA-PK over ATR was used as the lead for optimisation through SAR producing BAY-8400 (Berger et al., 2021). BAY-8400 was found to have an IC_{50} of 81 nM for DNA-PK and was modestly selective against PI3K (117 nM) and ATR (394 nM) (Berger et al., 2021). BAY-8400, in combination with the thorium-227 labelled alpha radiation emitter immune conjugate targeting prostrate specific membrane antigen (PSMA) PSMA-TTC BAY2315497, sensitised LNCaP prostrate cancer cells *in vitro.* BAY-8400 also demonstrated good aqueous solubility and oral bioavailability. BAY-8400 had little effect when given as a single agent, but sensitised the LNCaP tumour xenografts to the targeted alpha radiation, resulting in tumour growth inhibition (Berger et al., 2021).

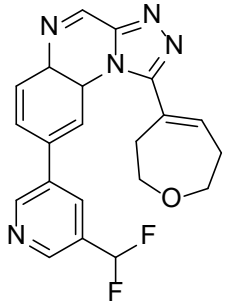

Figure 1.25. *Chemical Structure of BAY-8400.*

1.7 Issues with Inhibiting DNA-PKi

Inhibiting DNA-PK as a therapeutic strategy raises the potential of on-mechanism normal tissue toxicity. This normal tissue toxicity could arise from a number of interactions. Firstly, inhibition of DNA-PK function will sensitise any tissues to radiation-induced DSBs. Hence, normal tissue within the radiation field will be sensitised by systemic delivery of a DNA-PK inhibitor (J. M. Brown, 2019). Evidence for this has been described for several compounds; M3814, where although reversible, Grade 1 radiation-induced dermatitis was observed in three of the ten xenograft animals receiving the highest dose (50 mg/kg) (Zenke et al., 2020), and with AZD7648 (C. R. Hong et al., 2022) a significant level of radiosensitisation of the stem cells in the oral mucosa and small intestine was observed. Further, DNA-PK inhibition can also cause normal tissue toxicity both within the radiation field and in other tissues through some of the other roles of DNA-PK outside of DSB repair (Yue, Bai, Xie, Ma, & Zhou, 2020).

DNA-PK plays an important role in V(D)J recombination which is essential for antigen receptor diversity and the development of adaptive immunity. The identification of the radiosensitivity of the Severe Combined Immune Deficiency (SCID) mouse and attribution to a loss of DNA-PK function (Fulop & Phillips, 1990), (Biedermann et al., 1991) was the original catalyst for the development of DNA-PK inhibitors.

DNA-PK is also known to be involved in telomere maintenance. Telomeres are repetitive non-coding DNA sequences found at the end of chromosomes to protect the ends from degradation (Ting, Pohorelic, Yu, Lees-Miller, & Beattie, 2009). DNA-PKcs is known to associate with the shelterin complex. This complex is comprised of six subunits, one of which is the Protection of Telomeres Protein 1 (POT1) that out-competes RPA to prevent repair of the telomere overhang (Sui, Zhang, & Chen, 2020). The DNA-PKcs-Shelterin complex is therefore important for protection of telomere overhangs against degradation and fusion (Le, Maranon, Altina, Battaglia, & Bailey, 2013). In cells deficient in DNA-PKcs, uncapped telomeres are processed as DSBs and this impairs telomere function (Yue et al., 2020). DNA-PKcs is also known to phosphorylate the heterogenous nuclear riboprotein A1 (hnRNP A1) which removes Telomeric Repeat-containing RNA (TERRA) from chromatin allowing replication of telomeres in the S-phase and also allowing promotion of POT1 against RPA (Sui et al., 2020). Impairment of telomere function is associated with accelerated aging which may increase risk of cancer due to chromosomal instability and induction of cellular senescence (Von Figura, Hartmann, Song, & Rudolph, 2009).

DNA-PK also has important roles in cell cycle progression and is known to regulate the MDM2 interactions with p53, which when complexed together causes cell cycle arrest in G1 (Shangary & Wang, 2008). One-ended DSBs formed in S-phase are bound by RPA, and DNA-PK phosphorylates the RPA32 subunit at Ser4 and Ser8 causing Chk1 activation and arrest to delay mitotic entry due to damage (S. Liu et al., 2012).

Phosphorylation of DNA-PK at specific sites causes DNA-PKcs localisation to centrosomes during mitosis, where its activity is essential for successful division. For example, it has been observed that phosphorylation of DNA-Pkcs at Ser3205 by Polo Like Kinase 1 (PLK1) allows localisation of DNA-PKcs to the midbody in cytokinesis and Protein Phosphatase 6 (PP6) dephosphorylates the Ser3205 site when cells exit mitosis (B. Huang et al., 2014). This implies that phosphorylation of Ser3205 is required for mitotic entry and exit.

DNA-PK is a regulator of transcription. DNA-PKcs phosphorylates the TRIM28 factor at Ser824 which is required for RNA polymerase II activity (Bunch et al., 2015). DNA-PK phosphorylates

many transcription factors such as the TATA-binding protein (TBP), Transcription Factor IIB (TFIIB), Specificity Protein 1 (Sp1) and Octamer-binding transcription factors 1 and 2 (OCT1 and OCT2) (Mohiuddin & Kang, 2019). Studies on Chinese hamster ovarian cells deficient in Ku70/80, or DNA-PKcs, resulted in transcription decreasing by 2-7 fold (Woodard, Anderson, & Dynan, 1999).

Therefore, inhibition of DNA-PK in the context of cancer treatment raises clear potential for a range of ancillary effects mediated through the many roles of DNA-PK. Several strategies to minimise these off target effects can be considered. Many studies have demonstrated that transient and selective pharmacological delivery of DNA-PK inhibitors as single agents seems to be well tolerated in mice (Fok et al., 2019), (Zenke et al., 2020), (Fuchss et al., 2017) and evidence is developing for humans (Van Bussel et al., 2021). Another approach would be to target cancer cells specifically through tumour-selective drug delivery to avoid inhibition of DNA-PK in normal tissues.

1.8 Tumour Hypoxia

Hypoxia (low oxygen) is a common pathophysiological characteristic of solid tumours (Emami Nejad, 2021). Normal tissues have around 3-9% oxygen, while tissue is considered hypoxic at a level of below 2% (Thomas, 2016).

Solid tumours often have poor blood supply due to the increased cell proliferation which outstrips proper vasculogenesis. This results in the development of abnormal tumour vasculature, limiting oxygenation within a tumour (Linda Spiegelberg a, 2019).

Tumour hypoxia plays a major role in tumour progression and the response to clinical treatment (Dhani, Fyles, Hedley, & Milosevic, 2015). Tumour cells can display a 'hypoxia driver phenotype' (Dhani et al., 2015), where the tumour cells acquire pro-survival characteristics in response to hypoxic stress (Wilson & Hay, 2011), including mediating immune suppression (Muz, De La Puente, Azab, & Azab, 2015), while also contributing to the development of the tumour microenvironment (Singleton, Macann, & Wilson, 2021). The aggressive phenotype and the toxic tumour microenvironment is caused in large part due to hypoxia (Rohwer & Cramer, 2011), and therefore hypoxic cells contribute to the resistance to cancer therapy (Wilson & Hay, 2011), and hypoxia is considered to be a negative prognostic and predictive factor for patient outcomes (Vaupel & Mayer, 2007).

An international multi-centre study analysed the relationship between tumour hypoxia and the outcomes of patients diagnosed with advanced head and neck cancer being treated with radiation therapy alone or with chemoradiotherapy (Nordsmark et al., 2005). They found that the 5-year survival for patients with high hypoxic levels approached 0%. Another study conducted a prospective study on patients with cervix cancer treated with radiation therapy alone, to validate the prognostic impact of hypoxia, independent from other clinical and pathologic features such as tumour stage and size (Fyles et al., 2002). They found that tumour hypoxia was an indicator of poor progression-free survival and was related to an increased risk of distant metastases, which they thought could be due to the upregulation of the hypoxic response, resulting in the development of an aggressive phenotype (Fyles et al., 2002). Interestingly, they also found that tumour hypoxia was not associated with relapse within the irradiated pelvis, but with relapse in the distant metastases. They thought this was due to the reoxygenation during treatment overcoming the effects of hypoxia.

Radiotherapy in patients is particularly impaired by hypoxia. A study investigated the impact of tumour hypoxia using endogenous markers for factors involved in hypoxic pathway, in

patients involved in a previous randomised control trial; Continuous Hyperfractionated Accelerated Radiotherapy (CHART) in the United Kingdom that failed to show a benefit of accelerated radiotherapy over standard radiotherapy in HNSCC patients (Koukourakis et al., 2006). They found that the expression of the endogenous markers for the hypoxic pathways were strongly correlated with radiotherapy failure, and that these biomarkers can be used to identify subgroups within the HNSCC patient cohort that will either respond well to radiotherapy or respond well to hypoxia targeting drugs, depending on their hypoxic status. A study by (Evans et al., 2007) also found that hypoxia was associated with poor prognosis in HNSCC patients. They had utilised a 2-nitroimidazole hypoxia marker, EF5, which they believe could be developed into a non-invasive method of identifying hypoxia levels in patients by combining PET imaging with ^{18}F-EF5.

Hypoxic cells require 2-3-fold higher radiation doses than oxic cells for equivalent cell killing, because oxygen is required to convert radiation-induced DNA free radicals to DSB (see section 1.3.4). In the study conducted by (Koukourakis et al., 2006) they found that hypoxia was a major factor impairing the efficacy of accelerated radiotherapy, and that standard radiotherapy might be more beneficial in tumours that are able to undergo reoxygenation during the therapy – but that it is difficult to identify this subgroup of hypoxic tumours.

Similarly, the disorganised tumour vasculature also reduces the efficacy of many chemotherapeutic drugs because of disorganised blood flow and drug diffusion across relatively long inter-capillary distances limits drug exposure to cells in the tumour.

There are two main mechanisms that cause hypoxia in tumours. The first was discovered by Thomlinson and Gray in 1955 (Thomlinson & Gray, 1955) and is known as chronic hypoxia or diffusion limited hypoxia. The diffusion of oxygen is compromised by the increased diffusion distances and also by metabolic consumption in tumour cells. It was found that cells within the diffusion distance of oxygen (100 – 180 μm) remained viable and survived, whereas cells beyond this gradient were unable to survive and resulted in necrosis.

The second mechanism is acute or perfusion limited hypoxia, in which cells close to the blood vessels can also be hypoxic. This is a consequence of the poor quality of the tumour vasculature. These are often disorganised blood vessels that have large intercapillary distances and the architecture of the vessels is also usually poor (Varvara Petrova 2018). The vessels are often hyperpermeable due to a discontinuous endothelium and an absent basement membrane, and are also dilated due to a lack of smooth muscle cells. Structural abnormalities such as blind ends can also be present (Emami Nejad, 2021). These factors all affect the blood flow through the vasculature and result in unstable blood flow. Therefore oxygen concentrations of cells surrounding the blood vessel can vary transiently from normal to anoxia depending on the level of occlusion. These factors leads to both spatial and temporal heterogeneity of oxygen concentrations and this heterogeneity is problematic for measuring hypoxia in patient tumours as measurements taken then might not be representative of the tumour during the treatment.

The factors that limit the delivery of oxygen also limit transport of nutrients needed for tumour growth, increase interstitial fluid pressure and also causes acidosis (Singleton et al., 2021), (Rohwer & Cramer, 2011). A hallmark of cancer; metabolic reprogramming is induced by hypoxia where anaerobic glycolysis is favoured over aerobic glycolysis and therefore production of lactate from pyruvate is increased leading to lower pH levels (Emami Nejad, 2021). Low oxygen, pH and nutrients as well as high interstitial fluid pressure, together

contribute to tumour microenvironmental stress (Singleton et al., 2021), (Rohwer & Cramer, 2011).

Tumour microenvironmental stress promotes the selection of cells within the tumour that have better tolerance to these stresses. Hypoxia can induce apoptosis in normal and cancer cells, but hypoxia can also induce gene expression alterations that allow cancer cells to adapt and thrive in the hostile environment (Vaupel & Mayer, 2007). This leads to clonal selection of tumour cells that are more malignant and better adapted (Rohwer & Cramer, 2011). Mutations that confer an advantage under hypoxic conditions may be selected for and become the dominant cell population. For example, cells with knocked out p53 were selected for over cells with functional p53 under hypoxic conditions (Graeber et al., 1996).

1.9 Adaptation to Hypoxia

There are three main molecular pathways that mediate the adaptation of a cell to hypoxia; the HIF family deregulation, UPR and the mTOR pathways (Wilson & Hay, 2011).

Hypoxia Inducible Factors (HIF) are a group of transcription factors (HIF-1, HIF-2 and HIF-3) that are heterodimeric protein complexes consisting of the oxygen sensitive alpha subunits and the constitutively expressed beta subunits (Rohwer & Cramer, 2011). In the presence of oxygen the alpha subunit, HIF-1α or HIF-2α, are subjected to rapid degradation. Prolyl hydroxylases (PHDs) hydroxylate two proline amino acid sites at their Oxygen Dependent Degradation (ODD) Domain, using oxygen as a cofactor. Hydroxylated HIF-1α or HIF-2α are recognised by the Von Hippel Lindau (VHL) protein which recruits an E3 ubiquitin ligase, targeting HIF for ubiquitination and subsequent degradation (Weidemann & Johnson, 2008). Under hypoxic conditions the hydroxylation of HIF-1α or HIF-2α by VHL is impaired because oxygen is a required substrate for the PHD hydroxylation (Weidemann & Johnson, 2008). Thus, they are free to dimerise with the HIF-1β subunit to form the HIF-1 transcription factor which translocates to the nucleus and binds to the promoter region of the hypoxia response element (HRE). This binding causes upregulation of expression of genes such as vascular epidermal growth factor (VEGF) and inducible nitric oxide synthase (INOS) which promote angiogenesis and TGFβ and insulin growth factor-2 (IGF-2) which promote cell proliferation and metastasis (Weidemann & Johnson, 2008).

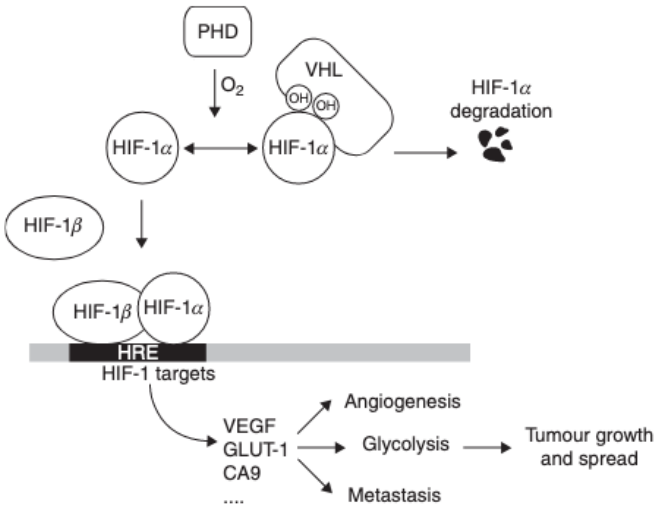

Figure 1.26. Hypoxia Inducible Factor-1 (*HIF-1) Regulation.* *The alpha subunit (*HIF-1α*) is subjected to rapid degradation under oxic conditions through oxygen dependent PHD hydroxylation, which marks it for*

degradation by VHL. Under hypoxic conditions the alpha subunit is free to dimerise with the beta subunit (HIF-1β) and translocate to the nucleus where it upregulates pro-survival genes such as those involved in proliferation or metastasis. (Joiner & van der Kogel, 2018).

The Unfolded Protein Response UPR is activated by the accumulation of misfolded proteins in the Endoplasmic Reticulum (ER) due to a dysregulation in ER homeostasis arising from hypoxic conditions (Hetz, 2012).

The three UPR stress sensors; Inositol Requiring Protein 1α (IRE1α), Protein Kinase RNA-like Endoplasmic Reticulum Kinase (PERK) and Activating Transcription Factor (ATF6) are activated rapidly and each activate a different transcription factor; XBP1, ATF4 and ATF6 respectively (Hetz, 2012). These activated transcription factors promote hypoxia tolerance mechanisms, such as autophagy, angiogenesis and metabolic reprogramming to resolve ER stress (Hetz, 2012). PERK also phosphorylates eIF2α blocking protein synthesis, which prevents further ER stress (Hetz, 2012). In the event of sustained stress IRE1α and PERK mediate a poorly understood process to induce apoptosis.

The mTOR pathway involves two mTOR complex kinases; MTOR Complex 1 (MTORC1) and MTOR Complex 2 (MTORC2) (Zou, Tao, Li, & Zhu, 2020). mTOR is a member of the PIKK family. MTORC1 is sensitive to many different signals from growth factors, oxygen levels, nutrients, energy and stress and regulated cell growth and metabolism. In contrast, MTORC2 is sensitive to growth factors, but not nutrients, and regulates cell proliferation and survival, and can also regulate the expression of MTORC1 (Zou et al., 2020).

MTORC1 and MTORC2 are involved in various signalling pathways (Zou et al., 2020). MTORC1 can be activated through phosphorylation and induction of the PI3K/Akt signalling pathway leading to activation of the Tuberous Sclerosis Complex 1 and 2 proteins (Tsc1/Tsc2) which act as a GTPase for Ras Homolog Enriched in Brain (RHEB) stimulating MTORC1 and thus promoting angiogenesis, autophagy, apoptosis and cell growth (Abdo Qaid et al., 2021). MTORC2 can regulate Akt activation and therefore MTORC1 activity (Zou et al., 2020). Overall, mTOR has been identified as a key player in tumorigenesis (Zou et al., 2020).

Activation of these hypoxia response pathways results in hypoxic cells that have malignant cell phenotypes with characteristics, such as reduced apoptotic potential and increased angiogenesis, which enable greater survival (Wilson & Hay, 2011). Radiotherapy can therefore select for the radioresistant hypoxic cancer cells by preferentially killing oxygenated tumour cells. The surviving hypoxic cells adapt to their environment and become more aggressive (J. M. Brown & Wilson, 2004). This leads to tumour progression, making hypoxia in tumours a negative prognostic and predictive factor in cancer patients.

1.10 Hypoxia Induced Treatment Resistance

Treatment of hypoxic tumour cells is difficult. As noted before, oxygen enhances radiotherapy through oxygen fixation of DNA radicals, and hypoxia leads to decreased damage fixation on the DNA. Hypoxic cells require higher doses of radiation to compensate the lower rate of damage fixation (Sørensen & Horsman, 2020). This is shown in the calculation of the Oxygen Enhancement Ratio as:

$$OER = \frac{Radiation\ Dose\ in\ Hypoxia}{Radiation\ Dose\ in\ Normoxia} \qquad \textit{Equation 14}$$

Although hypoxia not only impairs radiotherapy, it can increase indirectly drug resistance as well (J. M. Brown & Wilson, 2004). Factors that create the tumour microenvironment, such as poor vasculature of the tumour in combination with the low extracellular pH associated

with glycolysis, can impair drug delivery (Singleton et al., 2021). Hypoxia results in nutrient-deprived cells which have lower proliferation rates than oxygenated cells. Many classical anticancer chemotherapy drugs are anti-proliferative; that is, they are more cytotoxic towards proliferating cells. Therefore cytotoxic chemotherapy can spare non-proliferating hypoxic cells in a tumour. This is further accentuated by drug diffusion gradients with many chemotherapy drugs having limited extravascular drug diffusion, thus only killing cells close to blood vessels (J. M. Brown, 2002). This results in the previously hypoxic cells experiencing increased oxygen and nutrient supply from blood vessels and enabling regrowth. Selective repopulation of p53 knockout cells over wild type cells which undergo apoptosis due to the hypoxic conditions, leads to decreased sensitivity to a wide variety of anticancer treatments (Graeber et al., 1996).

Anticancer drugs that rely on active transport to get into cells, require ATP. Anaerobic glycolysis produces less ATP than oxidative phosphorylation. The increased lactate production under anaerobic glycolysis, which increases acidity, also impairs drugs that are weak bases from crossing the plasma membrane. However, hypoxia can also increase sensitivity to certain drugs, such as acidic drugs like the alkylating agent chlorambucil (Wilson & Hay, 2011).

1.11 Treatments for hypoxia

Hypoxia is a characteristic not common in normal tissues and therefore represents an opportunity for selective targeting, in order to improve the therapeutic ratio of radiation therapy (J. M. Brown & Wilson, 2004). Many different approaches have been taken in order to achieve this including trying to increase oxygen concentration in tumours, using high LET radiation due to their reduced OER, and using sensitisers to mimic oxygen (Jens Overgaard, 2007).

1.11.1 *Increasing Oxygen Delivery to Tumours*

Increasing oxygen delivery in tumours used methods such as Hyperbaric Oxygen (HBO) therapy where patients were placed in sealed chambers in pure oxygen with pressures around 3 atmospheres (Leach, Rees, & Wilmshurst, 1998). It was found that pure oxygen lead to vasoconstriction, therefore to combat this instead of using pure oxygen, a mixture called Carbogen which was 5% CO_2 and 95% O_2 was utilised (Coates, Skwarski, & Higgins, 2018). A vitamin B_3 analogue, nicotinamide, that was known to prevent transient blood flow fluctuations was used with carbogen to overcome perfusion-limited hypoxia, as well as diffusion-limited hypoxia (Jens Overgaard, 2007). The combination was used in the Accelerated Radiotherapy, Carbogen and Nicotinamide (ARCON) trials, but there was a lack of benefit seen in local tumour control in patients with advanced laryngeal cancers (Janssens et al., 2012). The HBO therapy was discontinued due to technical difficulties in the administration of radiation therapy inside a sealed chamber and patient compliance problems, as well as the fire risk associated with pure oxygen (Leach et al., 1998), (Joiner & van der Kogel, 2018).

Another approach was to use erythropoietin (EPO) to increase production of red blood cells and consequently oxygen delivery to tumour cells. However, the combination of EPO with radiation therapy lead to worse outcomes in patients with head and neck cancers. This was found to be due to EPO receptors also being expressed on squamous cell carcinoma cells causing proliferation of those tumour cells as well (Arcasoy et al., 2005).

Angiogenesis inhibitors have also been observed to increase tumour oxygenation – this is thought to be due to the normalisation of vasculature (Sørensen & Horsman, 2020).

1.11.2 *Oxygen-Mimetic Sensitisers*

There is a long history of the development of drugs that mimic the radiosensitising effect of oxygen in tumours (R. K. Jackson, Liew, & Hay, 2019). Oxygen readily reacts with radicals due to its electron affinic nature, and it was believed that small, lipophilic, electron affinic compounds would also be able to diffuse further than oxygen and react with DNA radicals to radiosensitise hypoxic cells in tumours (G.E. Adams & Cooke, 1969). The design criteria required the compounds to be selective for hypoxic cells, be chemically stable and have good aqueous solubility (G. E. Adams, 1978). Nitroimidazoles were found to fit these qualities and were able to radiosensitise hypoxic cells *in vitro* and in animal studies (Wardman, 2018).

The magnitude of the sensitising effect of radiosensitisers is given by the Sensitiser Enhancement Ratio (SER), which is analogous to the OER; the ratio of the radiation dose without sensitiser to radiation dose with sensitiser, to achieve the same biologic effect, and is calculated by (Joiner & van der Kogel, 2018):

$$SER = \frac{Radiation\ Dose\ without\ Sensitiser}{Radiation\ Dose\ with\ Sensitiser} \qquad Equation\ 15$$

SER_{10} values are often stated, as the SER for 10% survival.

2-Nitroimidazoles have higher electron affinity than 5-nitroimidazoles and were shown to be more efficient radiosensitisers in preclinical studies in solid murine tumours (J. M. Brown, 1975). The 2-nitroimidazole, misonidazole, was one of the first radiosensitisers to be clinically tested. It showed promising *in vitro* and animal study results, with a SER of 1.7-2.2 with a dose of 1 mg/g given 30 mins prior to irradiation (J. M. Brown, 1975). However, clinical results were disappointing with no significant improvements in patients observed, and the dose-limiting toxicity was found to be peripheral neuropathy which could progress to central nervous system toxicity with prolonged use (Dische, Saunders, Flockhart, Lee, & Anderson, 1979). This limited the dose that could be given and lowered the SER to ineffective levels. One study, the Danish Head and Neck Cancer (DAHANCA 2) trial, did demonstrate benefit in patients with pharyngeal tumours (J. Overgaard et al., 1989). Another 2-nitroimidazole, etanidazole, was estimated to have a SER of 1.5 at the higher doses, but significantly lower toxicity than misonidazole, due to its shorter half-life allowing a three-fold dose increase from misonidazole (Coleman et al., 1989). This was also tested clinically in combination with radiotherapy in advanced head and neck cancer patients, but no significant benefit was found (D.-J. Lee et al., 1995). Nimorazole, which is a 5-nitroimidazole and was estimated to have a lower SER of 1.4 (J Overgaard, Overgaard, & Timothy, 1983), was tested in clinical trial due to its lower toxicity. It was found that far larger doses of this compound could be administered and the DAHANCA 5 clinical trial found significant benefit in patients with supraglottic and pharyngeal carcinomas (Jens Overgaard et al., 1998).

Over the decades that oxygen-mimetic radiosensitisers were being developed, a change in approach developed from the nitroimidazole compounds. The idea stemmed from the observation that the nitroimidazoles explored above could also undergo enzyme reduction under hypoxia to form cytotoxic species and thus selectively kill hypoxic cells.

1.12 Hypoxia Activated Prodrugs (HAPs)

These bioreductive drugs are reduced only under hypoxic conditions to become a cytotoxic species. Under oxic conditions they are inactive, therefore sparing most normal tissue. These drugs are known as Hypoxia Activated Prodrugs (HAPs) (Li, Zhao, & Li, 2021). Reduction via one-electron reductases, such as cytochrome p450 oxidoreductase (POR), reduces the

inactive prodrug to a prodrug radical species, which can be further reduced in the absence of oxygen to form an activated drug or fragment into an active species (Figure 1.27) (Phillips, 2016). Alternatively two-electron reductases can directly reduce the inactive prodrug to form the active drug species, without producing an oxygen-sensitive prodrug radical intermediate, leading to drug activation in an oxygen independent manner (Phillips, 2016).

HAPs generally consist of three main components; a trigger which is activated only under hypoxic conditions through reduction by one and two electron reductases, an effector which is the cytotoxic component and a linker which is what keeps the other two components together and the effector inactive while still linked (Phillips, 2016).

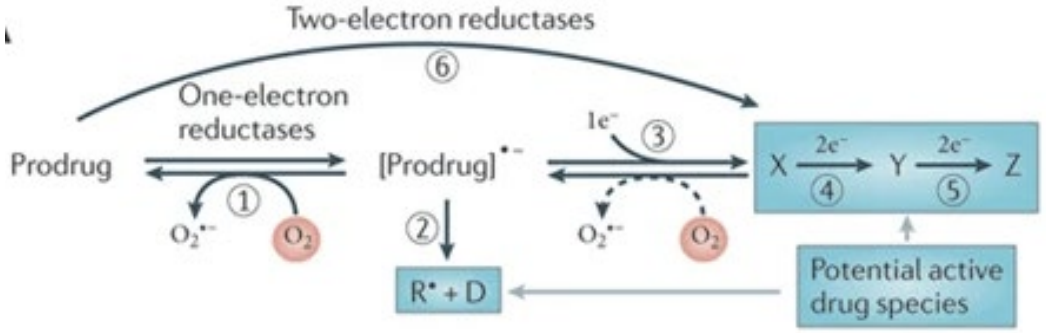

Figure 1.27. General *Reduction Pathways for HAPs.* *One-electron reduction generates a prodrug radical, that under oxic conditions can be re-oxidised back. Under hypoxic conditions the prodrug radical would be further reduced to the active drug either by fragmentation (2) or by further reductions (3), (4) and (5). Two-electron reductases compete against the one-electron reductases and are oxygen independent, therefore can directly form the active drug without producing the oxygen sensitive prodrug (6).* (Wilson & Hay, 2011).

There are five main chemical classes of HAPs that can be metabolised through enzymatic reduction in hypoxic conditions; quinones, nitroaryl compounds, aromatic *N*-oxides, aliphatic *N*-oxides and transition metals (Wilson & Hay, 2011).

Although the area of HAPs has gained a lot of interest and many HAP compounds have been developed and examined preclinically, only a few compounds have advanced to clinical trial and, although clearly active compounds, all have failed to demonstrate superiority to standard of care in clinical trials (Francis W Hunter, Wouters, & Wilson, 2016).

1.12.1 *Tirapazamine*

The first HAP to reach clinical trials was tirapazamine (3-amino-1,2,4-benzotriazine 1,4-dioxide) which is an aromatic *N*-oxide compound (Figure 1.28) (J. Brown, 1993). Tirapazamine is activated under hypoxic conditions through reduction by one-electron reductases and a series of reactions, generates either benzotriazinyl or hydroxyl radicals, which are damaging to DNA (Shinde, Hay, Patterson, Denny, & Anderson, 2009). Preclinical studies showed that tirapazamine preferentially killed tumour cells due to its toxicity in hypoxic conditions (J. Brown, 1993). It was also shown to synergise with radiation therapy *in vitro* (J. Brown, 1993). TPZ acted as a radiosensitiser in a range of tumour xenograft models in combination with both single-dose radiation (Zeman, Hirst, Lemmon, & Brown, 1988) and fractionated radiation (J. M. Brown & Lemmon, 1990), (Martin Brown & Lemmon, 1991). TPZ was synergistic in combination with cisplatin (Done & Brown, 1993) and this was shown to be due to the hypoxia-dependent inhibition of the repair of cisplatin-induced DNA cross-links (Kovacs et al., 1999), (Wouters, Wang, & Brown, 1999).

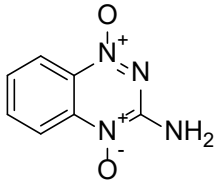

Figure 1.28. *Structure of tirapazamine.*

Tirapazamine underwent two distinct series of clinical trials. The initial focus was on the combination of tirapazamine with cisplatin in NSCLC. A phase II trial (Disilvestro et al., 2014) evaluating the combination of tirapazamine with cisplatin and radiation on a weekly dosing schedule, with lowered starting doses, found that it was acceptably tolerated, but had no improvement over cisplatin in combination with radiotherapy. Initial trials revealed tirapazamine was well tolerated up to 36–450 mg /m^2 as a single agent (Senan et al., 1997). Dose reductions to 260 mg m^2 were required in combination with cisplatin given every three weeks (Johnson et al., 1997). Tirapazamine induced nausea and vomiting, diarrhea, weight loss and muscle cramps, reversible hearing loss, and tinnitus (Reddy & Williamson, 2009). The phase III trial investigated the combination of cisplatin and tirapazamine in patients with Advanced Previously Untreated non–small-cell Lung Tumours (CATAPULT I) and found that tirapazamine enhanced the activity of cisplatin (Von Pawel et al., 2000). The CATAPULT II trial (F. Shepherd et al., 2000) found that the combination of tirapazamine and cisplatin was less active than etoposide and cisplatin for survival, but response rates were similar. Another phase III trial (Williamson et al., 2005) however, found that the addition of tirapazamine to paclitaxel and carboplatin did not improve survival outcomes in patients with advanced NSCLC, compared with paclitaxel and carboplatin alone. They also found that it increased toxicity. A study (Sandler et al., 2000) found improvement in overall survival with the combination of gemcitabine and cisplatin against cisplatin alone, in advanced NSCLC patients. Phase III trials in patients with advanced Non-Small Cell Lung Cancer (NSCLC) showed that tirapazamine enhanced cisplatin activity compared to cisplatin treatment alone (Von Pawel et al., 2000). However, in a subsequent trial the combination of tirapazamine and cisplatin was found to be inferior to the combination activity of cisplatin and etoposide and resulted in lower survival rates (F Shepherd et al., 2000). Another phase III trial also involving patients with NSCLC investigated tirapazamine with the combination of paclitaxel and carboplatin, but found that not only did the addition of tirapazamine to the two drugs in combination not improve patient responses, but it increased the toxicity of carboplatin and paclitaxel and was poorly tolerated (Williamson et al., 2005).

Trials in cervical cancer were also conducted. Phase I trials (Aghajanian et al., 1997) found that the combination of tirapazamine with cisplatin in patients with recurrent cervical cancer only resulted in response at the highest dose level of 330 mg/m^2 which included grade 3 and 4 toxicities, but also disease stabilisation in patients. A phase I/II trial found that tirapazamine in combination with cisplatin and pelvic radiotherapy, in patients with cervical cancer had, acceptable toxicity and that thirteen of the fifteen patients had complete control of pelvic disease at six months (Craighead, Pearcey, & Stuart, 2000). Other phase II trials, using a dosing schedule of every three weeks (Covens, Blessing, Bender, Mannel, & Morgan, 2006), found that the combination of tirapazamine and cisplatin had observable efficacy in patients with platinum sensitive ovarian or primary peritoneal cancer, but that it was also associated with significant grade 3 and 4 toxicities. The same combination was also tested in patients

with advanced recurrent cervical cancer and the toxicities observed were found to be acceptable (Maluf et al., 2006).

Despite these equivocal results another clinical avenue was pursued. Phase I trials of tirapazamine with and without radiation and with cisplatin in patients with advanced head and neck cancer showed good clinical responses and significant grade 3 and 4 toxicities (Rischin et al., 2001). A follow-up phase II trial suggested that TPZ, in combination with cisplatin chemoradiotherapy, was effective, with a trend in favour of the TPZ arm over 5-fluorouracil (5-FU) plus chemoradiotherapy (Rischin et al., 2005). This result was dependent on the patient's tumours being hypoxic as defined by 18F-misonidazole PET imaging, which was shown to be prevalent in patients with advanced and neck cancer (R. J. Hicks et al., 2005). This resulted in increased risk of locoregional failure in patients treated with platinum/fluorouracil chemoradiation compared to patients treated with the tirapazamine combination. (Rischin et al., 2006). A Phase III clinical trial investigated tirapazamine in combination with radiation and cisplatin against a cisplatin and radiation combination in patients with untreated advanced HNSCC. There was no improvement in survival from the addition of tirapazamine (D Rischin et al., 2008). The investigators stated that they had deviations in radiotherapy occurring in 20% of patients with the potential for an adverse impact on tumour control and that there was evidence of some treatment effect in patient who did not have major deviations (D Rischin et al., 2008). Importantly, the patients were not selected for the presence of hypoxia. The hypoxia biomarker used in the Phase II clinical trial was not adopted in the subsequent randomised phase III trial (Danny Rischin et al., 2008). A meta-analysis of the safety and efficacy of tirapazamine in clinical trials was conducted and concluded that, despite failing many clinical trials, it would be unjustifiable to label tirapazamine as a failed drug. Further, it suggested the proportion of hypoxic cells in patient tumours should be assessed prior to treatment. (Hiremath & Devendrappa, 2018).

1.12.2 *PR-104*

PR-104 is a phosphate ester pre-prodrug (Figure 1.29) of a nitroaromatic HAP that undergoes hydrolysis to the dinitrobenzamide mustard prodrug PR-104A (Christopher P Guise et al., 2014). PR-104A can be reduced by various oxidoreductases to hydroxylamine PR-104H and amine PR-104M which are cytotoxic metabolites that result in inter-strand DNA crosslinking (Christopher P Guise et al., 2014).

Pre-clinical studies showed that PR-104A was cytotoxic toward hypoxic cells *in vivo* in human SiHa cervical carcinoma, HT29 colorectal carcinoma, and H460 NSCLC tumour xenografts as a single agent and in combination with radiotherapy. PR-104 demonstrated greater activity than tirapazamine in combination with radiation (Patterson et al., 2007), but was less potent in the same cell lines *in vitro*, this was thought to be due to the greater tumour penetrability of PR-104 than tirapazamine (K. O. Hicks et al., 2007). PR-104 required more severe hypoxic levels for activation than tirapazamine. PR-104 was also found to synergise with gemcitabine and docetaxel in Panc-01 pancreatic and 22RV1 androgen-refractory prostate xenograft models, respectively, leading to increased mouse survival and was also able to increase survival as a single agent against H460 NSCLC tumour xenografts (Patterson et al., 2007).

Phase I clinical trials were conducted in patients with solid tumours that were refractory to standard therapy (Jameson et al., 2010). PR-104 was administered intravenously (IV) every three weeks as a one hour infusion (Jameson et al., 2010). The MTD was found to be 1,100 mg/m^2, above which the DLTs observed were febrile neutropenia (Jameson et al., 2010). It was found to be well tolerated with only one patient out of six who experienced a grade 3

toxicity at the 1,100 mg/m^2 dose rate; which was fatigue (Jameson et al., 2010). The AUC was found to be 20 μg h/mL (Jameson et al., 2010). This drug level produced significant tumour cell killing in human tumour xenografts (Benito et al., 2011). Although another phase I trial conducted on patients with advanced solid tumours, given one hour intravenous infusions on days; 1, 8 and 15 every 28 days with doses ranging from 135 mg/m^2 to 900 mg/m^2 found grade four toxicity of thrombocytopenia and neutropenia (McKeage et al., 2011). The MTD was found to be 675 mg/m^2 (McKeage et al., 2011). It was concluded that weekly administration of PR-104 might be suitable in clinical studies if given in a shorter course to avoid toxicity, with fractionated radiotherapy or haematopoietic stem cell support (McKeage et al., 2011).

Another phase I trial investigated PR-104 in combination with gemcitabine or docetaxel in patients with advanced solid tumours, but found severe myelotoxicity in both combinations, and further dose escalation of PR-104 in combination with gemcitabine was prevented by thrombocytopenia. Docetaxel dose escalation was able to be continued with use of prophylactic Granulocyte Colony Stimulating Factor (G-CSF) (McKeage et al., 2012).

A Phase II study in testing PR104 in small cell lung cancer was terminated due to the discovery that the Aldo-Keto Reductase family 1 member C3 (AKR1C3) is able to catalyse reduction of PR-104 to PR-104H in the presence of oxygen *in vitro* and *in vivo*. This discovery undermined the use of PR-104 as a HAP (C. P. Guise et al., 2010). AKR1C3 was detected in a minority of bone marrow cells and CD34 human myeloid progenitor cells were found to be positive for AKR1C3 mRNA. This was suggested to contribute to the myelotoxicities observed in clinical trials (C. P. Guise et al., 2010).

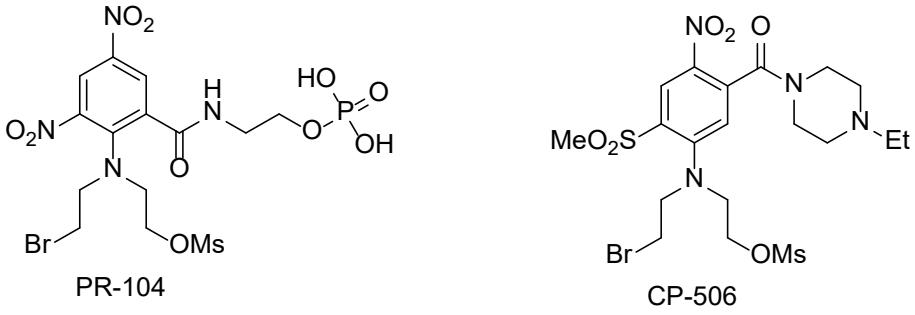

Figure 1.29. *Structure of PR104 and CP-506.*

The discovery that AKR1C3 was an unusual reductase spurred medicinal chemistry efforts to design out AKR1C3 activity. The leading AKR1C3-resistant analogue to replace PR-104A is CP-506.

CP-506 is converted to an oxygen sensitive radical anion by one electron reductases and under hypoxic conditions this intermediate is converted to the cytotoxic compound CP-506M. In the presence of oxygen the radical anion is re-oxidised back to the prodrug. CP-506 was designed to have more favourable properties than PR-104, in addition to being resistant to AKR1C3 it is also resistant to many metabolic clearance pathways that compromise PR-104 pharmacokinetic profile, such as glucuronidation and self-alkylation of the reduced ortho nitro-group (Van Der Wiel et al., 2021). It also has the potential to be orally bioavailable and has good diffusion properties allowing a strong bystander effect (Van Der Wiel et al., 2021), (Jackson-Patel et al., 2022). It was found to show selective cytotoxicity under hypoxic conditions, was inhibited under oxic conditions and was completely resistant to two electron metabolism by AKR1C3 (Van Der Wiel et al., 2021). CP-506 displayed dose-dependent growth

inhibition of H69 small-cell lung cancer and MDA-468 breast adenocarcinoma tumour xenografts and a range of activity against a panel of 15 tumour xenografts (Van Der Wiel et al., 2021). CP-506 is currently starting Phase I/II trials in monotherapy or in combination with carboplatin or immune checkpoint inhibitors in patients with solid tumours (NCT04954599).

1.12.3 *TH-302 (Evofosfamide)*

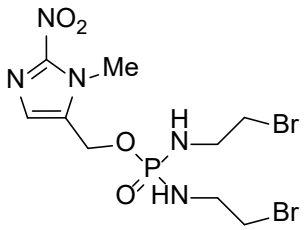

Figure 1.30. *Structure of TH-302.*

TH-302, a 2-nitroimidazole HAP, undergoes one-electron reduction under hypoxic conditions to produce a DNA cross-linking agent, Bromo-IsoPhosphoramide Mustard (Br-IPM) (Duan et al., 2008). In biological media the dibromo groups undergo rapid nucleophilic substitution by chloride ions resulting in formation of the dichloro analogue Isophosphoramide Mustard (IPM) (C. R. Hong, Dickson, et al., 2018). TH-302 reduction can occur in an oxygen-insensitive manner by 2-elecron reduction catalysed by nitroreductases to form the hydroxylamine (C. R. Hong, Dickson, et al., 2018).

Pre-clinical studies showed that TH-302 had greater anti-tumour activity in hypoxic conditions and provided dose-dependent tumour growth inhibition in the H460 NSCLC xenograft model. It also provided a range of growth inhibition in a panel of 11 xenograft models (J. D. Sun et al., 2012). It was observed to have greater dose potency than tirapazamine and was inhibited by oxygen to a greater extent as well (Meng et al., 2012). A significant bystander effect was observed in HCT116 cells overexpressing 2-electron nitroreductase (NfsA) which were sensitive to TH-302 under hyperoxia (Meng et al., 2012). However, (C. R. Hong, Dickson, et al., 2018) found that the bystander effect of TH-302 is lowered under hypoxia due to the instability of hydroxylamine which is produced under hypoxic conditions (Duan et al., 2008) and could possibly fragment to form Br-IPM, limiting diffusion.

The first phase I trial of TH-302 was in patients with advanced solid malignancies and the MTD was determined to be 575 mg/m^2 weekly and 670 mg/m^2 when given every three weeks (Weiss et al., 2011). The DLTs were grade three skin and mucosal toxicities, but good responses were observed in patients with metastatic small cell lung cancer (SCLC) and melanoma, with stable control of disease (Weiss et al., 2011).

A Phase II study investigating TH-302 in combination with doxorubicin in patients with advanced soft tissue sarcoma found good tumour response and overall survival (Chawla et al., 2014). Another phase II study investigating TH-302 in combination with gemcitabine in patients with advanced pancreatic cancer also found good tumour response and progression free survival (Borad et al., 2015).

These promising results prompted phase III trials; one which investigated the combination of TH-302 with doxorubicin in patients with advanced soft tissue sarcomas and failed to improve overall survival compared to doxorubicin alone (Tap et al., 2017). Another phase III trial investigating the combination of TH-302 with gemcitabine in patients with pancreatic ductal

adenocarcinoma (PDAC) also missed the primary endpoint of improved overall survival (Van Cutsem et al., 2016).

These disappointing results could be partly attributed to the lack of patient screening for the presence of tumour hypoxia (Linda Spiegelberg a, 2019). The phase III trial investigating TH-302 in combination with gemcitabine showed longer progression free survival and higher overall response rate in patients being treated with the combination therapy (Van Cutsem et al., 2016) and therefore the hypoxic status of tumours of each of the patients would have been very informative (Linda Spiegelberg a, 2019).

1.12.4 *Tarloxotinib*

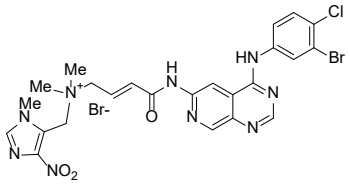

Figure 1.31. Structure of tarloxotinib bromide

Tarloxotinib is a 4-nitroimidazole HAP that is reduced through one-electron reduction to a nitro radical anion intermediate and in the presence of oxygen this radical anion can be oxidised back to the prodrug. Under hypoxic conditions the intermediate can be fragmented and produces an irreversible pan-ErbB effector which has inhibitory activity against members of the ErbB family (EGFR, HER2 and HER4) (Estrada-Bernal et al., 2021). Members of the ErbB family are involved in progression of cancer cell evolution processes such as proliferation, metastasis, metabolism and survival (Estrada-Bernal et al., 2021).

Preclinical studies show that tarloxotinib is converted to the effector (tarloxotinib-E) under hypoxic conditions and that the prodrug has diminished activity in normoxic conditions therefore sparing most wild type EGFR inhibition in normal tissue. Tarloxotinib-E was found to be a potent inducer of apoptosis *in vitro* as well, and inhibited tumour growth in *in vivo* ErbB-dependent xenograft models (E*strada-Bernal et al., 2021)*.

Phase I trials were conducted in patients with advanced solid tumours and the MTD was found to be 150 mg/m^2 when administered weekly as a one hour intravenous infusion (Estrada-Bernal et al., 2021). Tarloxotinib advanced to Phase II trial where it was investigated in patients with NSCLC (S. V. Liu et al., 2020). In this trial patients were separated into three cohorts; with patients harbouring an EGFR Exon 20 insertion were in Cohort A, patients with HER2 activating mutations were in Cohort B and patients with progressive disease after platinum based chemotherapy or harbouring NGR1, EGFR, HER2 or HER4 fusion mutations were in Cohort C (S. V. Liu et al., 2020). Tarloxotinib showed a tumour reduction in 44% of patients with HER2 activating mutations in Cohort B and 22% showed partial response (S. V. Liu et al., 2020). The best response in Cohort A was stable disease (55%) and progressive disease (45%) (S. V. Liu et al., 2020). Overall, tarloxotinib was found to be well tolerated, although grade 3 EGFR-related toxicities were observed such as rash and diarrhea, but these side effects were not prevalent (S. V. Liu et al., 2020). Another Phase II trial studied tarloxotinib in patients with recurrent or metastatic squamous cell carcinoma of the head and neck or skin (NCT02449681) (Rischin et al., 2016). Hypoxic PET scans were going to be obtained of the patients enrolled. But the trial was terminated by the funding company, Threshold Pharmaceuticals (ThresholdPharmaceuticals, 2016).

Despite clear indications of activity, no HAPs have progressed through Phase III trials to registration. One shortcoming in all Phase III trials of HAPs has been the lack of patient selection for hypoxic positive tumours. The use of HAPs is a targeted approach, yet the target is not being quantified in the patients being treated. Patients with low hypoxic fractions would not be expected to benefit from the treatment of HAPs (Linda Spiegelberg a, 2019). Much work has been done on identifying biomarkers of hypoxia in tumours, but there exist a multitude of sensitivity indicators and the transience of hypoxia makes personalised therapy difficult (Francis W Hunter et al., 2016). The innovations in imaging technology and molecular oncology are paving the way for better patient evaluation (Francis W Hunter et al., 2016) and therefore it is important for clinical trials to incorporate the latest imaging techniques and biomarker identification strategies into their investigations.

1.13 DNA-PKi delivered as HAPs in combination with Radiation Therapy

Radiation therapy has not often been used in combination with HAPs that have gone onto clinical trials – despite the fact that such a combination would be complementary because HAPs selectively target the radioresistant hypoxic cells. This combination would also result in fewer side effects and toxicities as the mechanism of both therapies is different to each other (Hamis et al., 2020) compared to combination with chemotherapies which can potentially exacerbate toxicities.

DNA-PK inhibitors can be utilised as the effector in HAPs to deliver the DNA-PK inhibitor to hypoxic tissues within tumours (Ishna N. Mistry, Mar 14, 2017.). Not only does this lead to hypoxic cell killing, but also reduces the exposure of normal cells within the radiation field to the cytotoxic effects of the DNA-PK inhibitor (Ishna N. Mistry, Mar 14, 2017.). This is expected to increase the therapeutic window by optimising tumour cell kill. This has benefits for the patient because increasing the radiosensitivity of radioresistant tumour cells can reduce the radiation dose and duration required to achieve effective tumour cell kill. This can mitigate the acute and chronic side effects that are associated with radiotherapy allowing treatment to be completed.

A study was conducted investigating the radiosensitisation by DNA-PK inhibitor IC87361 which was released from the HAP SN38023 under hypoxic conditions (Wong et al., 2019). SN38023 was reduced in cells overexpressing the one-electron reductase POR selectively under hypoxia and fragmented to release the DNA-PK inhibitor IC87361. The DNA-PK inhibitor radiosensitised PRKDC (DNA-PK catalytic subunit)-proficient HAP C631 cells, but did not radiosensitise paired PRKDC-deficient cells demonstrating that radiosensitisation is caused by inhibition of DNA-PK. The prodrug SN38023 was 24-fold less potent than the effector IC87361 in monolayer cell culture models. This relatively low selectivity was rationalised to be possibly due to SN38023 being able to occupy the ATP binding site through a morpholino-Leu3806 interaction. SN38023 produced similar cell kill in HCT116/POR spheroids as IC87361, suggesting hypoxic activation. Poor aqueous solubility limited the potential of the prodrug. IC87361 did not readily diffuse out of the cell it was produced in, resulting in high intracellular concentrations and a lack of observed bystander effect (Wong et al., 2019).

This preliminary study set the scene for prodrugs of DNA-PK inhibitors with better *in vitro* and *in vivo* properties and DNA-PK inhibitors that can elicit significant bystander effects are required for successful therapeutic HAP delivery of DNA-PKi to radiosensitise tumour cells (Wong et al., 2019).

1.14. Project Aims and Objectives

As part of a drug discovery programme conducted at the ACSRC a new class of DNA-PK inhibitors was discovered. This new class has been optimised and a lead DNA-PK inhibitor, SN39536, has been identified. A HAP of this lead compound has been prepared (SN39884).

This project will explore the properties and behaviour of the novel HAP SN39884 and the corresponding DNA-PK inhibitor SN39536 in cells under hypoxic and oxic conditions.

In particular, the project will determine whether the prodrug SN39884 is selectively metabolised under hypoxic conditions and releases the DNA-PK inhibitor SN39536 and whether the prodrug and effector can radiosensitise tumour cells under oxic and anoxic conditions.

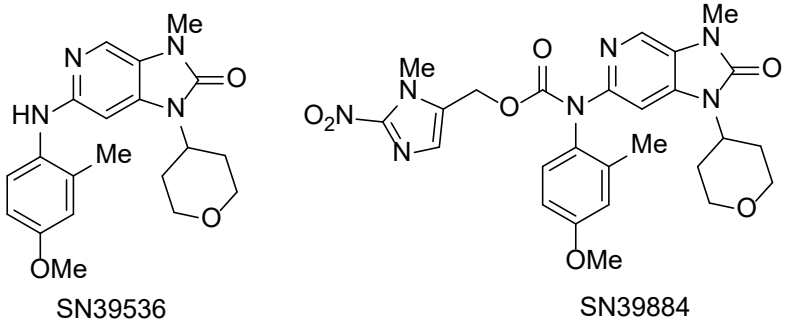

Figure 1.32. *DNA-PK inhibitor SN39536 and corresponding HAP SN39884*.

Aim 1: To explore the metabolic activation of the prodrug SN39884 and release of the effector SN39536 in cells constitutively expressing cytochrome P450 oxidoreductase (POR) (HCT116-G), overexpressing POR (POR-G) and under expressing POR (PORko-R) under oxic and anoxic conditions, using LCMS analysis to quantify metabolites.

Aim 2: To demonstrate hypoxia-selective sensitisation by prodrug SN39884 in monolayer cultures of HCT116-G, POR-G and PORko-R cells in combination with radiation using a growth inhibition endpoint under oxic and anoxic conditions.

Aim 3: To demonstrate hypoxia-selective radiosensitisation by prodrug SN39884 in monolayer cultures of HCT116-G, POR-G and PORko-R cells using a clonogenic survival endpoint under oxic and anoxic conditions.

2. Chapter 2. Materials and Methods

2.1 Materials

Material/Reagent	**Source/Supplier**
6, 24 and 96-well plates	Thermo Fisher Scientific Nunc, Roskilde, Denmark
500 mL bottle top filter	Corning Inc., NY, USA
Acetic acid	Thermo Fisher Scientific, Auckland, NZ
Acetonitrile	Thermo Fisher Scientific, Auckland, NZ
Alpha minimal essential media (αMEM)	Gibco New Zealand Ltd., Auckland, NZ
Analytical grade water	Milli Q purification system. Millipore Corporation, Bedford, USA.
Column for LC-MS (Zorbax SB-C18 3 x 150 MM, 5 uM. PN 883975-302, SN USDM002061)	Agilent Technologies, Inc., USA
Cell culture flasks (T75, T175)	Thermo Fisher Scientific Nunc, Roskilde, Denmark
Dimethyl sulfoxide (DMSO)	Ajax Chemicals, NSW, Australia
Disodium hydrogen phosphate (Na_2HPO_4)	Merck KGaA, Darmstadt, Germany
Foetal calf serum (FCS)	Moregate Biotech, Hamilton, NZ
Formaldehyde	Merck KGaA, Darmstdt, Germany
Formic acid	Merck KGaA, Darmstadt, Germany
Neomycin (G418)	Gibco New Zealand Ltd., Auckland, NZ
^{3}H-mannitol	American Radiolabeled Chemicals, Inc.
Liquid scintillation counter	Packard Tricarb Scintillation, Minnesota, USA)
Methanol	Merck KGaA, Darmstadt, Germany
Methylene Blue	Serva Electrophoresis, Heidelberg, Germany
Potassium dihydrogen phosphate (NaH_2PO_4)	Sigma-Aldrich, St. Louis, MO. USA
Penicillin-Streptomycin-Glutamine (P/S)	Gibco New Zealand Ltd., Auckland, NZ
Phosphate buffered saline (PBS)	Prepared in house
Puromycin	Gibco New Zealand Ltd., Auckland, NZ
Sodium chloride (NaCl)	Merck KGaA, Darmstadt, Germany
Sterile saline (NaCl 0.9%)	Multichem NZ Ltd., Auckland, NZ
Sulforhodamine B (SRB)	Sigma-Aldrich, St. Louis, USA
Trichloracetic acid (TCA)	ACSRC Laboratory, Auckland, NZ.
Trypan Blue	Invitrogen, Life Technology Corp, USA
Trypsin EDTA (0.5%), no phenol red	Gibco New Zealand Ltd., Auckland, NZ
Unbuffered Tris	Sigma-Aldrich, St. Louis, USA

2.2 Prodrug and DNA-PK inhibitor

The prodrug SN39884 and the DNA-PK inhibitor SN39536 that were the focus of this thesis were synthesised by Associate Professor Michael Hay (ACSRC). SN39884 and SN39536 were available in powder form, where SN39884 (batch number: NC5) had a molecular weight of 551.56 g/mol and SN39536 (batch number: NC3) had a molecular weight of 368.44 g/mol. These were dissolved in DMSO to produce a stock solution at a concentration of 30 mM. All stock solutions were kept at -80 °C.

2.3 Gamma irradiation

All irradiation was carried out using the Eldorado 78 cobalt-60 teletherapy unit (Atomic Energy of Canada Ltd). For *in vitro* experiments, plates were transferred to a metal box and for anoxic experiments, this was sealed in a Bactron Pd/H_2-scrubbed anaerobic chamber (Sheldon Manufacturing, Cornelius, OR). Dose rates for cell cultures were in the range 0.5 - 0.9 Gy/min. Dose rates were determined previously using ammonium thiocyanate-modified Fricke dosimetry (Fricke, 1966).

2.4 Cell Culture

2.4.1 Cell Lines

The colon cancer cell line HCT116 cells were initially purchased from ATCC and authenticated in-house by short tandem repeat profiling. HCT116 cells with forced expression of sPOR (soluble, cytosolic variant of P450 oxidoreductase) along with green fluorescent protein (copGFP) and puromycin resistance gene were used as the high POR expression cell line (POR-G). HCT116 cells with biallelic knockout of POR, expressing red fluorescent protein (mRuby) and neomycin (G418) resistance genes were used as the POR null cell line (PORko-R). HCT116 cells expressing copGFP and puromycin resistance genes were used as the cell line that constitutively expresses POR (HCT116-G) in this study. HCT116-G, POR-G and PORko-R were developed by Dr Hong (C. R. Hong, Bogle, et al., 2018). POR-G and HCT116-G cells were passaged in alpha Minimum Essential Medium (αMEM) + 5% foetal calf serum (FCS) + 2 µM puromycin and PORko-R cells were maintained in αMEM + 5% FCS + 1 mg/mL neomycin. All cell lines were passaged for <2 months (60 days) and all cells were mycoplasma-free by Plasmo Test (InvivoGen, San Diego, CA).

2.4.2 Growth and Maintenance

10^6 cells were frozen down in 20% DMSO and 80% FCS freezing media in a total volume of 1 mL and transferred into cryotubes, which are stored in isopropanol Mr. Frosty containers, in the -80°C freezer for a few days before being stored in the liquid N_2 cryostore.

Cells were taken from the liquid N_2 cryostore and were thawed immediately in a water bath at 37 °C. The 1 mL of cell solution was transferred into a 50 mL Falcon tube with 9 mL of culture media. Cell were pelleted by centrifugation (1000 rpm, 8 min at room temperature) and media removed by aspiration. The cells were then resuspended in fresh media, and put into a T75 flask (75 cm^2) in a total volume of 15 mL culture medium.

The cultured cells are kept in a 37 °C humidified, 20% oxygen and 5% carbon dioxide incubator. Cells were kept until they reached 10 days old, they were split to give ~90% confluence for experiments, and they were checked regularly under a light microscope to ensure there was no contamination present.

To harvest cells from culture flasks growth medium was discarded via aspiration and cells were washed with phosphate buffered saline (PBS, prepared in-house, 137 mM NaCl, 2.68

mM KCl, 1.47 mM KH_2PO_4, 8.16 mM, Na_2HPO_4, pH 7.4). PBS was aspirated and cells were treated with 3 mL of trypsin solution (0.05% trypsin- 0.5 mM EDTA in PBS) for 10 min at 37 °C. Cells were then resuspended in 7 mL of culture media; αMEM + 5% FCS + 2 µM puromycin for POR-G and HCT116-G, or αMEM + 5% FCS + 1 mg/mL neomycin for PORko-R cells to deactivate trypsin. Cells were resuspended 30 times to ensure a good single cell suspension. Cells were counted using a Countess automated cell counter (Countess II FL, Invitrogen, USA) or a Z2 Coulter particle counter and size analyser (Beckman Coulter Inc, FL, USA). Cell viability was determined by diluting 20 µL of cell suspension with 20 µL of trypan blue and 10 µL was added to each side of a Countess slide. Total number of live and dead cells were counted using a Countess automated cell counter or by manual counting under a light microscope. Any dead cells observed were noted and the number of viable cells was divided by the total of viable and dead cells and multiplied by 100 to give the cell viability.

2.5 Metabolism Assay

2.5.1 Cell Seeding

Cells were harvested at 70-90% confluence and cell viability and counts were determined using the methods detailed in section 2.4.2. Cells were trypsinised as described in section 2.4.2 and a final density of 5 x 10^5 cells/0.45 mL was achieved by diluting the cell suspension in αMEM + 10% FCS + 1% IC50 supplement (0.2 mM 2-deoxycytidine, 10 mM D-glucose) for all cell lines. Cells (5 x 10^5cells/0.45 mL) were plated in 24-well plates and incubated for 2 h at 37 °C for cell attachment. For anoxic experiments, the pelleted cells were taken into the Bactron anaerobic chamber (5% H_2/5% CO_2/ 90% N_2, palladium catalyst anaerobic chamber, Coy laboratories, MI USA) and resuspended with deoxygenated αMEM + 10% FCS + 1% IC50 media. Cells were incubated for 2 h inside the anaerobic chamber. The plasticware and culture medium used for treatment of cells under anoxia were pre-equilibrated in the anaerobic chamber more than 3 days.

2.5.2 Drug Treatment

Drug stock solutions in DMSO (30 mM) were diluted to 100 µM in culture media and 50 µL of 100 µM drug solution was added to each well (final concentration: 10 µM). Cells in 24-well plates were exposed to SN39536 under oxic conditions or SN39884 under oxic and anoxic conditions for 0 – 3 h. Cells were incubated 37 °C with drug for 0 hours, 1.5 h and 3 h under oxia and 1 h, 2 h and 3 h under anoxia in the anaerobic chamber.

2.5.3 Intracellular and Extracellular Processing

At the end of the incubation the plates were spun at 1000 rpm for 15 min at 4 °C and placed on ice. Extracellular samples were first collected from each well by carefully taking 100 µL of medium and transferring it into Eppendorf tubes containing 200 µL ice cold methanol.
The remaining extracellular medium was removed using 1 mL and 10 µL Eppendorf pipettes and the media discarded. Intracellular samples were collected by adding 100 µL ice cold methanol directly into each well.
All samples were vortexed at 600 rpm for 30 sec and stored in -80 °C until LC-MS analysis.

2.5.4 LC-MS Analysis

The methanolic extracts were centrifuged at 13,500 rpm for 5 min at 4 °C and the supernatant was transferred into HPLC vials.
SN39536 and SN39884 cell culture samples were analysed using an Agilent 1260 series HPLC with photodiode array detector coupled with the 6510 LC/MS model with jet stream electrospray ionisation source (Agilent Technologies, USA).

The column used was the AG-7 C18 column (Zorbax SB-C18 3 x 150 mm, 5 µM).
5 µL samples were injected from a refrigerated autosampler. The aqueous mobile phase was 4.5 mM formate buffer and the organic phase was 80% acetonitrile with 0.01% formic acid at a flow rate of 0.5 mL/min. The total run time was 12 min and the organic phase gradient was 40% at 0 min, 100% at 8 min, 40% at 9 min and 40% at 12min. SN39536 and SN39884 were analysed in positive mode by extraction of the *m/z* 369 ion and *m/z* 552 ion, respectively. Data were acquired and analysed with Agilent Open Lab CDS Chemstation software.
Concentrations of SN39884 and SN39536 in intracellular and extracellular samples were quantified using external standard calibration curves of SN39884 and SN39536 (30, 10, 3.33, 1.11, 0.37, 0.12, 0.04, 0.014 µM).

2.5.5 Estimation of residual extracellular medium in intracellular samples

The cell-excluded marker ^{3}H-mannitol was added to the extracellular medium (final concentration 0.2 pM) at the end of drug exposure. Radioactivity in aliquots of the final extracts was determined by scintillation counting (Packard Tricarb Scintillation, Minnesota, USA) and residual extracellular medium in intracellular samples was estimated as previously described (C. R. Hong, Dickson, et al., 2018). Contamination of intracellular samples from extracellular medium was corrected by subtracting the amount of the prodrug and metabolites (µmol) in residual extracellular medium (3.8 µL) from total amounts (µmol) in the intracellular samples. Intracellular volume was estimated using the Z2 Coulter counter as previously described (Hong 2018 et al).

2.6 Proliferation (IC_{50}) assay

2.6.1 Plating in 96-well plates

Cells were harvested at 70-90% confluence and cell viability and counts were determined using the methods detailed in section 2.4.2. Cells were centrifuged for 5 min at 1000 rpm and resuspended in αMEM + 10% FCS + 1% IC_{50} supplement media. Cell suspensions were diluted to achieve final cell density of 3000 cells/100 µL for POR-G and PORko-R cells and 1200 cells/100 µL for HCT116-G cells. 100 µL of diluted cell suspensions were added to each well in 96-well plates and incubated for 2 hours at 37 °C. For anoxic experiments the pelleted cells were taken into the Bactron anaerobic chamber, resuspended with deoxygenated αMEM + 10% FCS + 1% IC_{50} media, and incubated for 2 h inside the anaerobic chamber. The plasticware and culture medium used for treatment of cells under anoxia were pre-equilibrated in the anaerobic chamber more than 3 days.

2.6.2 Drug and radiation treatment

Drug stock solution in DMSO (30 mM) was diluted to 30 µM in culture media and 50 µL of 30 µM drug solution was added to each well (final concentration: 10 µM) in the bottom row and mixed gently so as not to disturb attached cells. 3-fold serial dilution of drug was performed in the plates by transferring 50 µL from the bottom row to the next row containing 100 µL medium. For a non-drug control, a solution of 50 µL of DMSO was diluted to 30 µM in cell culture media.
Cells in the 96-well plates were exposed to SN39536 under oxic conditions or SN39884 under oxic and anoxic conditions for 3 h.
Radiation treatment using the Cobalt-60 gamma source was given to oxic plates (plates treated with SN39884 or SN39536) at 2 Gy and anoxic plates at 4.6 Gy (plates treated with SN39884) at room temperature. After radiation, plates were returned to a standard humidified 5% CO_2 incubator without changing the medium. For anoxic treatment, plates were sealed in metal boxes in the anoxic chamber, irradiated and incubated under normoxia

for 18 h. 18 h after irradiation drugs were removed and cells were washed 2 times with 150 µL /well of αMEM + 5% FCS + 1% P/S and a final wash with antibiotic selective media αMEM + 5% FCS + 1% P/S + 2 µM puromycin (for HCT116-G and POR-G), or 1 mg/mL neomycin (PORko-R) to stop drug exposure, control wells were filled with 150 µL of αMEM + 5 % FCS + 1% P/S and all plates were incubated at 37 °C for another 4 days before Sulforhodamine B staining (section 2.6.3).

2.6.3 Sulforhodamine B (SRB) staining

After the incubation period the cells were fixed with 50 µL of cold 40% TCA added gently without mixing, giving a final concentration of 10%. The plates were incubated in a 4 °C fridge for 1 h. The plates were then rinsed with running tap water while submerged in a plastic box. Excess water was flicked off the plates and 50 µL of 0.4% SRB in 1% acetic acid was added to each well and the plates were incubated in a dark cupboard for 30 min.

Plates were destained by dipping the plates sequentially in four plastic box, filled with approximately 2 L of water and 20 mL acetic acid giving a final concentration of 1% each. This is done quickly to prevent leaching of the stain from cells.

The SRB stain is then solubilised by adding 100 µL of 10 mM unbuffered Tris to each well using (Multidrop™ Combi nL Reagent Dispenser, Thermo Fisher, Finland). Each of the plates were then wrapped in foil to keep them in the dark, and were left on a plate shaker for 30 min and cell density was measured using the spectrophotometer machine (ELx808 absorbance plate reader, Agilent Technologies, California, US) as previously described (Wong et al., 2019).

2.7 Clonogenic assay

2.7.1 Plating in 96-well plates

Cells were harvested at 70-90% confluence and cell viability and counts were determined using the methods detailed in section 2.4.2. The required number of cells was 1 x 10^5 cells per well in a 100 µL volume. The calculated amount of cell suspension was transferred into a 50 mL Falcon tube that was centrifuged for 5 min at 1000 rpm and resuspended in the required amount of media (including the extra 10 wells) αMEM + 10% FCS + 1% IC_{50} supplement for all cell lines. Cells were seeded (5 x 10^5 cells/100 µL) in 96-well plates and all empty wells were filled with 150 µL PBS and incubated for 2 h at 37 °C. For anoxic experiments the pelleted cells were taken into the Bactron anaerobic chamber, resuspended with deoxygenated αMEM + 10% FCS + 1% IC_{50} media and incubated for 2 h inside the anaerobic chamber.

2.7.2 Drug and radiation treatment

Drug stock solutions in DMSO (1000 µM) were diluted to 10 µM in culture media and 50 µL of 10 µM drug solution was added to each well (final concentration: 1 µM). For control wells 50 µL of DMSO diluted to 10 µM in culture media was added. Cells in 96-well plates were exposed to SN39536 under oxic conditions or SN39884 under oxic and anoxic conditions for 3 h at 37 °C. Plates were irradiated using a wedge-shaped lead shield as previously described (Wong et al., 2019) to generate a range of dose rates across each plate (2.1 – 9.2 Gy for oxic plates and 4.1 – 18.4 Gy for anoxic plates). After irradiation all plates were incubated at 37 °C under normoxia for 18 h.

2.7.3 Plating for Clonogenic Assay into 6-well plates

Plates were inspected under the microscope and any precipitation or large number of dead/floating cells were noted. Extracellular medium was discarded and cells were washed once with 100 µL PBS. 100 µL trypsin was added and plates were incubated at 37 °C for 10 minutes. 200 µL of medium (αMEM + 5% FCS + 1% P/S) was added and cells were

resuspended. Cells were pipetted up and down 10 times to achieve a good single cell suspension and this cell suspension was transferred to 1 mL titre tubes. Another 200 µL of medium (αMEM + 5% FCS + 1% P/S) was added to the wells and pipetted up and down to transfer any residual cells into the same titre tubes, making up a total volume of 500 µL in each titre tube. 10-fold serial dilutions were conducted by transferring 0.1 mL of cell suspension from titre to titre tubes containing 0.9 mL media (αMEM + 5% FCS + 1% P/S). Six-well plates were filled with 4.5 mL antibiotic-selective medium (αMEM + 5% FCS + 1% P/S + 2µM puromycin for POR-G and HCT116-G, or 1mg/mL G418 for PORko-R cells). The cell suspension dilutions were added to the wells. Cells were counted using a Coulter counter. Plates were incubated at 37 °C for 10 days.

2.7.4 Methylene blue staining

After the 10 days of incubation all plates were stained with methylene blue for 30 min. Colonies with >50 cells were counted manually.

2.7.5 Graphing and statistical analysis

Clonogenic Survival curves were fitted in GraphPad Prism using the linear quadratic model described by Chadwick and Leenhouts. The linear-quadratic relationship with radiation dose is used to determine the surviving fraction (Y) using the equation:

$$Y = -(\alpha x + \beta x^2)$$

As in equation 13 from section 1.4.3; α represents a single track event which is proportional to the dose and β represents two track events which are proportional to the square of the dose.

The D_{10} value is the radiation dose required for 90% cell killing, therefore leaving a survival fraction of 10%.

The sensitising effects of the drugs were calculated using survival fraction values in the sensitiser enhancement ratio (SER) equation (Equation 15 from section 1.7). If the SER is over 1 then this indicates radiosensitisation.

$$SER = \frac{D_{10}\ Control}{D_{10}\ Drug\ Treated}$$

3. Chapter 3. Metabolic Activation of SN39884 and Release of SN39536

3.1 Hypoxia activated prodrugs of DNA-PK inhibitor.

Researchers at the Auckland Cancer Society Research Centre (ACSRC) have developed a novel series of DNA-PK inhibitors represented by the lead compound SN39536 (**Figure 3.1**). This compound is a nanoM inhibitor of DNA-PK phosphorylation and inhibits DNA-PK autophosphorylation on Ser2056 in UT-SCC-54C head and neck squamous cell carcinoma cells (Hay et al., 2020). While SN39536 is an effective radiosensitiser of tumour cells, it is expected to also sensitise normal tissue within the radiation field and this could lead to a reduced therapeutic index for the compound. The recently developed clinical stage DNA-PKi compound, AZD7648 (Fok et al., 2019; Goldberg et al., 2020), was shown to cause normal tissue damage within the radiation field (C. R. Hong et al., 2022). SN39884 is a novel prodrug also developed by researchers at the ACSRC that is designed to release the effector SN39536 specifically under hypoxic conditions (**Figure 3.1**). SN39884 has been designed as a hypoxia activated prodrug (HAP) that may provide tumour selective delivery of the effector, SN39536,

and so selectively radiosensitise tumour cells only, resulting in an improved therapeutic index for this compound.

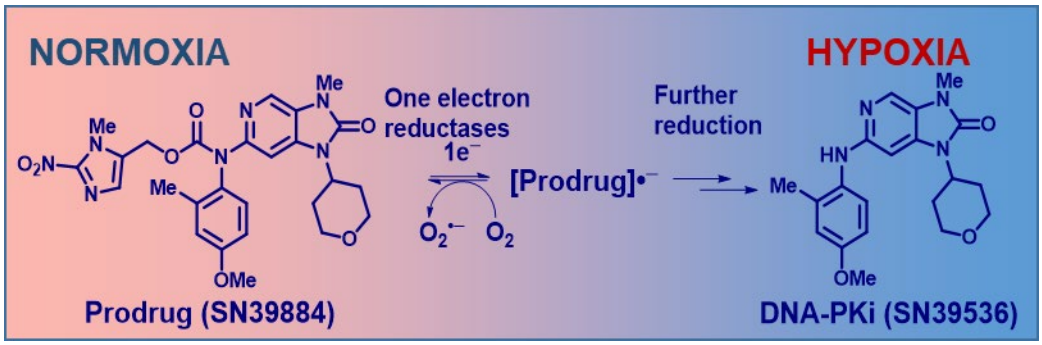

Figure 3.1: Proposed Mechanism of Action of SN39884 and its Selective Reduction Under Hypoxic Conditions. *SN39884 is reduced by one electron reductases to generate the prodrug radical that can be re-oxidised back to the prodrug under oxic conditions, but under hypoxic conditions the prodrug radical can be further reduced to form the effector SN39536 (Hay et al., 2020).*

An important aspect of the HAP design approach is whether SN39884 is stable under oxic conditions and is only activated under hypoxia to release the DNA-PK inhibitor SN39536. Researchers at ACSRC have established a cell culture method for determining the stability and metabolic activation of HAPs in monolayer cell cultures (Wong et al., 2019). They determined the metabolic activity and cellular uptake of the prodrug SN38023 and the DNA-PKi effector IC87361 by exposing cells to these compounds under oxic and anoxic conditions (Wong et al., 2019). They measured the concentrations of the prodrug and effector using LC/MS techniques and were able to show that the prodrug SN38023 was selectively reduced to the DNA-PKi IC87361 under anoxic condition, with no detectable IC87361 released under oxia in human colorectal carcinoma HCT116 cells.

Therefore, we wanted to determine the metabolic stability of the newly developed HAP SN39884, and the corresponding DNA-PKi effector SN39536, under oxic and anoxic conditions using this approach.

The one-electron reductase, cytochrome P450 oxidoreductase (POR) has been identified as the main reductase responsible for the activation of HAPs (Su et al., 2013), such as tirapazamine (Walton, Wolf, & Workman, 1992), SN30000 (Francis W. Hunter et al., 2015), PR104A (C. P. Guise et al., 2010) and TH-302 (Meng et al., 2012). The radical species formed from 1-electron reduction is back-oxidised under aerobic conditions, and therefore results in a futile cycle without activation/release of the effector. However, under hypoxic conditions the radical species can be further metabolised into the active effector (See Figure 1.27, Section 1.8). The stability of the prodrug under oxic conditions, and its susceptibility to oxygen-insensitive 2-electron reduction, represents off-target activation of the prodrug, (See Section 1.8) and therefore the behaviour of the prodrug under oxic conditions will also be investigated.

We used the HCT116 cell line and POR variants for this study as these cell lines have been used by ACSRC researchers in studies investigating bystander effects of HAPs (C. R. Hong, Bogle, et al., 2018) and investigating metabolism of the prototypic HAP SN38023 and corresponding DNA-PK inhibitor IC87361 (Wong et al., 2019). This line, POR-G, consists of HCT116 cells expressing a N-terminal truncated variant of POR along with copGFP fluorescent

proteins (superbright GFP variant from Pontellina plumata) and puromycin resistance genes (C. R. Hong, Bogle, et al., 2018). We used a POR-null cell line (PORko-R), consisting of HCT116 cells with biallelic knockout of POR, expressing mRuby and neomycin resistance genes (C. R. Hong, Bogle, et al., 2018). We also used HCT116 cells that constitutively express POR, having no alteration made to its POR expression (HCT116-G), as well as copGFP and puromycin resistance genes (C. R. Hong, Bogle, et al., 2018) in this study. LC-MS was utilised to quantify concentrations of SN39884 and SN39536 to understand the stability of compounds in culture medium, oxygen-dependent metabolism of SN39884 to SN39536 and cellular uptake of the prodrug and effector.

3.2 Aims

The overall aim of this chapter was to investigate metabolic activation of SN39884 and subsequent release of SN39536 under oxic and anoxic conditions. The first objective was to test whether SN39536 and SN39884 are stable in culture medium. The second objective was to investigate metabolism of SN39536 and SN39884 in human colorectal carcinoma HCT116 cells under oxic and anoxic conditions. The role of POR in activation of SN39884 was also explored using HCT116 cells that differ in POR expression (POR-G, PORko-R and HCT116-G). LC-MS was utilised to quantify intracellular and extracellular concentrations of SN39884 and SN39536 to understand cellular uptake.

1. To investigate the stability of SN39536 in culture medium and cellular uptake of SN39536 under oxia.
2. To investigate stability of SN39884 in culture medium and the cellular uptake of SN39884
3. To investigate hypoxia-selective activation of SN39884 and release of SN39536 under oxic and anoxic conditions.
4. To investigate the effect of POR on the activation of SN39884 under oxic and anoxic conditions in cells constitutively expressing POR (HCT116-G), over expressing POR (POR-G) and POR knockout (PORko-R).

3.3 Results

3.3.1 Chemical Stability of SN39536 in Culture Media

The metabolism assay protocol developed by (Wong et al., 2019) for testing the HAP SN38023 and DNA-PK inhibitor IC87361 was used for this study to determine the intracellular and extracellular concentrations of the novel HAP SN39884 and its DNA-PKi effector SN39536 under oxic and anoxic conditions. This study demonstrated the degree of oxygen sensitivity of the prodrug and its cellular penetrability. The varying POR expression levels in the three HCT116 cell lines allowed us to investigate the effect of POR expression on activation of prodrug SN39884 to the effector SN39536.

Firstly, the stability of the effector SN39536 was determined in culture medium in the absence of cells under oxic conditions (**Figure 3.2**). SN39536 (10 µM) was added to culture medium and concentrations of SN39536 were measured by LC-MS at 0 h, 1.5 h and 3 h.

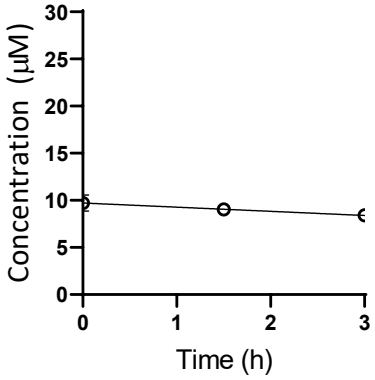

Figure 3.2: Average concentrations of SN39536 in culture medium under oxic conditions. *10 μM SN39536 (0.5 mL) was added to culture medium in 24-well plates and the plates were incubated for 0 h, 1.5 h or 3 h at 37 °C under oxia. Concentrations of SN39536 were measured by LC-MS. Mean and SE are from 3 independent experiments.*

The concentration of SN39536 decreased from 9.7 ± 0.9 μM at 0 h to 8.4 ± 0.4 μM at 3 h in culture medium, but there was no significant difference in SN39536 concentrations between 0 h and 3 h ($p = 0.227$, one-way ANOVA) indicating that the SN39536 does not undergo further transformation and remains stable in culture medium under oxic conditions (**Figure 3.2**).

3.3.2 Optimisation of Metabolism Assay

A pilot metabolism assay demonstrated that the concentration of SN39536 was unexpectedly high in the residual media left in each well after the culture medium was removed in the absence of cells (**Figure 3.3**). This residue could compromise the ability to accurately measure drug concentrations in intracellular samples. This prompted us to determine the amount of residual media being left behind once the extracellular medium had been removed from each well using a cell-impermeable marker, ^{3}H-mannitol, as previously described (C. R. Hong, Dickson, et al., 2018; Wong et al., 2019) to correct for contamination when collecting intracellular samples after extracellular medium removal.

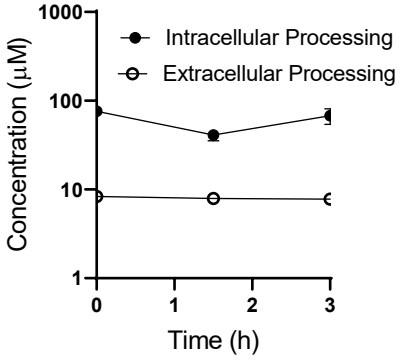

Figure 3.3 Concentration of SN39536 in media and after processing under oxic conditions. *10 μM SN39536 was added for 0 h, 1.5 h or 3 h to culture media without cells. The cell-excluded marker ^{3}H-mannitol was added to 0.5 mL medium (final concentration 0.2 pM) after the drug exposure. 100 μL medium was added to 200 μL MeOH to measure concentration of SN39536 in medium and the rest of medium was discarded. 100 μL MeOH was added to each well to measure concentration of SN39536 in residual media left in wells after whole medium was removed. Mean and SE are from 3 biological replicates.*

Table 3.1: Determination of contamination of intracellular samples by the extracellular medium using ^{3}H-mannitol as an extracellular marker. Mean and SE are from 3 biological replicates.

	Average residual medium per well (μL)
Blank	3.610 ± 0.007
PORko-R	3.601 ± 0.498
HCT116-G	3.981 ± 0.631
POR-G	3.290 ± 0.082
Average	3.650 ± 0.202

An average of 3.650 ± 0.202 μL of extracellular medium was being left behind after whole extracellular medium was removed (**Table 3.1**), resulting in contamination of the subsequent intracellular samples with compound from the residual extracellular medium. This results in the intracellular concentration of SN39536 appearing to be higher than anticipated (**Figure 3.3**). Contamination of intracellular samples from extracellular medium was corrected by subtracting total µmol of the prodrug and metabolites in residual extracellular medium (3.65 µL) from total µmol in the intracellular samples.

3.3.3 Cellular Uptake of SN39536

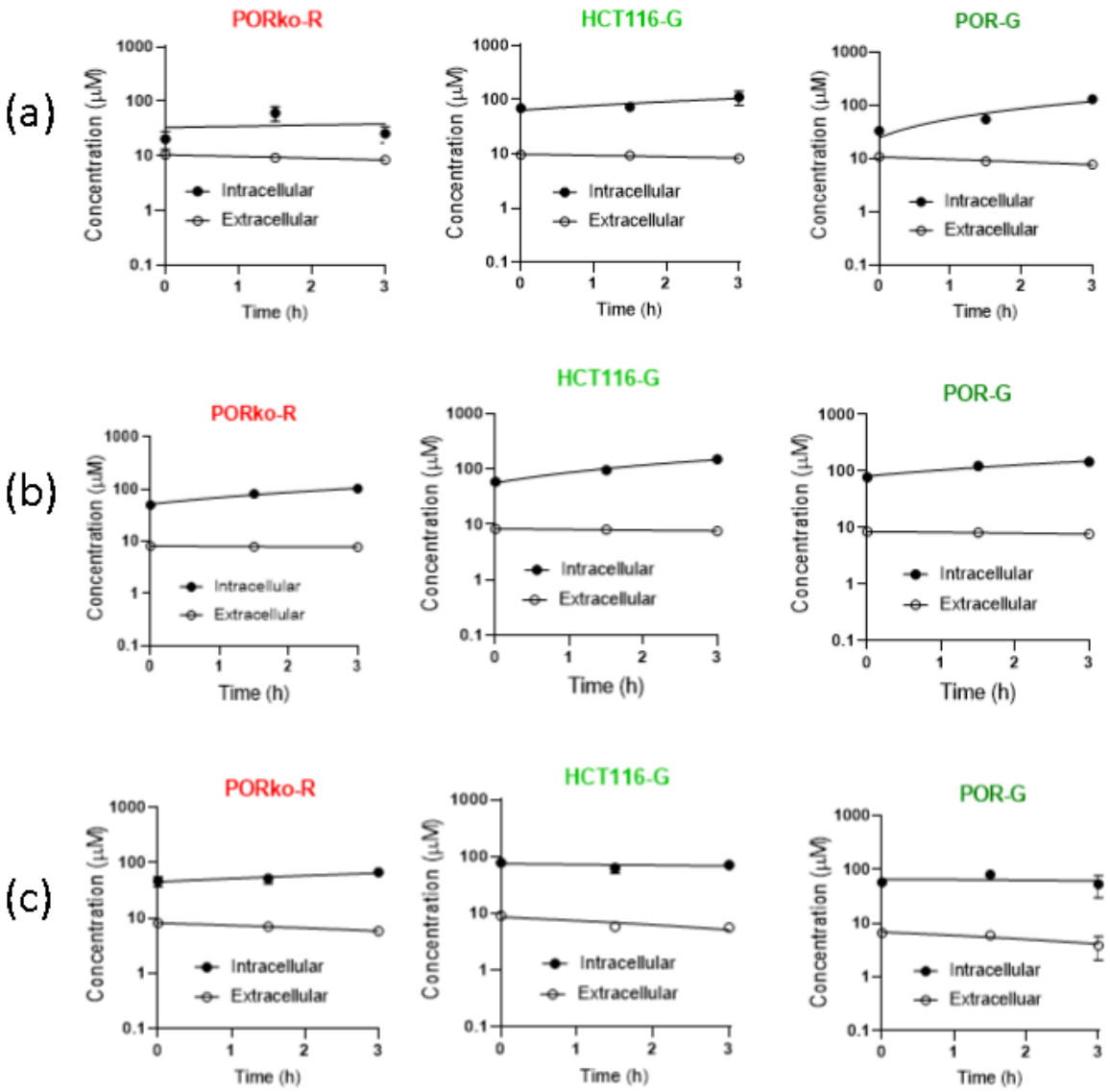

Figure 3.4: Intracellular and extracellular concentrations of SN39536 in PORko-R, HCT116-G and POR-G cells under oxia in three independent experiments (a), (b) and (c). *5 x 10^5 cells/0.5 mL were incubated for 2 h for cell attachment and exposed to 10 μM of SN39536. Plates were incubated for 0 h, 1.5 h or 3 h before intra- and extracellular samples were processed and analysed by LC-MS. Mean and SE are from 3 biological replicates.*

Metabolism assays were carried out in three cell lines; PORko-R, HCT116-G and POR-G treated with 10 μM SN39536 for 0 h, 1.5 h or 3 h under oxia (**Figure 3.4:**). The initial extracellular concentrations of SN39536 were approximately 10 μM for each of the cell lines and these concentrations appeared to decrease slightly over the time course of the experiment.

The intracellular concentrations of SN39536 were ca. 10-fold higher than the corresponding extracellular concentrations in all three cell lines (**Figure 3.4:**), except in PORko-R cells in **Figure 3.4:** a which have lower intracellular concentrations than expected across all three time points, despite having similar extracellular concentrations as HCT116-G and POR-G cells (approximately 10 μM).

The intracellular concentrations in all three cell lines showed more variation than the extracellular concentrations (**Figure 3.4**), indicating that there could have been procedural problems during intracellular processing. Most of the figures for the three cell lines illustrate

a rapid uptake of almost 10-fold to give intracellular concentrations of close to 100 μM. Continued, but smaller increases in intracellular concentrations were observed over the time course of the experiment. This data indicates that there was rapid uptake into cells with a steady state being established within the time course of the experiment.

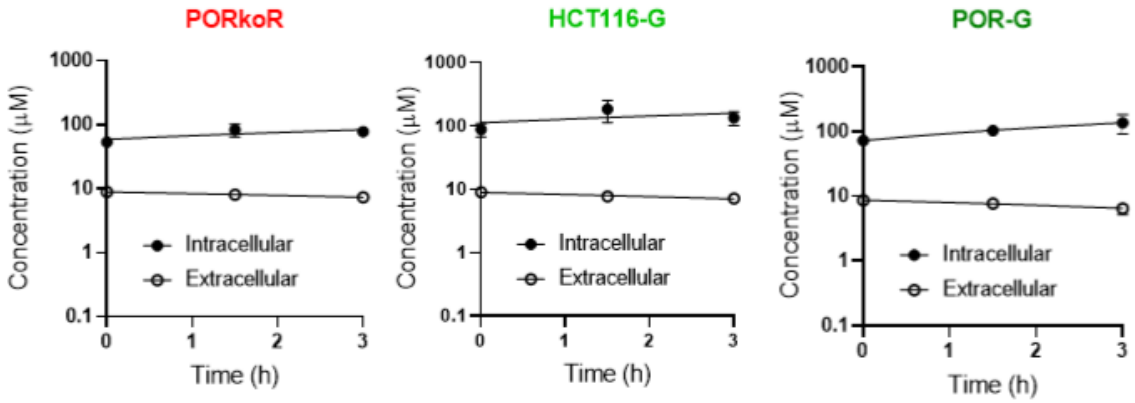

Figure 3.5: Average intracellular and extracellular concentrations of SN39536 in PORko-R, HCT116-G and POR-G cells under oxia from the three independent experiments (a), (b) and (c) in Figure 3.4: *. Cells were incubated for 2 h for cell attachment and then exposed to 10 µM of SN39536 and incubated for 0 h, 1.5 h or 3 h before intra- and extracellular samples were taken and analysed by LC-MS. Mean and SE are from 3 independent experiments.*

When the uptake experiments were averaged for each of the cell lines (**Figure 3.5**) from three independent experiments shown in (**Figure 3.4**), the initial extracellular concentration of SN39536 was close to 10 μM in all three cell lines with slight decreases observed over the time course. Initial intracellular concentrations were ca 8–10-fold higher at ca. 100 μM, with small observable increases thereafter (**Figure 3.5**).

When averaged, the ratio of the intracellular concentration (Ci) and the extracellular concentration (Ce), (Ci/Ce), across the three time points for POR-G was 9.3, for HCT116-G it was 12.9 and for PORko-R it was 8.94. Because the extracellular concentrations between the three cell lines were so similar (**Figure 3.5**), the lower PORko-R Ci/Ce ratio indicates lower cellular uptake; ca. 1.5-fold lower than POR-G and ca. 2-fold lower than HCT116-G. As mentioned previously, this could be due to procedural errors in intracellular processing that lead to low intracellular concentrations in PORko-R (**Figure 3.4:** a), which brings the average Ci/Ce down.

The intracellular concentrations and extracellular concentrations in the processed samples were totalled for all three experiments (**Figure 3.4:**) and averaged to determine if the SN39536 was stable in cells over the time frame of the experiment (**Figure 3.6**).

The total concentration of SN39536 decreased slightly over time when SN39536 was added to PORko-R, HCT116-G and POR-G cells, but there was no significant difference between 0 h and 3 h ($p > 0.05$, one-way ANOVA)(**Figure 3.6**). Previous work by ACSRC staff has also confirmed that SN39536 is stable in culture medium (98.5%) containing 5 % FCS over 24 h.

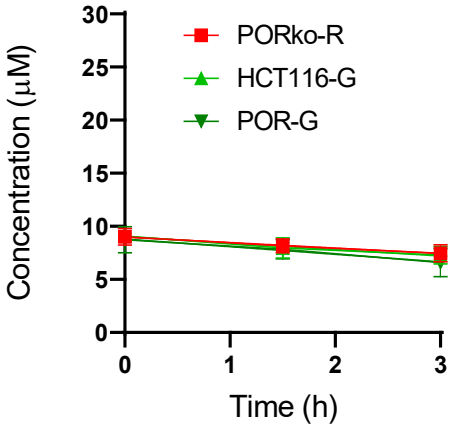

Figure 3.6: Average of the total intracellular and extracellular concentrations of SN39536 in PORko-R, HCT116-G and POR-G cells under oxia from three independent experiments. *Cells were incubated for 2 h for cell attachment and then exposed to 10 µM of the effector SN39536 for 0 h, 1.5 h or 3 h before intra- and extracellular samples were taken and analysed by LC-MS. Mean and SE are from 3 independent experiments.*

3.3.4 Investigation of the Stability and Metabolic Activation of SN39884 under Oxia

We evaluated the stability of the prodrug SN39884 under oxic conditions in culture medium (**Figure 3.7**). When 10 µM SN39884 was added to extracellular medium the concentration of SN39884 remained constant over three hours and a trace of SN39536 was detected. A low concentration of SN39536 is consistent with the previously observed effector impurity (0.90%) in the prodrug demonstrated in the initial purity analysis of SN39884 (See Chapter 2.2). This shows that SN39884 is stable in culture medium at 37 °C under oxic conditions.

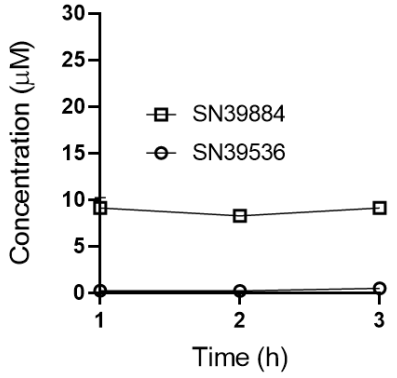

Figure 3.7 Average concentration of SN39884 and SN39536 in culture medium under oxic conditions. *10 µM SN39884 was added to culture medium for 0 h, 1.5 h or 3 h at 37 °C and concentrations were measured by LC-MS. Mean and SE are from 2 independent experiments.*

We then evaluated the stability of the prodrug SN39884 under oxic conditions in cells (**Figure 3.8**). Ideally, the HAP should be chemically stable in aqueous media and also should not undergo oxygen-insensitive reduction in cells. We conducted two replicates measuring intracellular and extracellular concentrations of prodrug SN39884 (**Figure 3.8**a) and

(Appendix 1) and intracellular and extracellular concentrations of the corresponding DNA-PK inhibitor SN39536 (**Figure 3.8**b) and (Appendix 1).

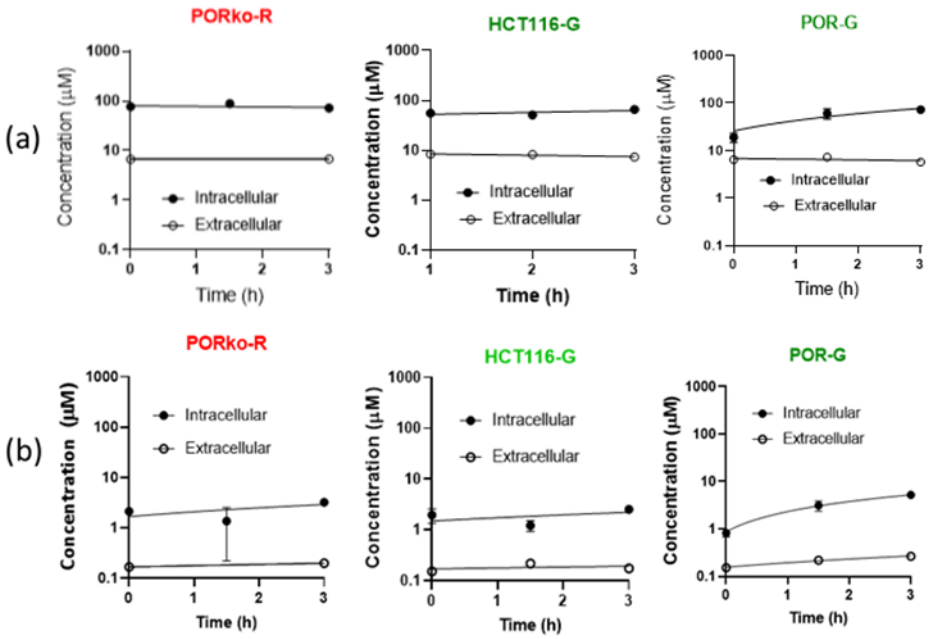

Figure 3.8: Intracellular and extracellular concentrations of SN39884 (a) and SN39536 (b) in PORko-R, HCT116-G and POR-G cells under oxia in one independent experiment (a and b). *Cells were incubated for 2 h for cell attachment and then exposed to 10 µM of SN39884 for 0 h, 1.5 h or 3 h before samples were taken and analysed by LC-MS. Mean and SE are from ≥ 2 biological replicates. Due to sample losses during the covid-19 lockdown extracellular concentration at 1.5 h in PORko-R cells (a,b) could not be measured.*

There was a rapid uptake of SN39884 into cells for each of the three cell lines. The average Ci/Ce ratios of SN39884 over 3 h were 11.1 ± 0.4 for PORko-R, 8.9 ± 0.3 for HCT116-G and 8.0 ± 2.8 for POR-G. This shows that the three cell line variants all had similar cellular uptakes of SN39884 under oxia.

Extracellular concentrations of SN39884 in all three cell lines in the first experiment (**Figure 3.8a**) were stable at the first two time points (0 h and 1.5 h). The intracellular SN39884 concentrations remained stable across the three cell lines, except in the POR-G cells in (**Figure 3.8a**), where the intracellular concentration of SN39884 at the 0 h time point is 19 μM, but the concentration increased at the later time points in 1.5 h (60 µM) and 3 h (73 µM) (**Figure 3.8a**).

However, in the second experiment (Appendix 1) the extracellular concentrations of SN39884 were close to 2 µM at the initial timepoint and decrease slightly over the time course of the experiment in all three cell lines. As the nominal concentration of drug added was 10 μM, the difference in extracellular SN39884 concentration (**Figure 3.8a**) and (Appendix 1a) indicates something occurred during drug addition or processing of samples that resulted in lower extracellular concentrations. As these samples were kept over the covid lockdown period (ca. 14 weeks) before being analysed by LC-MS, some of methanol extracts evaporated , this could have affected the standard curves that were generated resulting in apparent low concentrations (Appendix 1). Procedural errors such as in drug dilution could have resulted in less SN39884 being added at the 0 h time point.

The initial concentrations of the effector SN39536 (**Figure 3.8b**) were low and consistent with the previously observed effector impurity (0.90%) in the prodrug demonstrated in the initial purity analysis of SN39884 (See Chapter 2.2). The extracellular concentrations remained stable at around 0.1 μM and intracellular concentrations at approximately 1 μM (**Figure 3.8**). This shows that SN39884 was not being converted to significant levels of SN39536 in PORko-R and HCT116-G cells. However, POR-G cells demonstrated a slight increase in intracellular concentration of SN39536, which at 1.5 h is 3.21 μM and at 3 h is 5.21 μM in one experiment (**Figure 3.8b**) compared to the other two cell lines. There was a rapid uptake of SN39536 into cells for each of the three cell lines. The average Ci/Ce ratios of SN39536 over 3 h were 9.4 ± 1.8 for PORko-R, 8.1 ± 1.1 for HCT116-G and 8.1 ± 4.0 for POR-G. This shows that cellular uptake of SN39536 is similar in these cell lines.

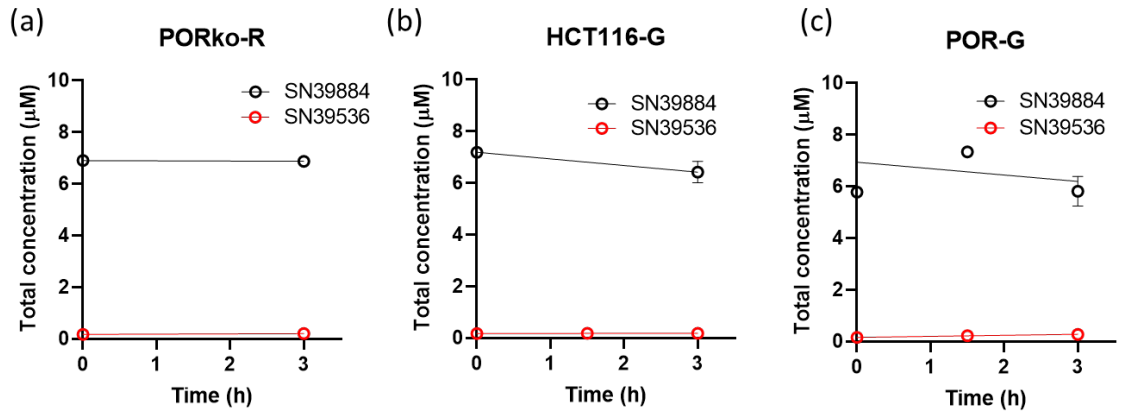

Figure 3.9: Total concentrations of SN39884 or SN39536 in PORko-R, HCT116-G and POR-G cells under oxia. *Cells were incubated for 2 h cell attachment and exposed to 10 µM SN39884 under oxia. Drug concentrations were measured by LC-MS. Intracellular and extracellular concentrations in (**Figure 3.8**) were summed. Mean and SE are from ≥ 2 biological replicates, except SN39536 and SN39884 concentrations at 1.5 h in HCT166-G and 0 h in POR-G (n=1) respectively.*

Total intra- and extracellular concentrations of SN39884 remained stable in PORko-R cells, but decreased slightly in HCT116-G and POR-G cells (**Figure 3.9**). Total SN39536 concentrations were very low when SN39884 was added to cells under oxia, but concentrations of SN39536 increased in POR-G cells from 0.15 to 0.27 µM over three hours (**Figure 3.9**), suggesting that POR overexpression may contribute to oxygen-insensitive activation of SN39884. However, due to loss of samples during the lockdown and the discrepancy between the initial prodrug concentrations in the two independent experiments (**Figure 3.8** and Appendix 1) we need to repeat this experiment to explore this hypothesis.

3.3.5 Investigation of the Stability and Metabolic Activation of SN39884 under Anoxia

We analysed the metabolism of the prodrug SN39884 and release of the effector SN39536 under anoxic conditions (**Figure 3.10**), (**Figure 3.11**).

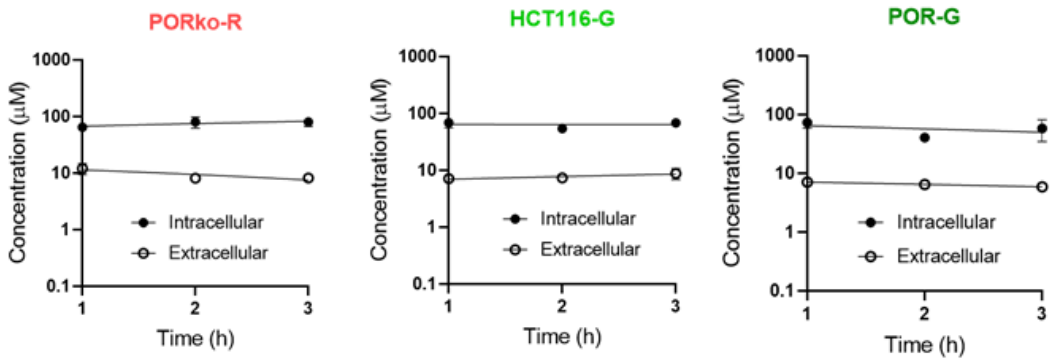

Figure 3.10: Average intracellular and extracellular concentrations of SN39884 in PORko-R, HCT116-G and POR-G cells under anoxia from the two independent experiments Appendix 2 (a) and (c). *Cells were incubated for 2 h for cell attachment and then exposed to 10 μM of the effector SN39884 for 0 h, 1.5 h or 3 h before samples were taken and analysed by LC-MS. Mean and SE are from 2 independent experiments.*

When averaged, the concentration of SN39884 under anoxia (**Figure 3.10**) from the two independent experiments (**Appendix 2**), showed there was a rapid uptake of SN39884 in all three cell lines. The Ci/Ce ratios of SN39884 remained constant over 3 h (8.34 for PORko-R, 8.25 for HCT116-G and 8.80 for POR-G) (**Figure 3.10**). This shows that the three cell line variants all had similar cellular uptakes of SN39884 under anoxia.

There was an increase in intracellular concentrations of SN39536 for each cell line, with PORko-R concentration at 1 h of 5.23 μM, HCT116-G concentration at 1 h of 6.29 μM and POR-G concentration at 1 h of 25.89 μM (**Figure 3.11**). The extracellular concentrations also increased over time (**Figure 3.11**) around approximately 1 μM, but in HCT116-G, concentration was skewed at 3 h by the outlier value from (**Appendix 2d**). The extracellular concentration of SN39536 were highest in POR-G and lowest in PORko-R, following the trend observed for the intracellular concentrations (**Figure 3.11**).

The Ci/Ce ratios of SN39536 were 14.08 for PORko-R, 21.60 for HCT116-G and 20.71 for POR-G and therefore uptake of SN39884 was similar across HCT116-G and POR-G cells, but slightly lower in PORko-R (**Figure 3.11**).

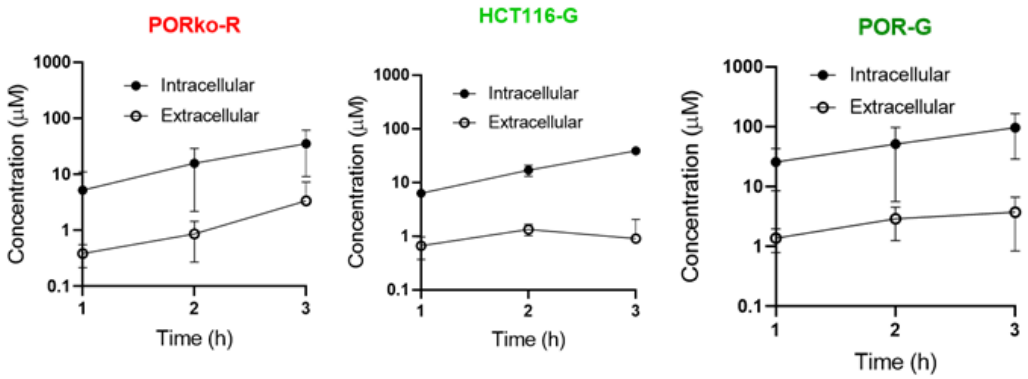

Figure 3.11. Average intracellular and extracellular concentrations of SN39536 in PORko-R, HCT116-G and POR-G cells under anoxia from the two independent experiments Appendix 2 (b) and (d). *Cells were incubated for 2 h for cell attachment and then exposed to 10 μM of the effector SN39884 for 0 h, 1.5 h or 3 h before samples were taken and analysed by LC-MS. Mean and SE are from 2 independent experiments.*

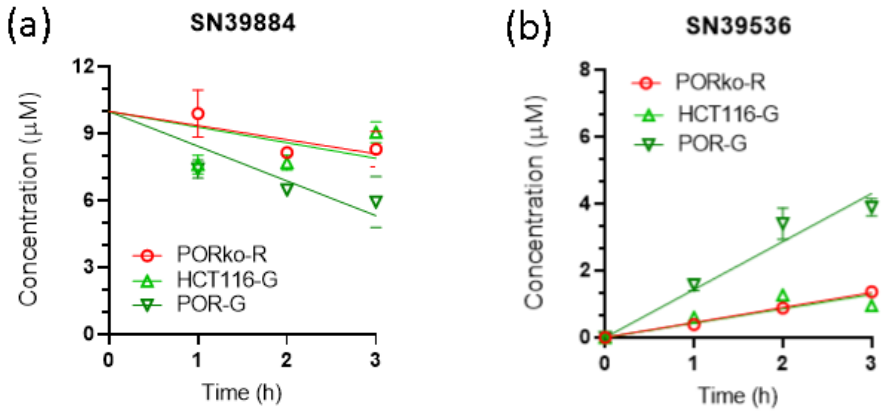

Figure 3.12 Average total concentration of SN39884 (a) and SN39536 (b) in PORko-R, HCT116-G and POR-G cells under anoxia from the two independent experiments in (Appendix 2). *Cells were incubated for 2 h for cell attachment under anoxia and then exposed to 10 μM of the effector for 1 h, 2 h or 3 h before samples were taken and analysed by LC-MS. Intracellular and extracellular concentrations of SN39884 (**Figure 3.10**) and SN39536 (**Figure 3.11**) were summed. Mean and SE are from 2 independent experiments.*

The average total concentration of SN39884 under anoxic conditions (***Figure 3.12***a) shows that SN398884 drug concentration decreased over time from the 10 μM concentration that was added. POR-G had the largest decrease, which went down to approximately 6 μM, and we see a corresponding increase in SN39536 concentration in POR-G cells to 4 μM at the 3 h time point (***Figure 3.12***b). This is approximately 2.84 and 4.07-fold higher than the concentration of SN39536 at the 3 h timepoint in PORko-R and HCT116-G cells, respectively (***Figure 3.12***b). This demonstrates the conversion of SN39884 to SN39536 under anoxic conditions, and shows that POR significantly increases the rate of SN39884 metabolism.

The concentrations of SN39884 and SN39536 in PORko-R and HCT116-G cells were very similar at all time points (**Figure 3.12**). This shows that POR knockout had no effect on the rate of metabolism of SN39884 and therefore other reductases have a role in metabolism of SN39884 under anoxia.

3.4 Discussion

This chapter uses LC-MS analytical methods to quantify the intracellular and extracellular concentrations of the newly developed prodrug SN39884 and the corresponding DNA-PKi effector SN39536 to investigate their chemical stability in culture medium, cellular metabolism of SN39884 to SN39536 under oxic and anoxic conditions and cellular uptake in HCT116 cells with varying POR expression levels. This experimental procedure had previously been employed by (Wong et al., 2019) to investigate the metabolic activity and cellular uptake of the prodrug SN38023 and its corresponding DNA-PK inhibitor IC87361.

Previous studies have shown that POR plays a major role as a reductase in the metabolism of tirapazamine, SN30000 and PR104A (Su et al., 2013) (Francis W. Hunter et al., 2015). (Su et al., 2013) showed that concentration of the metabolites from the reduction of prodrugs PR104A and SN30000 were significantly higher in POR overexpressing cells under anoxia. Therefore cell lines that overexpress POR, or do not have functional POR, provide valuable tools to assess the POR dependence of metabolism of HAPs such as SN39884. The HCT116 cell variants had been previously used to investigate the effects of POR expression on metabolic activity of hypoxia activated prodrugs (C. R. Hong, Bogle, et al., 2018; Su et al., 2013).

SN39536 was stable in culture medium and cells under oxic condition. When cells were exposed to SN39884 under oxia, there was a slight decrease in SN39884 in HCT116-G and POR-G cells (**Figure 3.9**). However, concentrations of SN39536 remained very low over 3 h under oxia compared to anoxic conditions (**Figure 3.12**) and this was consistent with the previously observed effector impurity (0.90%) in the prodrug. We plan to repeat this experiment to confirm whether POR overexpression contributes to oxygen-independent activation of SN39884.

When SN39884 was added to cells under anoxia concentrations of SN39536 were higher in POR-G cells compared to HCT116-G and PORko-R cells under anoxia, indicating that SN39884 is a substrate for POR. (Su et al., 2013) has shown that knocking out POR only had a minor change in the anoxic reductive metabolism of PR-104A and SN30000. Consistent with this, POR knockout had no effect on metabolism of SN39884 under anoxia (**Figure 3.12**), suggesting that there are other reductases that can activate SN39884. (Wong et al., 2019) found that conversion of SN38023 in HCT116 cells overexpressing POR was 8-fold faster than parental HCT116 cells under anoxia, whereas we saw that SN39536 concentrations in HCT116-G were only 4.07-fold lower than POR-G at the 3 h time point. This further supports that SN39884 activation is less reliant on POR compared to other HAPs.

(Wong et al., 2019) investigated the cellular metabolism of the prodrug SN38023 and DNA-PKi effector IC87361 in the same cell lines we tested in this project and they found very high cellular uptake of both SN38023 and IC87361. Intracellular concentrations of SN38023 and IC87361 in HCT116 cells were ~ 75- and 179-fold higher than extracellular concentrations, respectively, at the 4 h time point. This indicates that there is considerable intracellular entrapment of the effector and IC87361 cannot readily diffuse from the cells where it is produced. (C. R. Hong et al., 2021) has shown that high intracellular binding of drug decreases penetration of the drug through layers of cells using a multicellular layers (MCLs) model. This infers that diffusion of SN38023 into hypoxic zones will be highly compromised by this sequestration in cells. (Wong et al., 2019) also conducted an experiment where they added IC87361 itself to HCT116-G cells under anoxia and their data shows that there was an

approximately 400-fold difference between intracellular and extracellular concentrations at the 3 h time point.

In this project we also measured intracellular and extracellular concentrations in order to investigate the extent of intracellular uptake of SN39884 and SN39536. There was a rapid uptake of SN39536 and SN39884 and the cellular uptake of SN39884 and SN39536 was approximately around 8-10-fold (Ci/Ce ratio) in PORko-R, HCT116-G and POR-G. This suggests that SN39884 can produce more efficient bystander effects than SN30823. This bystander effect is considered to be particularly important for the activity of HAPs to overcome limited delivery of prodrugs and the spatial heterogeneity of their activation in tumours (Singleton et al., 2021). It would be interesting to investigate whether SN39884 has more efficient bystander effects than SN38023 in the future using the 3D spheroid co-culture model (Wong et al., 2019).

In conclusion, SN39884 was selectively activated under hypoxia to release SN39536. POR could metabolise SN39884 under hypoxia, but SN39884 was less reliant on POR for activation and there were other reductases that could activate SN39884. SN39536 also appeared to diffuse out of cells more quickly than IC87361, and therefore SN39884 could potentially lead to increased bystander effects, and greater antitumour activity.

4 Chapter 4. Radiation Growth Inhibition by SN39884 and SN39536

4.1 Introduction:

The desired cytotoxicity profile of a DNA-PK inhibitor being developed in the context of radiotherapy requires the inhibitor to have low cytotoxicity without radiation, but to potently sensitise tumour cells to the effect of radiation. For effective Hypoxia Activated Prodrugs (HAPs) of DNA-PK inhibitors, the HAP should demonstrate low cytotoxicity under oxic conditions, both alone, and in combination with radiation. Under anoxic conditions, the HAP should undergo activation to release the DNA-PK inhibitor which should also display low toxicity under anoxic conditions as a single agent, but provide potent sensitisation of radiation.

Researchers at the ACSRC have adapted a regrowth assay format to be able to screen large numbers of compounds in a short time using a 96-well plate format and select compounds for further *in vitro* and *in vivo* testing. This assay was used to determine the cell regrowth after irradiation with drug exposure of the previously developed HAP SN38023 and its corresponding DNA-PK inhibitor IC87361 to evaluate their radiosensitising capability (Wong et al., 2019).

The half-maximal inhibitory concentration, (IC_{50}) is an *in vitro* measure that is used to evaluate the concentration of drug required to inhibit a biological effect by 50%; indicating the potency of an antagonist drug (Aykul & Martinez-Hackert, 2016). IC_{50} assays are commonly used in the anti-cancer drug discovery field as a high throughput screening method to evaluate drug potency and identify lead compounds. The assay is relatively quick; cells are grown for 4 days after treatment exposure, which is enough time for the cells to divide several times. In addition, the analysis of results is straightforward through the use of a colorimetric endpoint to measure cell density. Colorimetric assays are rapid and therefore frequently used in chemosensitivity testing using *in vitro* tumour cell lines. Many variations in the stains have been utilised, such as methylthiazoldiphenyl tetrazolium (MTT) dye (Keepers et al., 1991).

The density of cell growth in this chapter will be determined using Sulforhodamine B (SRB) staining, as used in (Wong et al., 2019). SRB staining is often used to determine cell density as a measure of cytotoxicity (Vichai & Kirtikara, 2006). SRB is a protein dye that binds to protein basic amino acid residues of trichloroacetic acid fixed cells (Voigt, 2005), and the absorbance is measured with a microplate reader. SRB has high sensitivity when compared to other conventional stains (Vichai & Kirtikara, 2006) and better linearity with cell number than the MTT dye (which is reliant on mitochondrial activity), while also shown to not stain cellular debris (Keepers et al., 1991). Therefore, SRB assays are suitable for large-scale drug screening applications and are highly reproducible (Voigt, 2005), although this depends on maintaining a good single cell suspension.

Although the (IC_{50}) antiproliferative assay measures inhibition of cell growth, it does not directly measure cell death, and does not differentiate between proliferating cells and non-proliferating cells. Therefore, the decreased cell number observed after exposure to drug could be due to either increased cell death or inhibition of cell proliferation (Berrouet, Dorilas, Rejniak, & Tuncer, 2020).

In this chapter we have utilised the IC_{50} growth assay to determine the amount of drug required to inhibit cell growth by 50%, with or without irradiation; thus giving a measure of

cytotoxicity of the prodrug SN39884 and effector SN39536 as well as radiosensitisation by the prodrug SN39884 and effector SN39536 under oxic and anoxic conditions. We used HCT116 cells with differential expression of POR (HCT116-G, PORko-R and POR-G) as for the metabolism studies in Chapter 3. We found that overexpression of POR increased activation of SN39884 by ca. four-fold under hypoxia. In this chapter we will investigate the effect of POR on radiosensitisation by SN39884 under oxic and anoxic conditions.

4.2 Aims:

The overall aim of this chapter was to investigate the radiosensitisation of SN39536 and SN39884 under oxic and anoxic conditions. The first objective was to determine the optimal cell density and radiation dose to be within the linear range of the calibration curve. The second objective was to investigate the level of radiosensitisation of SN39884 and SN39536 in human colorectal carcinoma HCT116 cells, under oxic and anoxic conditions. The role of POR in radiosensitisation by SN39884 was also explored using HCT116 cells that differ in POR expression (POR-G, PORko-R and HCT116-G). SRB staining was used to quantify cell regrowth after exposure.

1. To optimise radiation regrowth assay by identifying appropriate cell seeding density of PORko-R, HCT116-G and POR-G cells and the radiation dose that are within the linear range of the calibration curve.
2. To investigate radiosensitisation by SN39536 under oxic conditions.
3. To investigate radiosensitisation by SN39884 under oxic and anoxic conditions
4. To investigate the effect of POR on radiosensitisation by SN39884 under oxic and anoxic conditions.

4.3 Results:

4.3.1 Optimisation of Radiation Regrowth Assay

The radiation regrowth assay protocol developed by (Wong et al., 2019) for testing the radiosensitisation effect of the DNA-PK inhibitor IC87361 was used in this study to determine the cell regrowth after exposure to radiation and the novel HAP SN39884 and its DNA-PKi effector SN39536 under oxic and anoxic conditions.

Firstly, we tested if the methods described in (Wong et al., 2019) were ideal for estimating optical cell density for PORko-R, HCT116-G and POR-G cells after irradiation. To accurately measure cell density, the optical density should be linearly related to cell counts. Furthermore, each 96-well should be seeded with an appropriate cell number to ensure that cell growth is in the exponential phase during the experiment and radiosensitisation is not affected by high confluency (stationary phase).

Previous work by Ms Way Wong at ACSRC has shown that cell numbers producing absorbances between 0.1-0.5 is within the linear range of the calibration curve and is ideal for accurate IC_{50} estimation. Therefore, we investigated if the initial cell seeding density used in (Wong et al., 2019) fell within this range after irradiation.

We first used a similar cell density (1000 cells/well for PORko-R and POR-G and 400 cells/well for HCT116-G) with a 3 Gy radiation dose as described in (Wong et al., 2019) in our pilot experiment using SN39536 under oxia (**Figure 4.1**). The SRB absorbance was above 0.1 in

unirradiated plates, but 3 Gy irradiation alone resulted in absorbances < 0.1, suggesting that either, the cell density needs to be higher, or the radiation dose needs to be lowered (**Figure 4.1**).

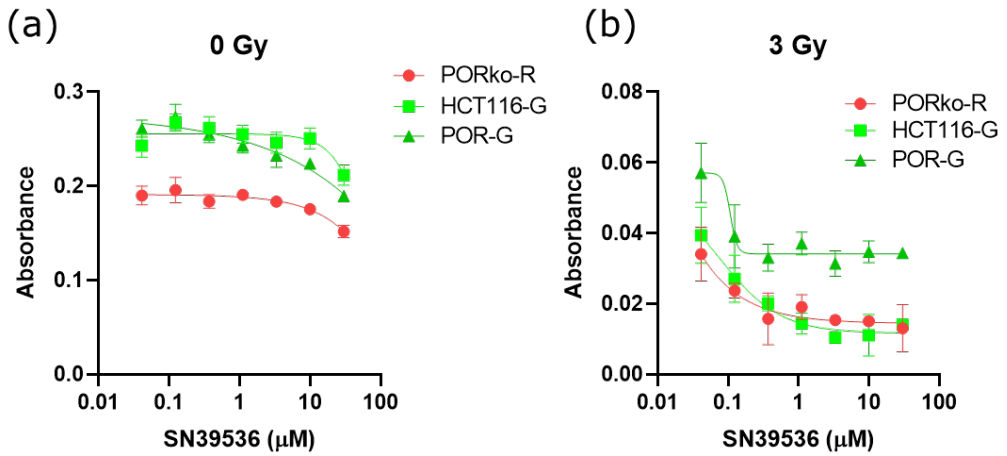

Figure 4.1: SRB absorbance per cell plated for unirradiated (a) and 3 Gy (b) treated wells. *1000 cells/well for PORko-R and POR-G cells and 400 cells for HCT116-G cells were seeded in 96-well plates. After 2 h incubation, cells were exposed to SN39536 under oxia for 3 h before, during and for 24 h after 0 Gy (a) and 3 Gy (b) irradiation. After 4 days incubation, cells were stained with SRB to determine optical density. Mean and SE are from 3 biological replicates.*

In the subsequent experiment, we compared the absorbance in the plates seeded at 1500 and 3000 cells/well for PORko-R and POR-G cells, and 600 and 1200 cells/well for HCT116-G cells at 4 days after 0, 2 and 3 Gy irradiation without drug treatment. The absorbance was higher in the plates seeded at higher initial cell seeding number as expected (**Figure 4.2** a and b). The plates seeded at lower cell seeding density (**Figure 4.2**a) showed the absorbance was less than 0.1 for PORko-R and HCT116-G cells after 2 Gy irradiation and the absorbance was lower than 0.1 in all three cell lines after 3 Gy treatment. The plates seeded at higher cell density (**Figure 4.2**b) showed the absorbance between 0.1-0.5 after 2 Gy irradiation in all 3 cell lines, but not after 3 Gy treatment. Overall, these results suggest that the higher cell density of 3000 cells/well for PORko-R and POR-G cells and 1200 cells/well for HCT116-G are ideal for investigating radiosensitisation by SN39536 and SN39884 after 2 Gy irradiation.

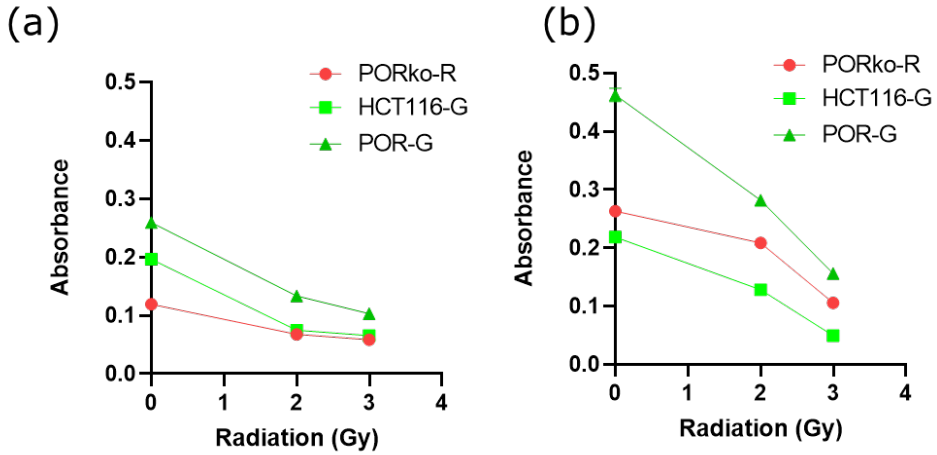

Figure 4.2: SRB absorbance per cell plated treated with 0, 2 or 3 Gy radiation only. *(a) 1500 cells for PORko-R and POR-G, 600 cells/well for HCT116-G. (b) 3000 cells/well for PORko-R and POR-G, 1200 cells/well for HCT116-G. n=3 biological replicates.*

The regrowth fraction was determined as the ratio of the absorbance for irradiated/unirradiated cells to determine the effect of radiation alone. We observed that 2 Gy irradiation reduced the cell density to 48.8 ± 3.01% and 50.9 ± 3.6% in the 3 cell lines when seeded at low (a) and high (b) cell seeding densities, respectively (**Figure 4.3** a and b). The higher radiation dose of 3 Gy resulted in a reduction of cell density to 40.8 ± 2.3 % (**Figure 4.3**a) and 32.1 ± 2.6 % (**Figure 4.3**b) in the 3 cell lines which was a minor decrease in the absorbance from 2 Gy to 3 Gy when seeded at lower cell density.

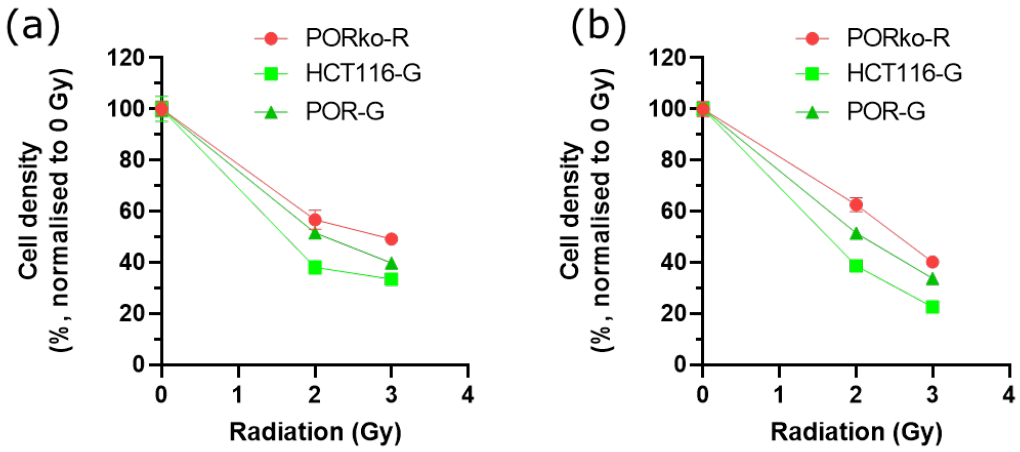

Figure 4.3: SRB absorbance per cell treated with 0, 2 or 3 Gy radiation only, data from (Figure 4.2) normalised to 0 Gy. *(a) 1500 cells for PORko-R and POR-G, 600 cells/well for HCT116-G. (b) 3000 cells/well for PORko-R and POR-G, 1200 cells/well for HCT116-G. n=3 biological replicates.*

4.3.2 Radiosensitisation by SN39536 under oxia

The effect of SN39536 was determined as a single agent and in combination with 2 Gy of radiation in the cell line panel (**Figure 4.4**). When used as a single agent SN39536 displayed low toxicity with a small decrease in cell density at 10 µM. This effect was consistent in each of the HCT116 cell lines.

Radiation alone at 2 Gy reduced cell viability to 72.6 ± 4.7%, 54.1 ± 3.2% and 65.4 ± 5.4 % in PORko-R, HCT116-G and POR-G cells, respectively. This difference was not statistically significant (p=0.166). The Regrowth Fraction was determined as the ratio of the absorbance for drug-treated/non-drug treated cells at each radiation dose to normalise for the effect of the radiation alone. SN39536 produced clear concentration-dependent radiosensitisation in each of the cell lines with similar IC_{50} values suggesting that radiosensitisation by SN39536 is independent of POR expression (**Table 4.1**).

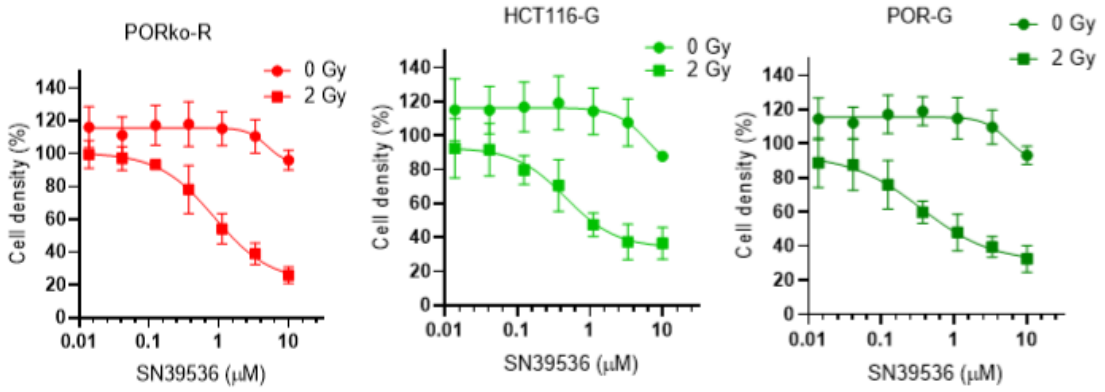

Figure 4.4: Cell density, normalised to 0 µM SN39536 controls, after treatment with differing concentrations of SN39536 with or without 2 Gy radiation. *Cells were incubated for 2 h for cell attachment and then exposed to serial dilutions of 10 µM of the effector SN39536, and irradiated at 2 Gy, 3 h later. Cells were incubated for 24 h before media was replaced with fresh media. After 4 days the cells were stained with SRB to determine density. Mean and SE are from 3 biological replicates.*

Table 4.1: Average IC_{50} values of SN39536 under oxia in cells exposed to 2 Gy radiation in (Figure 4.4), n=3 biological replicates.

SN39536 Oxia 2 Gy	Average IC_{50} (µM)	S.E.
PORko-R	1.52	0.383
HCT116-G	1.07	0.315
POR-G	1.43	0.855

4.3.3 Radiosensitisation by SN39884 under oxia

Next, we evaluated the radiosensitisation of SN39884 under oxia (**Figure 4.5**). The cell density did not decrease with increasing concentrations of SN39884, but at the highest concentration of 10 µM SN39884, there was a sharp drop in cell density by ~20% in both irradiated and non-irradiated cells. This shows that the prodrug does have some cytotoxicity at higher drug concentrations above 10 µM, but that the consistency of this effect across the cell line panel suggests this effect is unlikely to be a result of metabolism of SN39884 by POR under oxia. Similarly, SN39884 produced no additional cytotoxicity in the presence of 2 Gy of radiation across the cell line panel. There was a similar drop in cell density at 10 µM of SN39884. This data suggests that SN39884 is not undergoing significant metabolism under oxic conditions to release SN39536.

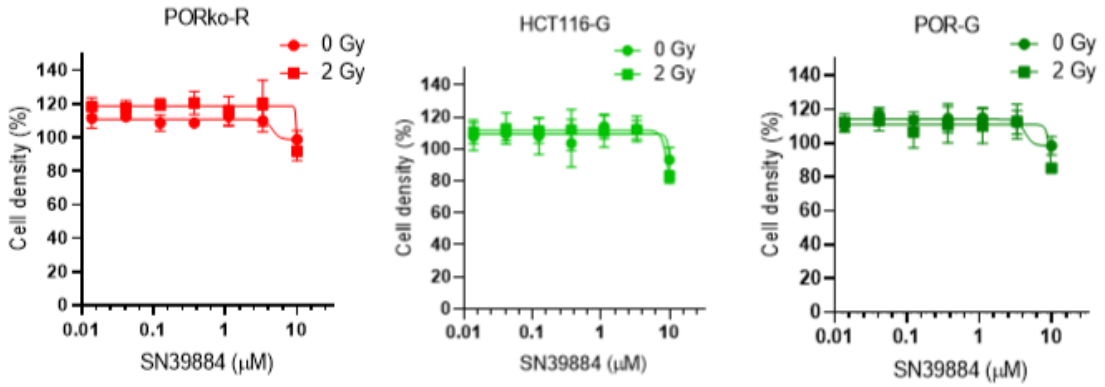

Figure 4.5: Cell density, normalised to 0 µM SN39884 controls, after treatment with differing concentrations of SN39884 with or without 2 Gy radiation. *Cells were incubated for 2 h for cell attachment and then exposed to serial dilutions of 10 µM of the effector SN39884, and irradiated at 2 Gy, 3 h later. Cells were incubated for 24 h before media was replaced with fresh media. After 4 days the cells were stained with SRB to determine density. Mean and SE are from 3 biological replicates.*

Table 4.2: Average IC_{50} values of SN39884 under oxia in cells exposed to 2 Gy radiation in (Figure 4.5), n=3 biological replicates.

SN39884 Oxia	0 Gy Average IC_{50} (µM)	2 Gy Average IC_{50} (µM)
PORko-R	>10	>10
HCT116-G	>10	>10
POR-G	>10	>10

4.3.4 Radiosensitisation by SN39884 under anoxia

Lastly, the radiosensitisation with SN39884 under anoxic conditions was investigated. Under anoxic conditions a higher dose of radiation (4.6 Gy) was required to induce similar growth inhibition compared to 2 Gy under oxia. The optical cell density after 4.6 Gy alone under anoxia was 70.7 ± 3.4%, 58.0 ± 0.9 % and 69.9 ± 1.4% for PORko-R, HCT116-G and POR-G, respectively; similar to 2 Gy alone (oxia) (See Section 4.3.2). The differences between PORko-R and HCT116, and between POR-G and HCT116-G, were statistically significant (p=0.018 and p=0.023, respectively). Treatment with SN39884 alone was tolerated up until ca. 10 µM where growth inhibition was observed across the cell line panel (Figure 4.6). In contrast, SN39884 did inhibit cell growth in combination with radiation under anoxia. HCT116-G cells showed the lowest IC_{50} for SN39884 with PORko-R cells being the most resistant (Table 4.3). Unfortunately, one experiment did not reach IC_{50} (the data in Fig 4.6 is from two experiments and so we cannot determine whether this difference is significant).

Treatment of PORko-R cells with SN39884 and 4.6 Gy under anoxia reduces the cell density to approximately 50% at 10 µM. The calculated IC_{50} value in PORko-R cells is the highest at 9.8 µM, which is similar to the SN39884 IC_{50} values under oxia (Table 4.2). This is consistent with a lower rate of conversion from SN39884 to SN39536 in the absence of POR, and also shows that other reductases have the ability to convert SN39884 to SN39536 under anoxia to produce a radiosensitising effect – although not as strongly as with POR, as we saw in Chapter 3. The level of cell growth inhibition observed in HCT116-G cells and POR-G cells implies that radiosensitisation is not strongly affected by POR overexpression. The IC_{50} value for SN39884 in HCT116-G under anoxia is 2.4 µM and in POR-G it is 4.8 µM.

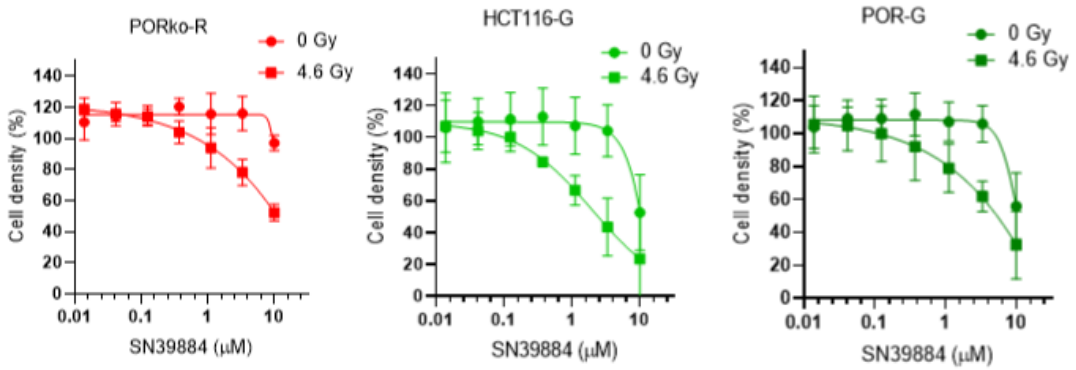

Figure 4.6: Cell density, normalised to 0 µM SN39884 controls, after treatment with differing concentrations of SN39884 with or without 4.6 Gy radiation under anoxia. *Cells were incubated for 2 h for cell attachment and then exposed to serial dilutions of 10 µM of the effector SN39884, and irradiated at 2 Gy, 3 h later. Cells were incubated for 24 h before media was replaced with fresh media. After 4 days the cells were stained with SRB to determine density. Mean and SE are from 2 biological replicates.*

Table 4.3: Average IC_{50} values of SN39884 under anoxia in cells exposed to 4.6 Gy radiation in (Figure 4.6), n=2 biological replicates (one replicate did not reach IC_{50}).

SN39884 Anoxia 4.6 Gy	Average IC_{50} (µM)	S.E.
PORko-R	9.8	0.17
HCT116-G	2.4	1.0
POR-G	4.8	1.2

4.4 Discussion

In this chapter we used growth inhibition assays to evaluate the radiosensitisation capability of the newly developed prodrug SN39884 and the corresponding DNA-PKi effector SN39536, under oxic and anoxic conditions, in HCT116 cells with different POR expression levels. This experimental procedure had previously been employed by (Wong et al., 2019) to investigate radiosensitisation by IC87361 and the corresponding HAP SN38023 in UT-SCC-54C HNSCC cells.

We determined that SN39536 displayed low cytotoxicity as a single agent (Figure 4.4). At the highest concentration SN39536 did show some growth inhibition. If we had been able to extend the range of drug concentrations to higher concentrations we may have been able to determine an IC_{50} value for SN39536, but the aqueous solubility of the compound limited our ability to increase the drug concentration. There are a number of reasons that may explain why SN39536 appeared to induce growth inhibition at higher concentrations. DNA-PK does have roles other than mediating NHEJ and inhibition of these processes may have resulted in an effect on cell growth (see Chapter 1.7). However, the most likely explanation is that the selectivity of SN39536 is not perfect. Inhibition of other targets, such as related PI3K isoforms or other PIKKs, may occur at the higher concentrations. This wider inhibition of kinases may result in cytotoxicity that is independent of radiation.

When SN39536 was combined with 2 Gy radiation it demonstrated efficient radiosensitisation in all three HCT-116 cell lines, with cell density being just above 20% at the highest 10 µM concentration of SN39536 after 4 days incubation. The IC_{50} values ranged from 1.1 to 1.5 µM

(**Table 4.1**) across the HCT116 panel and the radiosensitisation was independent of POR expression. The results indicate that SN39536 is a relatively effective radiosensitiser of the HCT116 cell lines with ca. 10-fold increase in cytotoxicity when combined with 2 Gy radiation (**Figure 4.1**).

We determined that SN39884 displayed low cytotoxicity under oxic conditions both, as a single agent, and when combined with 2 Gy of radiation (**Figure 4.5**). This implies that the prodrug is relatively stable under the conditions of the assay, at least under oxic conditions. At the highest concentrations of SN39884 there was an indication of impairment of cell growth across the cell line panel, but again the aqueous solubility of SN39884 prevented us from exploring higher drug concentrations in this assay. Several possible explanations may contribute to the cytotoxicity observed, but as cell density of all three cell lines was similar at the 10 µM SN39884 drug concentration (**Figure 4.5**), therefore, this observed cytotoxicity is unlikely to be due to increased POR metabolism. Oxygen-independent metabolism to release SN39536 is one possible explanation for the small increase in cytotoxicity seen in (**Figure 4.5**). It is also possible that hydrolysis of the carbamate linker may release SN39536 in a non-enzymatic process. It is also possible that SN39884 may inhibit other kinases that are required for cell growth. While each of these explanations is possible, they play a relatively minor role in determining the cytotoxicity of SN39884 in the HCT116 cell panel. It would be good in the future to conduct an experiment testing the stability of SN39884 in media over 24 hours to determine whether chemical instability leads to toxicity.
When SN39884 was tested in the cell line panel under anoxia we saw a clear change in behaviour. SN39884 appeared to be more cytotoxic alone under anoxia compared to oxic conditions, at least in the POR-G and HCT116-G cell lines (**Figure 4.6**), but we were not able to quantitate this. Cytotoxicity in the PORko-R cells under anoxia (**Figure 4.6**) appeared to be similar to SN39884 cytotoxicity observed in cells under oxia (**Figure 4.5**), whereas the cytotoxicity in HCT116-G and POR-G was comparable to the combination treatment under anoxia (**Figure 4.6**). This implies that POR is an important reductase for SN39884 metabolism. SN39884 provided an increase in cytotoxicity in combination with 2 Gy of radiation across the cell line panel and this radiosensitisation was most pronounced in the POR-G and HCT116-G cell lines (**Figure 4.6**). SN39884 displays radiosensitisation under anoxic conditions, but is potentially cytotoxic alone at higher concentrations, especially in POR expressing cells.
We saw in Chapter 3 that PORko-R cells were able to metabolise SN39884 to produce a similar concentration of SN39536 as HCT116-G cells under anoxia, but the POR overexpressing cells, POR-G, had the highest concentration of SN39536 under anoxia at 3 h. Radiosensitisation by SN39884 is expected to be dependent on the rate of metabolism of SN39884 (amount of SN39536 produced). Increased metabolism of SN39884 by POR should increase radiosensitisation by SN39884 (as effector SN39536). However, we did not see increased radiosensitisation in POR-G, compared to HCT116-G (**Figure 4.6**), presumably because these IC_{50} assays may not be accurate enough to see this effect (only 2-4 fold increase in metabolism in POR-G) because the assay doesn't quantify reproductive cell survival. It should be noted that we couldn't calculate IC_{50} values from one experiment where a mistake in drug addition or oxygen contamination led to invalid results. Unfortunately, this prevents us from drawing a firm conclusion.

However, our data does demonstrate that POR contributes to the metabolism of SN39884 to release SN39536, and to radiosensitise cells, but it is likely that other reductases also contribute to metabolism and subsequent radiosensitisation.

The growth inhibition assay provides an efficient screen of the cytotoxicity and radiosensitisation of cells using a colorimetric endpoint. However, the assay does have limitations. We observed in this chapter that 10 μM of the effector SN39536 under oxic conditions resulted in slightly above 20% cell density in all three lines after 4 days incubation. We know from chapter 3 that SN39536 concentrations are stable over time.

While an efficient assay, we cannot be sure the cells remaining after treatment are still able to divide and produce sizeable colonies, or whether they have lost their reproductive integrity. Therefore, radiosensitising ability could be understated using this assay.

Consequently, we will evaluate the radiosensitisation caused by SN39884 and SN39536 using a clonogenic survival endpoint. A clonogenic assay will allow us to determine whether the cells which have survived still have reproductive capability. This assay is considered the gold standard in assessing reproductive cell death.

5. Chapter 5. Clonogenic Survival of Cells Treated with SN39884 and SN39536

5.1. Introduction

In Chapter 3, we demonstrated that SN39536 is stable in culture medium and cells, and that the SN39884 prodrug is selectively metabolised to SN39536 under anoxic conditions. Consistent with this result, SN39536 showed potent radiosensitisation under oxic conditions and the combination of SN39884 with radiation treatment resulted in significant cell growth inhibition only under anoxic conditions in Chapter 4.

As discussed in Chapter 4, growth inhibition assays can provide survival data for high sample throughput in less time and with less effort than clonogenic assays, but growth inhibition assays cannot distinguish between proliferating cells and cells that are still viable, yet have no reproductive capability, which in the context of radiotherapy of tumours, these cells are essentially considered dead. Therefore growth inhibition assays do not directly measure clonogenic cell killing, and may overestimate cells that have survived after treatment.

The classic assay utilised to evaluate clonogenic cell survival is the clonogenic assay, which evaluates the ability of cells to proliferate and form colonies (defined as exceeding 50 cells), therefore determining the number of proliferating cells that are left after treatment and the ability of the tumour to grow back, which is a major clinical concern.

Clonogenic assays are considered the “gold standard” approach to measure radiation dose-survival curves, because this assay is more accurate at measuring clonogenic cell survival and also give accurate results when using higher radiation doses (Pauwels et al., 2003).

The clonogenic assay has previously been utilised by researchers at ACSRC to determine the survival of clonogenic cells after irradiation with drug exposure under hypoxia of the previously developed prodrug SN38023, and its corresponding inhibitor IC87361, in order to evaluate their hypoxia-dependent radiosensitising capability (Wong et al., 2019).

Utilising a similar technique, we wanted to determine cell survival after irradiation in combination with SN39884, or the effector SN39536, to assess their radiosensitisation potency under oxic and anoxic conditions. The set of experiments in this chapter were conducted by Dr Cho Rong Hong at ACSRC during the COVID-19 lockdown due to lack of access to the labs during level 3 and 4 lockdown and limited access during level 2.

The key difference between clonogenic assays and growth inhibition assays used in this thesis, is that the former investigates the effect of differing radiation doses on cells treated with the same dose of drug, allowing us to calculate the SER_{10} value (Sensitising Enhancement Ratio) which is calculated using the D_{10} values which is the radiation dose required for 10% survival. The SER_{10} values allow us to compare efficacy in radiosensitisation between compounds. Whereas the growth inhibition assay investigates the effect of differing drug doses on cells treated with the same radiation dose (as in Chapter 4), which allows us to calculate the drug concentration required for 50% growth inhibition (RIC_{50}) at one radiation dose. This is useful for comparing the activity of drugs at clinically relevant doses.

5.2. Aims

The overall aim of this chapter was to investigate the radiosensitisation of SN39536 under oxia and SN39884 under oxic and anoxic conditions. In this chapter we utilise the clonogenic survival as the endpoint to accurately determine the surviving population and to evaluate the hypoxia radiosensitisation by SN39884, and effect of POR on radiosensitisation by SN39884 under oxic and anoxic conditions.

1. To investigate radiosensitisation by SN39536 under oxic conditions.
2. To investigate radiosensitisation by SN39884 under oxic and anoxic conditions
3. To investigate the effect of POR on radiosensitisation by SN39884 under oxic and anoxic conditions.
4. Determine the Sensitising Enhancement Ratio (SER_{10})

5.3. Results

5.3.1 Radiosensitisation by SN39536 under oxia

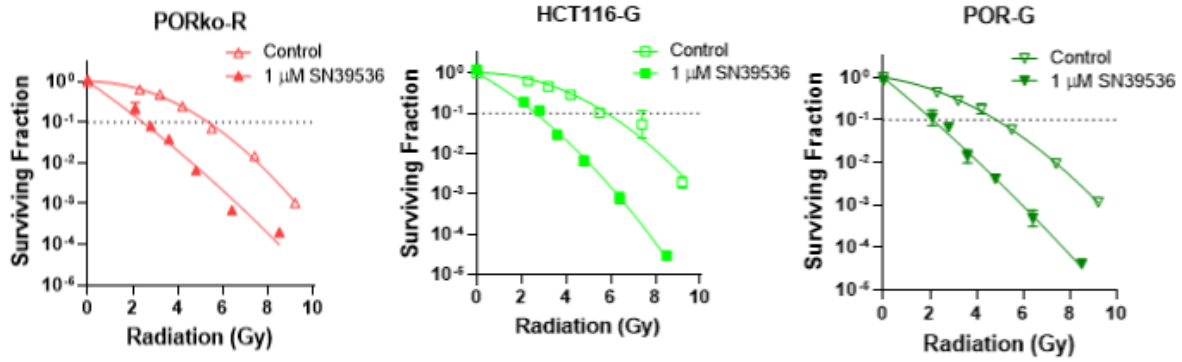

Figure 5.1: Radiation survival curves for PORko-R, HCT116-G and POR-G cells exposed to either 1 µM or 0 µM SN39536 under oxic conditions. *Cells were seeded at 1 x 10^5 cells per well and allowed to attach for 2 h, then treated with drug 3 h prior to irradiation using a lead wedge to create range of radiation doses from 1.89 Gy to 9 Gy. Cells were then incubated for 18 h before plating. Mean and SE are from 3 biological replicates.*

First, we examined radiosensitisation of PORko-R, HCT116-G and POR-G cells by SN39536 under oxic conditions at 18 h after irradiation (**Figure 5.1**). When cells were exposed to SN39536 alone, the surviving fractions for PORko-R, HCT116-G and POR-G cells were 1.107 ± 0.030, 1.256 ± 0.165 and 0.839 ± 0.085, respectively, suggesting that 1 µM SN39536 did not induce clonogenic cell death (**Figure 5.1**). The D_{10} values in cells exposed to radiation alone were 5.35 Gy, 5.84 Gy and 4.84 Gy in PORko-R, HCT116-G and POR-G cells, respectively, suggesting that the radiosensitivity of the three cell lines was similar under oxia. SN39536 demonstrated effective radiosensitisation in all three cell lines (**Figure 5.1**) with sensitising enhancement ratios (SER_{10}) of 2.19, 2.21 and 2.29 in PORko-R, HCT116-G and POR-G cells, respectively. This showed that SN39536, in combination with radiation, could achieve 90% cell killing at less than half the radiation dose required to achieve the same alone. The similar SER values suggested that POR expression levels did not have any effect on radiosensitisation by SN39536.

5.3.2 Radiosensitisation by SN39884 under oxia.

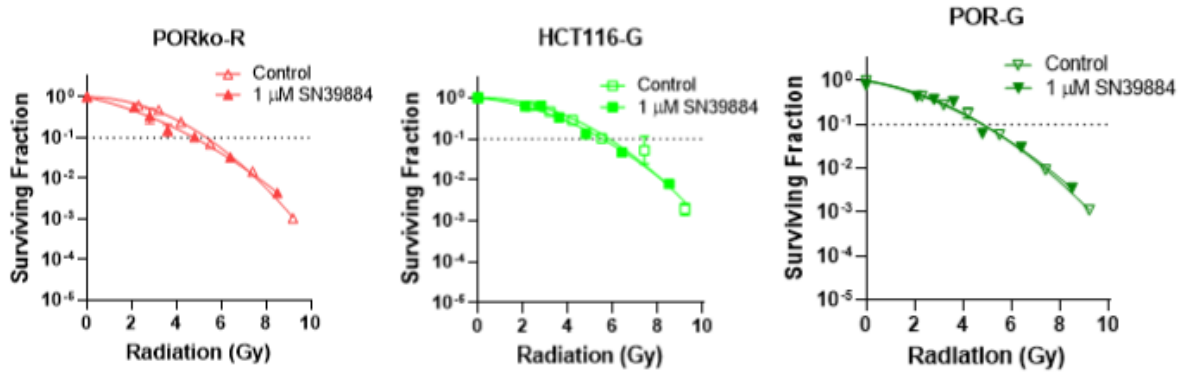

Figure 5.2: Radiation survival curves for PORko-R, HCT116-G and POR-G cells exposed to either 1 µM or 0 µM SN39884 under oxic conditions. *Cells were seeded at 1 x 10^5 cells per well and allowed to attach for 2 h, then treated with drug 3 h prior to irradiation using a lead wedge to create range of doses from 1.89 Gy to 9 Gy. Cells were then incubated for 18 h before plating. Mean and SE are from 3 biological replicates.*

Next, we evaluated radiosensitisation by 1 µM SN39884 under oxic conditions. Treatment with drug alone was relatively non-toxic with the surviving fractions at 0 Gy radiation dose for PORko-R, HCT116-G and POR-G cells of 1.04 ± 0.07, 1.02 ± 0.11 and 0.80 ± 0.05, respectively (**Figure 5.2**). The clonogenic cell survival after combined treatment of SN39884 and radiation was similar to that of radiation alone (**Figure 5.2**) with SER_{10} values of 1.12, 1.05 and 1.01 in PORko-R, HCT116-G and POR-G cells, respectively, suggesting that SN39884 did not radiosensitise cells under oxia.

5.3.3 Radiosensitisation by SN39884 under anoxia.

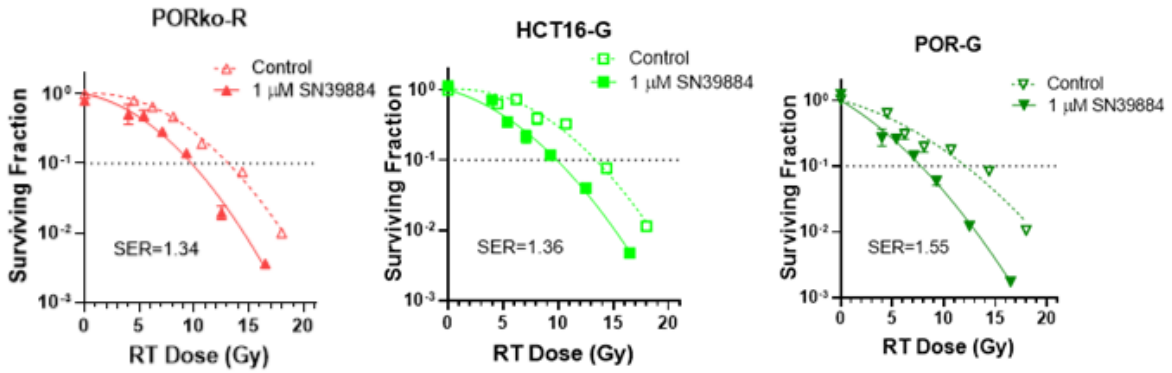

Figure 5.3: Radiation survival curves for PORko-R, HCT116-G and POR-G cells exposed to either 1 µM or 0 µM SN39884 under anoxic conditions. *Cells were seeded at 1 x 10^5 cells per well and allowed to attach for 2 h, then treated with drug 3 h prior to irradiation using a lead wedge to create range of doses from 5 Gy to 18 Gy. Cells were then incubated for 18 h before plating. Mean and SE are from 3 biological replicates.*

We investigated whether SN39884 could radiosensitise cells under anoxic conditions.

Drug alone toxicity with was negligible and surviving fractions for PORko-R, HCT116-G and POR-G cells were 1.259 ± 0.116, 0.813 ± 0.090 and 1.136 ± 0.022, respectively (**Figure 5.3**). As expected, cells were more resistant to radiation under anoxia than oxia with an oxygen enhancement ratio of 10% survival (OER_{10}) of 2.45, 2.30 and 2.50 in PORko-R, HCT116-G and

POR-G cells, respectively. Similar D_{10} values for PORko-R, HCT116-G and POR-G cells (13.12, 13.40 and 12.12, respectively), indicated that POR expression levels had little to no effect on the radiosensitivity of the cells under anoxia. We observed efficient radiosensitisation by SN39884 under anoxic conditions (**Figure 5.3**).

This implied that SN39884 was activated to SN39536 and radiosensitised cells under anoxia. POR-G cells demonstrated greater radiosensitisation by SN39884 with a SER_{10} of 1.55 compared to PORko-R and HCT116-G cells (SER_{10} 1.34 and 1.35), suggesting that POR contributed to metabolism of SN39884 under anoxia and lead to enhanced radiosensitisation.

5.4 Discussion

This chapter used clonogenic survival assays to evaluate radiosensitisation by the newly developed prodrug, SN39884, and the corresponding DNA-PKi effector, SN39536, under oxic and anoxic conditions in HCT116 cells with varying POR expression levels.

Cells treated with radiation and 1 μM SN39536 under oxic conditions had lower survival fractions than cells treated with radiation only, with similar SER values between the three cell lines (**Figure 5.1**). This correlates with our findings from Chapter 4, where radiosensitisation, as measured by the growth inhibition assays, was similar between the three cell lines, regardless of POR expression levels.

Cells treated with radiation and 1 μM SN39884, under oxic conditions had similar survival fractions to cells treated with radiation only, at all radiation doses ranging from 0 to 10 Gy, with SER_{10} values ranging from 1.01 – 1.12 across the three different cell lines (**Figure 5.2**). This observation confirmed that SN39884 was not a radiosensitiser itself, and was not activated to SN39536 under oxia. This was consistent with data from Chapter 3 where only very low concentrations of SN39536 were observed in all three cell lines.

In contrast, the addition of 1 μM of SN39884 to anoxic HCT116 cells under anoxia resulted in additional cell killing in combination with radiation treatment compared to radiation alone, consistent with the growth inhibition results in Fig 4.6.

As the concentration of SN39536 produced under anoxic conditions from SN39884 was greatest in POR-G cells in Chapter 3, this led us to the conclusion that POR overexpression contributed to increased metabolism of SN39884 under anoxia. In this chapter we saw that, POR-G cells had the highest cell killing at the maximal dose, and the highest SER value of 1.55, whereas HCT116-G and PORko-R cells had similar SER values 1.36 and 1.34, respectively (**Figure 5.3**). Therefore, we can conclude that POR overexpression did lead to increased cell killing, due to increased metabolism of SN39884, resulting in higher concentrations of SN39536. But as PORko-R cells were still able to produce comparable SN39536 concentrations as HCT116-G cells (Chapter 3), this implied that other reductases were capable of metabolising SN39884 to SN39536 at similar levels to the constitutive levels of POR (HCT116-G). This resulted in similar levels of radiosensitisation.

The results observed from the clonogenic assays in this chapter highlight the ability to distinguish small differences between the efficacy of the different cell lines. As the difference in SN39536 production under anoxia between HCT116-G and PORko-R compared to POR-G was approximately 2.3 fold (Chapter 3), this difference was too small for the radiation growth inhibition assay to distinguish in Chapter 4, but the clonogenic assay was able to demonstrate this effect on radiosensitisation.

The clonogenic assay has a longer incubation time of around 10 days to allow colonies to form. This extended time, relative to the growth inhibition assay, provides time for irradiated cells to die through mitotic death, which is the main mechanism of radiation-induced cell death (Citrin, 2016). This cell death can take a few cycles before the cell dies by attempting to divide (Citrin, 2016). But these cells fated to die soon might not be differentiated by the growth inhibition assay, and therefore would be considered viable.

A study found that the SRB assay measuring growth inhibition produced highly comparable results to the clonogenic assay in four different cell lines at low, clinically relevant radiation doses (0-6 Gy) when evaluating chemotherapy and radiotherapy interactions (Pauwels et al., 2003). Although, they did find minor differences in results between the two assays at higher doses of radiation.

(Pauwels et al., 2003) considered optimising the growth inhibition assay by increasing incubation time and using 46 well plates instead of 96 well plates to avoid over confluency and plating less cells – in order to allow time for cells to go through multiple divisions before counting. This is something to consider, as growth inhibition assays are high-throughput. However, in this particular situation where only two drugs are being compared across three cell lines the clonogenic survival assay is the best option.

A study by (C. R. Hong et al., 2022) explored radiosensitisation by the DNA-PKi, AZD7648, in murine SCCVII cells. AZD7648, at 1 µM, gave a SER of 6.1 under oxic conditions demonstrating that AZD7648 is a potent radiosensitiser. Further examination of AZD7648 (75 mg/kg ip) in C3H mice bearing SCCVII tumour xenografts treated with whole body irradiation demonstrated a SER of 2.5 for the SCCVII tumour cells. The other key observation from the study was that similar levels of radiosensitisation were observed in stem cells in the oral mucosa and crypts of Lieberkühn (C. R. Hong et al., 2022). This highlights the potential of DNA-PK inhibitors to sensitise normal tissue within the radiation field. The potential of SN39884 to provide oxygen-sensitive radiosensitisation has been demonstrated *in vitro* in this chapter. Moving forward, the key experiment will be to determine whether this oxygen selectivity can provide tumour selective activation of SN39884 with an increase in tumour cell killing while sparing the normal tissues within the radiation field.

In conclusion, SN39536 was an effective radiosensitiser under oxic conditions, with SER_{10} values ca 2.2 when used at 1 µM. SN39884 was found to be stable in HCT116 cells with varying expression of POR under oxic conditions in combination with high radiation doses up to 10 Gy. SN39884 was activated under anoxic conditions to release SN39536 and to provide robust radiosensitisation. High POR expression increased cell kill, but the absence of POR lead to similar amounts of cell killing as seen for cells constitutively expressing POR. This observation is in agreement with the metabolism studies in Chapter 3 where we saw SN39536 production under anoxia was greatest in POR overexpressing cells, and similar production of SN39536 in PORko-R and HCT116-G. Therefore, the clonogenic assay, even though it is more laborious and time consuming, gave us an accurate representation of radiosensitisation compared to the growth inhibition assay.

6 Chapter 6. Concluding Discussion

6.1 Introduction

This thesis explored the hypoxic selective metabolism of the hypoxia-activated prodrug SN39884, and the associated DNA-PK inhibitor SN39536, and evaluated their ability to radiosensitise human colorectal carcinoma cells under oxic and anoxic conditions.

We evaluated metabolic activation and cellular uptake under oxic and anoxic conditions, in three different HCT116 cell lines that each vary in POR expression, so we could also investigate the effect that POR has on SN39884 metabolism in Chapter 3. From the results obtained in the chapter we concluded that SN39884 is selectively activated under hypoxia and releases SN39536. We found that POR can metabolise SN39884 under hypoxia, but SN39884 is less reliant on POR for activation than other HAPs such as tirapazamine (Francis W. Hunter et al., 2015), SN30000 (Francis W. Hunter et al., 2015) and PR104A (Su et al., 2013) and there are other reductases that can activate SN39884. SN39536 demonstrated efficient diffusion out of cells in which it was formed compared with the previously developed DNA-PK inhibitor IC87361 (Wong et al., 2019). This suggests that efficient diffusion of SN39536 from hypoxic cells into surrounding cells could contribute to killing of a wider population of better-oxygenated cells and overcome any limitations in the extravascular transport of SN39884.

In Chapter 4 we assessed the abilities of SN39884 and SN39536 to radiosensitise HCT116 cells varying in POR expression under oxia and anoxia using a growth inhibition assay. The results demonstrated that SN39536 has some toxicity at 10 µM as a single agent under oxic conditions. Two possible interpretations can be drawn from this data. The DNA-PK inhibitor could be interfering with DNA-PK's roles outside of NHEJ such as glucose metabolism, genomic stability and regulation of inflammatory and immune responses (Goodwin & Knudsen, 2014). Alternatively, SN39536 may be inhibiting other kinases for which it has some activity against, such as the PI3-K isoforms and other PIKK enzymes such as ATM, ATR and mTOR. We also observed slight radiosensitisation at 10 µM SN39884 under oxia regardless of POR expression, which suggests that either the prodrug itself may have some growth inhibition effect, or that there are some mechanisms that release SN39536, such as reduction by oxygen independent 2-electron reductases, or chemical degradation (hydrolysis) of the carbamate linker causing release of effector from the trigger component of the HAP. The latter is unlikely since very little production of SN39536 was observed under oxic conditions in Chapter 3. Under anoxic conditions we saw that the prodrug produced similar increases in radiosensitisation in both POR expressing cells and cells with no POR expression. This contrasts with the Chapter 3 results which clearly demonstrated that POR overexpressing cells had a 3-4 fold higher production of SN39536 than HCT116-G and PORko-R cells.

We concluded the similarity in radiosensitisation across the three cell lines was due to the inability of the growth inhibition assay to differentiate between small differences in drug concentrations. This may be a consequence of a lack of discrimination between proliferating and non-proliferating cells. We also saw in Chapter 4 that the cell density started to plateau above 20% at the highest dose of SN39536 under oxia, which led us to believe that the assay was overestimating number of proliferating cells.

In Chapter 5 we went on to conduct clonogenic assays, which are considered the gold standard in assessing radiosensitisation. We saw that for SN39536 treatment under oxic

conditions the surviving fraction did not plateau at the highest radiation doses, suggesting that this assay is more accurately demonstrating clonogenic cell killing than growth inhibition assays. SN39536 was an effective radiosensitiser under oxic conditions, with SER_{10} values of ca 2.2 when used at 1 μM. There was no significant difference in SER_{10} values between the cell lines, demonstrating that radiosensitisation by the DNA-PK inhibitor was independent of POR expression levels.

We saw that the radiosensitisation induced by the prodrug SN39884 at 1 uM under oxic conditions did not differ significantly from the control cells treated with only radiation, with SER_{10} values ranging from 1.01 – 1.12 for the cell lines. This further demonstrated that the prodrug was stable under oxic conditions. In contrast, under anoxia, SN39884 resulted in additional cell killing in combination with radiation compared to radiation alone, with SER_{10} values ranging from 1.34 – 1.55. Radiosensitisation was greatest in the POR overexpressing cells, while similar radiosensitisation was seen in PORko-R and HCT116-G cells. The radiosensitisation induced in POR overexpressing cells is in agreement with the higher concentration of effector produced in POR-G cells than HCT116-G and PORko-R cells observed in chapter 3. We considered that reduction of SN39884 could be carried out by other enzymes in addition to POR and this effect compensated for the loss of POR expression in PORko-R cells and resulted in the similar levels of radiosensitisation observed in the clonogenic survival assay for those two cell lines. We can conclude that SN39884 is relatively stable under oxic conditions and can be activated by POR, and other reductases, under anoxia to release SN39536 and to produce effective radiosensitisation of HCT116 cells *in vitro*.

Overall, this thesis provides evidence of the efficacy of the hypoxia-activated prodrug SN39884 and its DNA-PK inhibitor SN39536 in *in vitro* studies. Future studies investigating these drugs is warranted as these drugs show good stability, cellular uptake and hypoxia selective radiosensitisation.

6.2 Future Directions

The drug discovery process aims to develop an effective and safe drug to target a protein or pathway for a therapeutic purpose. High Throughput Screening processes are undertaken to screen large compound libraries against the target. Characteristics, such as potency and selectivity are assessed and used to rank the molecules to generate lead compounds, that may be optimised to increase efficacy (Hughes, Rees, Kalindjian, & Philpott, 2011).

The assays used in this thesis are variations of methods currently employed to screen HAPs and their effectors by pharmaceutical companies and universities. Biochemical assays that utilise stable mammalian cell lines that overexpress a certain gene or have a gene knockout such as the HCT116 cell lines we have used throughout this study, which was modified to overexpress cytochrome P450 oxidoreductase (POR-G) or knocked out (PORko-R), are commonly used to investigate activation of HAPs under anoxic conditions (Su et al., 2013), (Francis W. Hunter et al., 2015), (Wong et al., 2019).

Using the three cell lines with variable POR expression in this study we were able to learn that POR only increased SN39884 metabolism under anoxia when overexpressed, but at constitutive levels, metabolism rates are not significantly different from when POR is absent. This lead us to conclude that other reductases have the ability to metabolise SN39884 when POR is knocked out. Therefore, it is possible that other reductases, if overexpressed, could lead to similar increases in SN39884 metabolism as when POR was overexpressed. The

identification of reductases responsible for activation of SN39884 is a critical requirement for its clinical development. Previously, the ACSRC has used various methods to identify reductases that are responsible for activation of HAPs such as genome-scale shRNA screens (Francis W. Hunter et al., 2015) and testing correlations between rates of metabolism of HAPs and expression of reductases in a panel of cell lines (C. P. Guise et al., 2010), (Francis W Hunter et al., 2014). These approaches could be used to identify the reductases responsible for activation of SN39884.

In this study we saw that the radiosensitising effect of the prodrug in constitutively expressing POR (HCT116-G) and overexpressing POR (POR-G) was not as well differentiated in the growth inhibition assay compared to the clonogenic assay. The growth inhibition assay was used in this study because of its efficiency. This assay is used for drug screening purposes because it allows the investigation of multiple cell lines and drugs in a short amount of time in 96-well plates, and the endpoint can be counted automatically by spectrophotometry. Therefore, the growth inhibition assay would be ideal as a primary assay to screen radiosensitisation in potential drug candidates, with only the better candidates further investigated in the more accurate clonogenic assay. The clonogenic assay requires manual counting and laborious plating of cells in 6-well plates, followed by a 10 day incubation period.

Further optimisation of this screening process can be made by utilising the metabolism assay conducted in Chapter 3, after the growth inhibition assay, so that the prodrugs selected can be investigated for their ability to produce the effector to a significant level selectively under hypoxia, before proceeding onto assessment by the clonogenic assay. As we saw in Chapter 3, the cell line that overexpressed POR produced the largest SN39536 levels under anoxia when treated with SN39884, and this lead to the greatest SER value under anoxia in Chapter 5. Therefore, how efficiently a prodrug can be metabolised and release the DNA-PK inhibitor gives an indicator of the efficacy of the prodrug, further narrowing down the potential drug candidates for testing in the clonogenic assay.

(Wong et al., 2019) found that SN38023 was selectively metabolised under hypoxic conditions to IC87361, which was found to be a potent radiosensitiser in growth inhibition and clonogenic assays. They investigated the cytotoxicity and radiosensitising ability of the prodrug SN38023, and its associated effector IC87361, in a spheroid model using a mixture of POR expressing cell lines POR-G and HCT116-G as activator cells and the POR null cell line PORko-R as the target cells. There was no evidence for a bystander effect because there was no difference in killing of target cells, irrespective of the presence of activator cells. This result implied residual activation of SN38023 by 1-electron reductases other than POR. They also found that SN38023 had comparable cytotoxicity to IC87361 in POR-G cells under hypoxic, which they did not find in their monolayer assays. They attributed this to the fact that their monolayer assays used higher cell densities than their spheroid assay, which was protective as they found the cellular uptake of the drugs to be very high from the metabolism assay and this would therefore limit the availability of the drugs.

In Chapter 3 we found that the ratio between SN39536 effector concentrations intracellularly and extracellularly (Ci/Ce) under anoxia was much smaller (~8-10 fold) than the Ci/Ce of IC87361 observed by (Wong et al., 2019) (~400 fold). (C. R. Hong et al., 2021) has shown that high intracellular binding decreases penetration of a drug through layers of cells, therefore based on our metabolism assay results, we hypothesise that SN39884 would generate a more efficient bystander effect than the prodrug SN38023. (C. R. Hong, Bogle, et al., 2018) studied the hypoxia activated prodrugs, SN30000 and PR104A, in the same spheroid model as (Wong

et al., 2019) and found that bystander effects of PR104A contribute to antitumour activity while the tirapazamine analogue SN30000 demonstrated that increasing activator cells reduced killing of target cells, which was in contrast to PR104A. They confirmed that the lack of bystander effect was due to rapid metabolic consumption of SN30000 which limited penetration. Therefore, it would be interesting to investigate the bystander effect of SN39884 using the co-culture spheroid model.

As mentioned in Section 1.8, the tumour microenvironment can impair drug activity and hypoxic regions are difficult to target with drugs due to the disorganised vasculature. Therefore, the potential for local diffusion of the prodrug or active metabolite to produce a 'bystander effect' is an important characteristic of hypoxia activated prodrugs (C. R. Hong, Bogle, et al., 2018). Multicellular layer (MCL) diffusion assays can be used to measure extravascular transport of the drug and its metabolites.

A major limitation with spheroid models is that information on drug penetration is indirectly measured by the cell killing and drugs that are not fluorescently or radio-labelled cannot be differentiated through analytical techniques. However, MCLs measure drug transport across a planar surface over time, therefore the concentration of prodrug and effector can be determined and differentiated, allowing quantification of concentration gradients (C. R. Hong et al., 2021). The MCL diffusion assay would have been good for confirming the diffusion of SN38023 through the multicellular layer. Investigating the diffusion of SN39884 through a MCL model utilising the activator and target mixed cell model would provide a high spatial resolution for its distribution.

(C. R. Hong et al., 2022) used 5'-ethynyl-2'-deoxyridine (EdU) to detect regenerating crypts in the ileum and oral mucosa in murine HNSCC tumour xenograft models to compare radiosensitisation of HNSCC tumour and normal tissues by a clinical stage DNA-PKi, AZD7648. They found that AZD7648 radiosensitises normal tissues and tumour similarly, suggesting that the DNA-PK inhibitor has poor tumour selectivity. Therefore we hypothesise that selective delivery of DNA-PK inhibitor to radioresistant hypoxic tissue would enhance tumour selectivity. It will be of interest to investigate therapeutic ratio of SN39536 and SN39884 using the methodology described in (C. R. Hong et al., 2022) to test our hypothesis.

6.3 Conclusion

DNA-PK inhibitors have significant potential as radiosensitisers for the treatment of human tumours. Concerns about on-mechanism toxicity within the radiation field pose a challenge to identify a tumour selective approach to radiosensitisation. The work presented in this thesis identifies that SN39884 is a hypoxia-activated prodrug of the potent DNA-PK inhibitor SN39536. SN39884 undergoes hypoxia-selective metabolism to release SN39536 and this provides radiosensitisation under hypoxia. While there is still considerable work to fully validate SN39884, it would appear to have significant potential as a hypoxia selective prodrug for use in combination with radiotherapy.

Appendix 1.

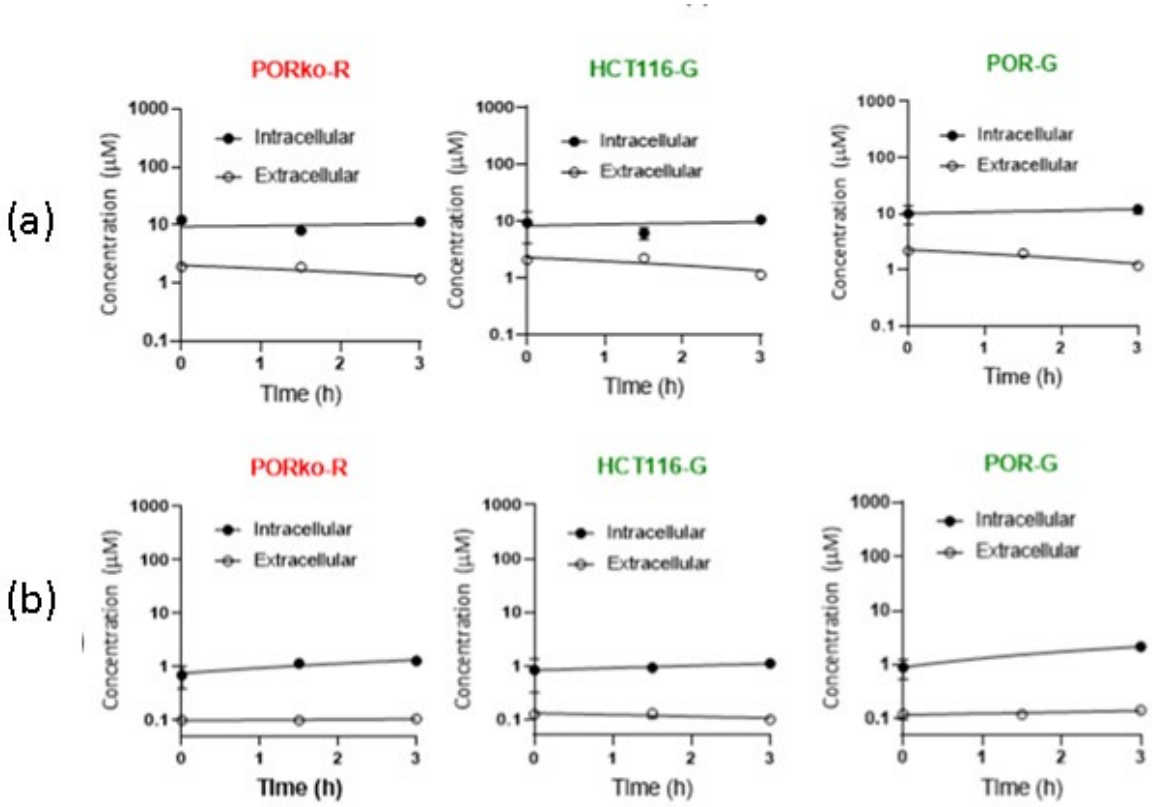

Appendix 1. Intracellular and extracellular concentrations of SN39884 (a) and SN39536 (b) in PORko-R, HCT116-G and POR-G cells under oxia . *Cells were incubated for 2 h for cell attachment and then exposed to 10 µM of SN39884 for 0 h, 1.5 h or 3 h before samples were taken and analysed by LC-MS. Mean and SE are from ≥ 2 biological replicates. Due to sample losses during the covid-19 lockdown extracellular concentration at 1.5 h in PORko-R cells (a,b) could not be measured.*

Appendix 2.

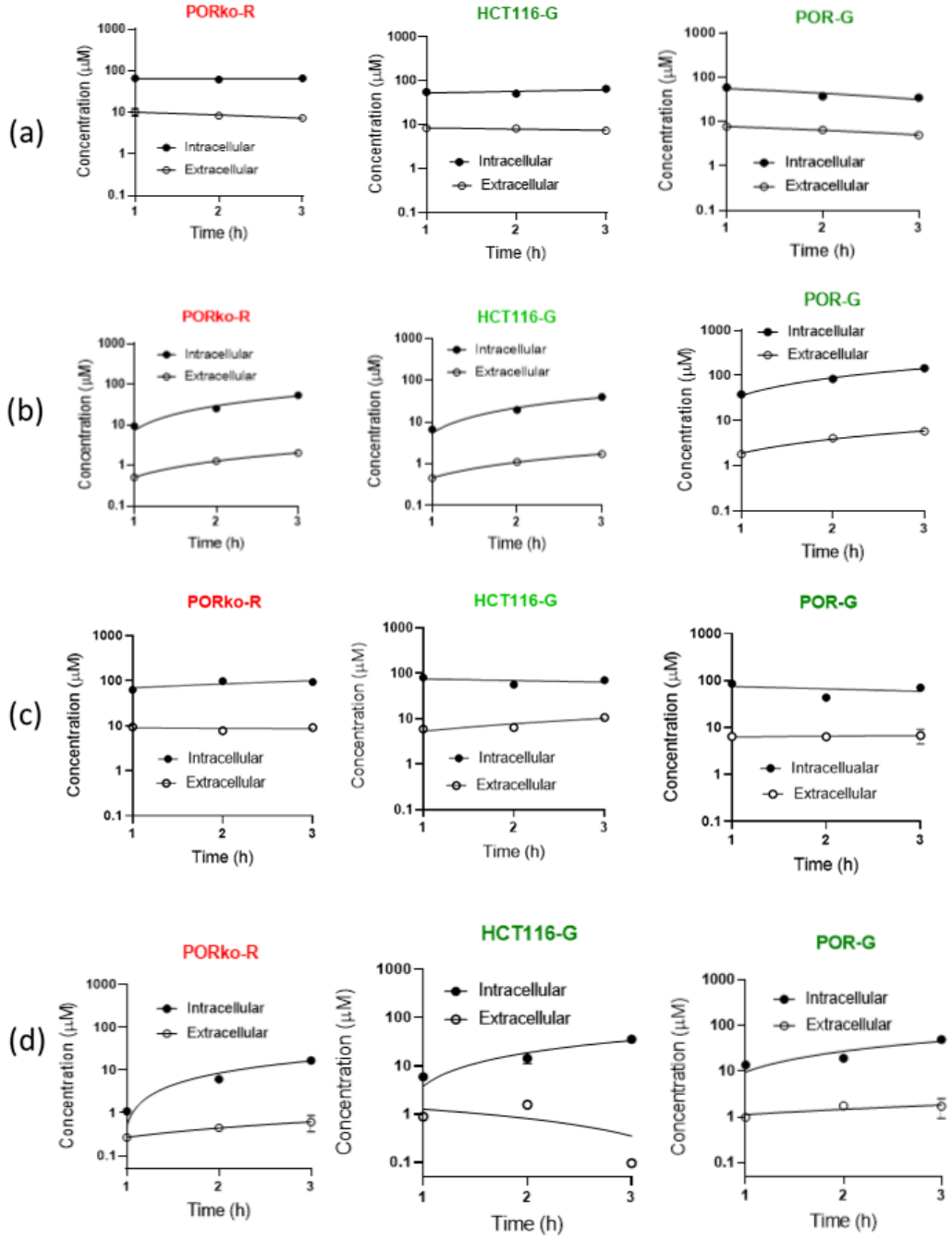

Appendix 2. Intracellular and Extracellular Concentrations of SN39884 (a) and (c) and SN39536 (b) and (d) in PORko-R, HCT116-G and POR-G cells under Anoxia in Two Independent Experiments (a and b), (c and d). *Cells were incubated for 2 h for cell attachment under anoxia and then exposed to 10 µM of the effector SN39884 for 0 h, 1.5 h or 3 h before samples were taken and analysed by LC-MS. Mean and SE are from 3 biological replicates.*

Bibliography:

Abbotts, R., & Wilson, D. M. (2017). Coordination of DNA single strand break repair. *Free Radical Biology and Medicine, 107*, 228-244. doi:10.1016/j.freeradbiomed.2016.11.039

Abdo Qaid, E. Y., Zulkipli, N. N., Zakaria, R., Ahmad, A. H., Othman, Z., Muthuraju, S., & Sasongko, T. H. (2021). The role of mTOR signalling pathway in hypoxia-induced cognitive impairment. *International Journal of Neuroscience, 131*(5), 482-488. doi:10.1080/00207454.2020.1746308

Abraham, R. T. (2004). PI 3-kinase related kinases:'big'players in stress-induced signaling pathways. *DNA Repair, 3*(8-9), 883-887.

Adams, G. E. (1978). Hypoxic cell sensitizers for radiotherapy. *International Journal of Radiation Oncology*Biology*Physics, 4*(1), 135-141. doi:https://doi.org/10.1016/0360-3016(78)90129-3

Adams, G. E., & Cooke, M. S. (1969). Electron-affinic sensitization. *International Journal of Radiation Biology and Related Studies in Physics, Chemistry and Medicine, 15*(5), 457-471. doi:10.1080/09553006914550741

Aghajanian, C., Brown, C., O'Flaherty, C., Fleischauer, A., Curtin, J., Roemeling, R. V., & Spriggs, D. R. (1997). Phase I study of Tirapazamine and Cisplatin in patients with recurrent cervical cancer. *Gynecologic Oncology, 67*(2), 127-130. doi:10.1006/gyno.1997.4841

Al-Minawi, A. Z., Saleh-Gohari, N., & Helleday, T. (2007). The ERCC1/XPF endonuclease is required for efficient single-strand annealing and gene conversion in mammalian cells. *Nucleic Acids Research, 36*(1), 1-9. doi:10.1093/nar/gkm888

Andrs, M., Korabecny, J., Jun, D., Hodny, Z., Bartek, J., & Kuca, K. (2015). Phosphatidylinositol 3-Kinase (PI3K) and phosphatidylinositol 3-kinase-related kinase (PIKK) inhibitors: importance of the morpholine ring. *Journal of Medicinal Chemistry, 58*(1), 41-71.

Arcasoy, M. O., Amin, K., Chou, S.-C., Haroon, Z. A., Varia, M., & Raleigh, J. A. (2005). Erythropoietin and erythropoietin receptor expression in head and neck cancer: relationship to tumor hypoxia. *Clinical Cancer Research, 11*(1), 20-27.

Aykul, S., & Martinez-Hackert, E. (2016). Determination of half-maximal inhibitory concentration using biosensor-based protein interaction analysis. *Analytical Biochemistry, 508*, 97-103. doi:10.1016/j.ab.2016.06.025

Azzam, E. I., Jay-Gerin, J.-P., & Pain, D. (2012). Ionizing radiation-induced metabolic oxidative stress and prolonged cell injury. *Cancer Letters, 327*(1-2), 48-60. doi:10.1016/j.canlet.2011.12.012

Bahassi, E. M., Ovesen, J. L., Riesenberg, A. L., Bernstein, W. Z., Hasty, P. E., & Stambrook, P. J. (2008). The checkpoint kinases Chk1 and Chk2 regulate the functional associations between hBRCA2 and Rad51 in response to DNA damage. *Oncogene, 27*(28), 3977-3985. doi:10.1038/onc.2008.17

Bartlett, E. J., & Lees-Miller, S. P. (2018). Established and emerging roles of the DNA-dependent Protein Kinase catalytic subunit (DNA-PKcs). In *Cancer Drug Discovery and Development* (pp. 315-338): Springer International Publishing.

Baskar, R., Lee, K. A., Yeo, R., & Yeoh, K.-W. (2012). Cancer and radiation therapy: current advances and future directions. *International Journal of Medical Sciences, 9*(3), 193-199. doi:10.7150/ijms.3635

Beamish, H. J. (2000). The C-terminal conserved domain of DNA-PKcs, missing in the SCID mouse, is required for kinase activity. *Nucleic Acids Research, 28*(7), 1506-1513. doi:10.1093/nar/28.7.1506

Begg, A. C., Stewart, F. A., & Vens, C. (2011). Strategies to improve radiotherapy with targeted drugs. *Nature Reviews Cancer, 11*(4), 239-253. doi:10.1038/nrc3007

Benito, J., Shi, Y., Szymanska, B., Carol, H., Boehm, I., Lu, H., . . . Konopleva, M. (2011). Pronounced hypoxia in models of murine and human leukemia: high efficacy of hypoxia-activated prodrug PR-104. *PLoS ONE, 6*(8), e23108. doi:10.1371/journal.pone.0023108

Berger, M., Wortmann, L., Buchgraber, P., Lücking, U., Zitzmann-Kolbe, S., Wengner, A. M., . . . Siemeister, G. (2021). BAY-8400: A novel potent and selective DNA-PK inhibitor which shows synergistic efficacy in combination with targeted alpha therapies. *Journal of Medicinal Chemistry, 64*(17), 12723-12737. doi:10.1021/acs.jmedchem.1c00762

Bernier, J., Hall, E. J., & Giaccia, A. (2004). Radiation oncology: a century of achievements. *Nature Reviews Cancer, 4*(9), 737-747. doi:10.1038/nrc1451

Berrouet, C., Dorilas, N., Rejniak, K. A., & Tuncer, N. (2020). *Comparison of drug inhibitory effects (IC $_{50}$) in monolayer and spheroid cultures*. Cold Spring Harbor Laboratory.

Bhargava, R., Onyango, D. O., & Stark, J. M. (2016). Regulation of single-strand annealing and its role in genome maintenance. *Trends in Genetics, 32*(9), 566-575. doi:10.1016/j.tig.2016.06.007

Biedermann, K. A., Sun, J., Giaccia, A. J., Tosto, L. M., & Brown, J. M. (1991). scid mutation in mice confers hypersensitivity to ionizing radiation and a deficiency in DNA double-strand break repair. *Proceedings of the National Academy of Sciences, 88*(4), 1394-1397.

Blasiak, J. (2021). Single-strand annealing in cancer. *International Journal of Molecular Sciences, 22*(4), 2167.

Bolus, N. E. (2017). Basic review of radiation biology and terminology. *Journal of Nuclear Medicine Technology, 45*(4), 259-264. doi:10.2967/jnmt.117.195230

Borad, M. J., Reddy, S. G., Bahary, N., Uronis, H. E., Sigal, D., Cohn, A. L., . . . Ryan, D. P. (2015). Randomized phase II trial of Gemcitabine plus TH-302 versus Gemcitabine in patients with advanced pancreatic cancer. *Journal of Clinical Oncology, 33*(13), 1475-1481. doi:10.1200/jco.2014.55.7504

Boucher, D., Hillier, S., Newsome, D., Wang, Y., Takemoto, D., Gu, Y., . . . Maxwell, J. (2016). Preclinical characterization of the selective DNA-dependent protein kinase (DNA-PK) inhibitor VX-984 in combination with chemotherapy. *Annals of Oncology, 27*, vi122.

Boucher, D., Hoover, R., Wang, Y., Gu, Y., Newsome, D., Ford, P., . . . Hillier, S. (2016). Potent radiation enhancement with VX-984, a selective DNA-PKcs inhibitor for the treatment of NSCLC. *Cancer Research*, 76(14_Supplement), 3716-3716

Bray, F., Ferlay, J., Soerjomataram, I., Siegel, R. L., Torre, L. A., & Jemal, A. (2018). Global cancer statistics 2018: GLOBOCAN estimates of incidence and mortality worldwide for 36 cancers in 185 countries. *CA: A Cancer Journal for Clinicians, 68*(6), 394-424. doi:10.3322/caac.21492

Bridges, C. B. (1922). The origin of variations in sexual and sex-limited characters. *The American Naturalist, 56*(642), 51-63.
Brown, J. (1993). SR 4233 (Tirapazamine): a new anticancer drug exploiting hypoxia in solid tumours. *British Journal of Cancer, 67*(6), 1163-1170. doi:10.1038/bjc.1993.220
Brown, J. M. (1975). Selective radiosensitization of the hypoxic cells of mouse tumors with the nitroimidazoles Metronidazole and Ro 7-0582. *Radiation Research, 64*(3), 633. doi:10.2307/3574253
Brown, J. M. (2002). Tumor microenvironment and the response to anticancer therapy. *Cancer Biology & Therapy, 1*(5), 453-458.
Brown, J. M. (2019). Beware of clinical trials of DNA repair inhibitors. *International Journal of Radiation Oncology, Biology, Physics, 103*(5), 1182-1183.
Brown, J. M., & Attardi, L. D. (2005). The role of apoptosis in cancer development and treatment response. *Nature Reviews Cancer, 5*(3), 231-237. doi:10.1038/nrc1560
Brown, J. M., Carlson, D. J., & Brenner, D. J. (2014). The tumor radiobiology of SRS and SBRT: are more than the 5 Rs involved? *International Journal of Radiation Oncology*Biology*Physics, 88*(2), 254-262. doi:10.1016/j.ijrobp.2013.07.022
Brown, J. M., & Lemmon, M. J. (1990). Potentiation by the hypoxic cytotoxin SR 4233 of cell killing produced by fractionated irradiation of mouse tumors. *Cancer Research, 50*(24), 7745-7749.
Brown, J. M., & Wilson, W. R. (2004). Exploiting tumour hypoxia in cancer treatment. *Nature Reviews Cancer, 4*(6), 437-447. doi:10.1038/nrc1367
Bryant-Friedrich, A. C. (2010). Fate of DNA sugar radicals. In *Advances in Molecular Toxicology* (pp. 127-155): Elsevier.
Bunch, H., Lawney, B. P., Lin, Y.-F., Asaithamby, A., Murshid, A., Wang, Y. E., . . . Calderwood, S. K. (2015). Transcriptional elongation requires DNA break-induced signalling. *Nature Communications, 6*(1), 10191. doi:10.1038/ncomms10191
Burger, K., Ketley, R. F., & Gullerova, M. (2019). Beyond the trinity of ATM, ATR, and DNA-PK: multiple kinases shape the DNA damage response in concert with RNA metabolism. *Frontiers in Molecular Biosciences, 6*, 61.
Bürkel, F., Jost, T., Hecht, M., Heinzerling, L., Fietkau, R., & Distel, L. (2020). Dual mTOR/DNA-PK Inhibitor CC-115 induces cell death in melanoma Cells and has radiosensitizing potential. *International Journal of Molecular Sciences, 21*(23), 9321. doi:10.3390/ijms21239321
Caldecott, K. W. (2014). DNA single-strand break repair. *Experimental Cell Research, 329*(1), 2-8. doi:https://doi.org/10.1016/j.yexcr.2014.08.027
Cameron, M., Cornelius, I., Cutajar, D., Davis, J., Rosenfeld, A., Lerch, M., & Guatelli, S. (2017). Comparison of phantom materials for use in quality assurance of microbeam radiation therapy. *Journal of Synchrotron Radiation, 24*(4), 866-876. doi:10.1107/s1600577517005641
Cano, C., Harnor, S. J., Willmore, E., & Wedge, S. R. (2018). Targeting DNA-PK as a therapeutic approach in oncology. In *Targeting the DNA Damage Response for Anti-Cancer Therapy* (pp. 339-357): Springer.
Cano, C. l., Saravanan, K., Bailey, C., Bardos, J., Curtin, N. J., Frigerio, M., . . . Menear, K. A. (2013). 1-substituted (Dibenzo [b, d] thiophen-4-yl)-2-morpholino-4 H-chromen-4-ones endowed with dual DNA-PK/PI3-K inhibitory activity. *Journal of Medicinal Chemistry, 56*(16), 6386-6401.

Casagrande, F., Bacqueville, D., Pillaire, M.-J., Malecaze, F., Manenti, S., Breton-Douillon, M., & Darbon, J.-M. (1998). G1 phase arrest by the phosphatidylinositol 3-kinase inhibitor LY 294002 is correlated to up-regulation of p27Kip1 and inhibition of G1 CDKs in choroidal melanoma cells. *FEBS letters, 422*(3), 385-390.

Chang, Y.-F., Imam, J. S., & Wilkinson, M. F. (2007). The nonsense-mediated decay RNA surveillance pathway. *Annual Review of Biochemistry, 76*(1), 51-74. doi:10.1146/annurev.biochem.76.050106.093909

Chaplin, A. K., Hardwick, S. W., Liang, S., Kefala Stavridi, A., Hnizda, A., Cooper, L. R., . . . Blundell, T. L. (2021). Dimers of DNA-PK create a stage for DNA double-strand break repair. *Nature Structural & Molecular Biology, 28*(1), 13-19. doi:10.1038/s41594-020-00517-x

Chapman, R., J., Taylor, R. G., Martin, & Boulton, J., Simon. (2012). Playing the end game: DNA double-strand break repair pathway choice. *Molecular Cell, 47*(4), 497-510. doi:10.1016/j.molcel.2012.07.029

Chawla, S. P., Cranmer, L. D., Van Tine, B. A., Reed, D. R., Okuno, S. H., Butrynski, J. E., . . . Ganjoo, K. N. (2014). Phase II study of the safety and antitumor activity of the hypoxia-activated prodrug TH-302 in combination with Doxorubicin in patients with advanced soft tissue sarcoma. *Journal of Clinical Oncology, 32*(29), 3299-3306. doi:10.1200/jco.2013.54.3660

Citrin, D. E. (2016). Short-term screening assays for the identification of therapeutics for cancer. *Cancer Research, 76*(12), 3443-3445. doi:10.1158/0008-5472.can-16-1299

Cleary, J. M., & Shapiro, G. I. (2010). Development of phosphoinositide-3 kinase pathway inhibitors for advanced cancer. *Current Oncology Reports, 12*(2), 87-94.

Coates, J. T., Skwarski, M., & Higgins, G. S. (2018). Targeting tumour hypoxia: shifting focus from oxygen supply to demand. *The British Journal of Radiology*, 20170843. doi:10.1259/bjr.20170843

Coleman, C. N., Lisa Noll, R. N., Howes, A. E., Harris, J. R., Zakar, J., & Kramer, R. A. (1989). Initial results of a phase I trial of continuous infusion SR 2508 (etanidazole): A radiation therapy oncology group study. *International Journal of Radiation Oncology*Biology*Physics, 16*(4), 1085-1087. doi:10.1016/0360-3016(89)90922-x

Collis, S. J., Deweese, T. L., Jeggo, P. A., & Parker, A. R. (2005). The life and death of DNA-PK. *Oncogene, 24*(6), 949-961. doi:10.1038/sj.onc.1208332

Cook, D., Long, S., Stanton, J., Cusick, P., Lawrimore, C., Yeh, E., . . . Bloom, K. (2021). Behavior of dicentric chromosomes in budding yeast. *PLOS Genetics, 17*(3), e1009442. doi:10.1371/journal.pgen.1009442

Cornell, L., Munck, J. M., Alsinet, C., Villanueva, A., Ogle, L., Willoughby, C. E., . . . Burt, A. D. (2015). DNA-PK—A candidate driver of hepatocarcinogenesis and tissue biomarker that predicts response to treatment and survival. *Clinical Cancer Research, 21*(4), 925-933.

Covens, A., Blessing, J., Bender, D., Mannel, R., & Morgan, M. (2006). A phase II evaluation of tirapazamine plus cisplatin in the treatment of recurrent platinum-sensitive ovarian or primary peritoneal cancer: a gynecologic oncology group study. *Gynecologic Oncology, 100*(3), 586-590. doi:10.1016/j.ygyno.2005.09.032

Cowell, I. G., Durkacz, B. W., & Tilby, M. J. (2005). Sensitization of breast carcinoma cells to ionizing radiation by small molecule inhibitors of DNA-dependent protein kinase and ataxia telangiectsia mutated. *Biochemical Pharmacology, 71*(1-2), 13-20.

Craighead, P. S., Pearcey, R., & Stuart, G. (2000). A phase I/II evaluation of Tirapazamine administered intravenously concurrent with Cisplatin and radiotherapy in women with locally advanced cervical cancer. *International Journal of Radiation Oncology*Biology*Physics, 48*(3), 791-795. doi:10.1016/s0360-3016(00)00720-3

Davidson, D., Amrein, L., Panasci, L., & Aloyz, R. (2013). Small molecules, inhibitors of DNA-PK, targeting DNA repair, and beyond. *Frontiers in pharmacology, 4*, 5.

Davidson, D., Coulombe, Y., Martinez-Marignac, V. L., Amrein, L., Grenier, J., Hodkinson, K., . . . Panasci, L. (2012). Irinotecan and DNA-PKcs inhibitors synergize in killing of colon cancer cells. *Investigational New Drugs, 30*(3), 1248-1256. doi:10.1007/s10637-010-9626-9

Davidson, D., Grenier, J., Martinez-Marignac, V., Amrein, L., Shawi, M., Tokars, M., . . . Panasci, L. (2012). Effects of the novel DNA dependent protein kinase inhibitor, IC486241, on the DNA damage response to doxorubicin and cisplatin in breast cancer cells. *Investigational New Drugs, 30*(4), 1736-1742. doi:10.1007/s10637-011-9678-5

Deng, S. K., Gibb, B., De Almeida, M. J., Greene, E. C., & Symington, L. S. (2014). RPA antagonizes microhomology-mediated repair of DNA double-strand breaks. *Nature Structural & Molecular Biology, 21*(4), 405-412. doi:10.1038/nsmb.2786

Desouky, O., Ding, N., & Zhou, G. (2015). Targeted and non-targeted effects of ionizing radiation. *Journal of Radiation Research and Applied Sciences, 8*(2), 247-254. doi:10.1016/j.jrras.2015.03.003

Dhani, N., Fyles, A., Hedley, D., & Milosevic, M. (2015). The clinical significance of hypoxia in human cancers*. Paper presented at the Seminars in nuclear medicine*.Vol. 45. No. 2. WB Saunders, 2015.

Dische, S., Saunders, M. I., Flockhart, I. R., Lee, M. E., & Anderson, P. (1979). Misonidazole—a drug for trial in radiotherapy and oncology. *International Journal of Radiation Oncology*Biology*Physics, 5*(6), 851-860. doi:10.1016/0360-3016(79)90070-1

Disilvestro, P. A., Ali, S., Craighead, P. S., Lucci, J. A., Lee, Y.-C., Cohn, D. E., . . . Monk, B. J. (2014). Phase III randomized trial of weekly Cisplatin and irradiation versus Cisplatin and Tirapazamine and irradiation in stages IB2, IIA, IIB, IIIB, and IVA cervical carcinoma limited to the pelvis: a gynecologic oncology group study. *Journal of Clinical Oncology, 32*(5), 458-464. doi:10.1200/jco.2013.51.4265

Dobzhansky, T. (1946). Genetics of natural populations. XIII. Recombination and variability in populations of Drosophila pseudoobscura. *Genetics, 31*(3), 269.

Done, M. J., & Brown, J. M. (1993). Tumor-specific, schedule-dependent interaction between tirapazamine (SR 4233) and cisplatin. *Cancer Research, 53*(19), 4633-4636.

Duan, J. X., Jiao, H., Kaizerman, J., Stanton, T., Evans, J. W., Lan, L., . . . Matteucci, M. (2008). Potent and highly selective hypoxia-activated achiral phosphoramidate mustards as anticancer drugs. *Journal of Medicinal Chemistry, 51*(8), 2412-2420. doi:10.1021/jm701028q

Eisenreich, A., & Rauch, U. (2011). PI3K inhibitors in cardiovascular disease. *Cardiovascular Therapeutics, 29*(1), 29-36. doi:10.1111/j.1755-5922.2010.00206.x

Emami Nejad, A., Najafgholian, S., Rostami, A. et al. (2021). The role of hypoxia in the tumor microenvironment and development of cancer stem cell: a novel approach to developing treatment. *Cancer Cell International, 21 62*.

Eriksson, D., & Stigbrand, T. (2010). Radiation-induced cell death mechanisms. *Tumor Biology, 31*(4), 363-372. doi:http://dx.doi.org/10.1007/s13277-010-0042-8

Eschwège, M. T., Francois. (2000). Conformal radiotherapy and intensity-modulated Radiotherapy: Clinical Data. *Acta Oncologica, 39*(5), 555-567. doi:10.1080/028418600750013249

Estrada-Bernal, A., Le, A. T., Doak, A. E., Tirunagaru, V. G., Silva, S., Bull, M. R., . . . Doebele, R. C. (2021). Tarloxotinib Is a hypoxia-activated pan-HER kinase inhibitor active against a broad range of HER-family oncogenes. *Clinical Cancer Research, 27*(5), 1463-1475. doi:10.1158/1078-0432.ccr-20-3555

Evans, S. M., Du, K. L., Chalian, A. A., Mick, R., Zhang, P. J., Hahn, S. M., . . . Koch, C. J. (2007). Patterns and levels of hypoxia in head and neck squamous cell carcinomas and their relationship to patient outcome. *International Journal of Radiation Oncology*Biology*Physics, 69*(4), 1024-1031. doi:10.1016/j.ijrobp.2007.04.067

Fell, V. L., & Schild-Poulter, C. (2012). Ku regulates signaling to DNA damage response pathways through the Ku70 von Willebrand A Domain. *Molecular and Cellular Biology, 32*(1), 76-87. doi:10.1128/mcb.05661-11

Fidler, M. M., Bray, F., & Soerjomataram, I. (2018). The global cancer burden and human development: A review. *Scandinavian Journal of Public Health, 46*(1), 27-36. doi:10.1177/1403494817715400

Fok, J. H. L., Ramos-Montoya, A., Vazquez-Chantada, M., Wijnhoven, P. W. G., Follia, V., James, N., . . . Cadogan, E. B. (2019). AZD7648 is a potent and selective DNA-PK inhibitor that enhances radiation, chemotherapy and olaparib activity. *Nature Communications, 10*(1). doi:10.1038/s41467-019-12836-9

Folkert, M. R., & Timmerman, R. D. (2017). Stereotactic ablative body radiosurgery (SABR) or stereotactic body radiation therapy (SBRT). *Advanced Drug Delivery Reviews, 109*, 3-14.

Fricke, H. (1966). Chemical dosimetry. *Radiation dosimetry, 2*, 167-239.

Fuchss, T., Mederski, W. W., Emde, U., Buchstallter, H.-P., Zenke, F., Zimmermann, A., . . . Urbahns, K. (2017). Highly potent and selective DNA-PK inhibitor M3814 with sustainable anti-tumor activity in combination with radiotherapy. Cancer Research, 77(13_Supplement), 4198-4198.

Fulop, G. M., & Phillips, R. A. (1990). The scid mutation in mice causes a general defect in DNA repair. *Nature, 347*(6292), 479-482. doi:10.1038/347479a0

Fyles, A., Milosevic, M., Hedley, D., Pintilie, M., Levin, W., Manchul, L., & Hill, R. P. (2002). Tumor hypoxia has independent predictor impact only in patients with node-negative cervix cancer. *Journal of Clinical Oncology, 20*(3), 680-687. doi:10.1200/jco.2002.20.3.680

Giglia-Mari, G., Zotter, A., & Vermeulen, W. (2011). DNA damage response. *Cold Spring Harbor Perspectives in Biology, 3*(1), a000745-a000745. doi:10.1101/cshperspect.a000745

Goldberg, F. W., Finlay, M. R. V., Ting, A. K. T., Beattie, D., Lamont, G. M., Fallan, C., . . . Dean, E. (2020). The discovery of 7-Methyl-2-[(7-methyl[1,2,4]triazolo[1,5*a*]pyridin-6-yl)amino]-9-(tetrahydro-2*H*-pyran-4-yl)-7,9-dihydro-8*H*-purin-8-one (AZD7648), a potent and selective DNA-dependent protein kinase (DNA-PK) inhibitor. *Journal of Medicinal Chemistry, 63*(7), 3461-3471. doi:10.1021/acs.jmedchem.9b01684

Gonzalez, D. L., Giannerini, S., & Rosa, R. (2019). On the origin of degeneracy in the genetic code. *Interface Focus, 9*(6), 20190038. doi:10.1098/rsfs.2019.0038

Goodarzi, A. A., & Jeggo, P. A. (2012). Irradiation induced foci (IRIF) as a biomarker for radiosensitivity. *Mutation Research/Fundamental and Molecular Mechanisms of Mutagenesis, 736*(1-2), 39-47.

Goodwin, J. F., & Knudsen, K. E. (2014). Beyond DNA repair: DNA-PK function in cancer. *Cancer Discovery, 4*(10), 1126-1139. doi:10.1158/2159-8290.cd-14-0358

Graeber, T. G., Osmanian, C., Jacks, T., Housman, D. E., Koch, C. J., Lowe, S. W., & Giaccia, A. J. (1996). Hypoxia-mediated selection of cells with diminished apoptotic potential in solid tumours. *Nature, 379*(6560), 88-91.

Griffin, R. J., Fontana, G., Golding, B. T., Guiard, S., Hardcastle, I. R., Leahy, J. J., . . . Stockley, M. (2005). Selective benzopyranone and pyrimido [2, 1-a] isoquinolin-4-one inhibitors of DNA-dependent protein kinase: synthesis, structure− activity studies, and radiosensitization of a human tumor cell line in vitro. *Journal of Medicinal Chemistry, 48*(2), 569-585.

Griffin, R. J., Fontana, G., Golding, B. T., Guiard, S., Hardcastle, I. R., Leahy, J. J. J., . . . Smith, G. C. M. (2005). Selective benzopyranone and Pyrimido[2,1-*a*]isoquinolin-4-one Inhibitors of DNA-dependent protein kinase: synthesis, structure−activity studies, and radiosensitization of a human tumor cell line in vitro. *Journal of Medicinal Chemistry, 48*(2), 569-585. doi:10.1021/jm049526a

Guise, C. P., Abbattista, M. R., Singleton, R. S., Holford, S. D., Connolly, J., Dachs, G. U., . . . Patterson, A. V. (2010). The bioreductive prodrug PR-104A is activated under aerobic conditions by human aldo-keto reductase 1C3. *Cancer Research, 70*(4), 1573-1584. doi:10.1158/0008-5472.can-09-3237

Guise, C. P., Mowday, A. M., Ashoorzadeh, A., Yuan, R., Lin, W.-H., Wu, D.-H., . . . Ding, K. (2014). Bioreductive prodrugs as cancer therapeutics: targeting tumor hypoxia. *Chinese Journal of Cancer, 33*(2), 80.

Guo, Z., Deshpande, R., & Paull, T. T. (2010). ATM activation in the presence of oxidative stress. *Cell Cycle, 9*(24), 4805-4811.

Gupta, A. K., Cerniglia, G. J., Mick, R., Ahmed, M. S., Bakanauskas, V. J., Muschel, R. J., & McKenna, W. G. (2003). Radiation sensitization of human cancer cells in vivo by inhibiting the activity of PI3K using LY294002. *International Journal of Radiation Oncology* Biology* Physics, 56*(3), 846-853.

Hall, E. J., Giaccia, Amato J. (2006). *Radiobiology for the radiologist* (6th . ed.). Philadelphia: Philadelphia : Lippincott Williams & Wilkins c2006.

Hamis, S., Kohandel, M., Dubois, L. J., Yaromina, A., Lambin, P., & Powathil, G. G. (2020). Combining hypoxia-activated prodrugs and radiotherapy in silico: Impact of treatment scheduling and the intra-tumoural oxygen landscape. *PLOS Computational Biology, 16*(8), e1008041. doi:10.1371/journal.pcbi.1008041

Han, J., & Huang, J. (2020). DNA double-strand break repair pathway choice: the fork in the road. *Genome Instability & Disease, 1*(1), 10-19.

Hanahan, D. (2022). Hallmarks of cancer: new dimensions. *Cancer Discovery, 12*(1), 31-46. doi:10.1158/2159-8290.cd-21-1059

Hanahan, D., & Robert. (2011). Hallmarks of cancer: the next generation. *Cell, 144*(5), 646-674. doi:10.1016/j.cell.2011.02.013

Hanahan, D., & Weinberg, R. A. (2000). The hallmarks of cancer. *Cell, 100*(1), 57-70. doi:10.1016/s0092-8674(00)81683-9

Harnor, S., Brennan, A., & Cano, C. (2017). Targeting DNA-dependent protein kinase for cancer therapy. *ChemMedChem*. 12.12 (2017): 895-900

Hartley, K. O., Gell, D., Smith, G. C., Zhang, H., Divecha, N., Connelly, M. A., . . . Jackson, S. P. (1995). DNA-dependent protein kinase catalytic subunit: a relative of phosphatidylinositol 3-kinase and the ataxia telangiectasia gene product. *Cell, 82*(5), 849-856.

Hay, M., Liew, L., Wong, W., Dickson, B., Cheng, G., Hong, C. R., . . . Jamieson, S. (2020). 25 Poster Discussion - Hypoxia-activated prodrugs of DNA-dependent protein kinase as radiosensitisers. *European Journal of Cancer, 138*, S13-S14. doi:https://doi.org/10.1016/S0959-8049(20)31099-6

Hetz, C. (2012). The unfolded protein response: controlling cell fate decisions under ER stress and beyond. *Nature Reviews: Molecular Cell Biology, 13*(2), 89-102. doi:10.1038/nrm3270

Hicks, K. O., Myint, H., Patterson, A. V., Pruijn, F. B., Siim, B. G., Patel, K., & Wilson, W. R. (2007). Oxygen dependence and extravascular transport of hypoxia-activated prodrugs: comparison of the dinitrobenzamide mustard PR-104A and Tirapazamine. *International Journal of Radiation Oncology*Biology*Physics, 69*(2), 560-571. doi:https://doi.org/10.1016/j.ijrobp.2007.05.049

Hicks, R. J., Rischin, D., Fisher, R., Binns, D., Scott, A. M., & Peters, L. J. (2005). Utility of FMISO PET in advanced head and neck cancer treated with chemoradiation incorporating a hypoxia-targeting chemotherapy agent. *European Journal of Nuclear Medicine and Molecular Imaging, 32*(12), 1384-1391. doi:10.1007/s00259-005-1880-2

Hiremath, S. B., & Devendrappa, S. L. (2018). Safety and efficacy of tirapazamine as anti-cancer drug: a meta-analysis of randomized controlled trials. *International Journal of Basic Clinical Pharmacology, 7*, 783.

Hoeijmakers, J. H. J. (2001). Genome maintenance mechanisms for preventing cancer. *Nature, 411*(6835), 366-374. doi:10.1038/35077232

Holley, A. K., Miao, L., St. Clair, D. K., & St. Clair, W. H. (2014). Redox-modulated phenomena and radiation therapy: the central role of superoxide dismutases. *Antioxidants & Redox Signaling, 20*(10), 1567-1589. doi:10.1089/ars.2012.5000

Hollick, J. J., Golding, B. T., Hardcastle, I. R., Martin, N., Richardson, C., Rigoreau, L. J., . . . Griffin, R. J. (2003). 2, 6-disubstituted pyran-4-one and thiopyran-4-one inhibitors of DNA-Dependent protein kinase (DNA-PK). *Bioorganic & Medicinal Chemistry Letters, 13*(18), 3083-3086.

Hong, C. R., Bogle, G., Wang, J., Patel, K., Pruijn, F. B., Wilson, W. R., & Hicks, K. O. (2018). Bystander effects of hypoxia-activated prodrugs: agent-based modeling using three dimensional cell cultures. *Frontiers in Pharmacology*, 1013.

Hong, C. R., Buckley, C. D., Wong, W. W., Anekal, P. V., Dickson, B. D., Bogle, G., . . . Wilson, W. R. (2022). Radiosensitisation of SCCVII tumours and normal tissues in mice by the DNA-dependent protein kinase inhibitor AZD7648. *Radiotherapy and Oncology, 166*, 162-170. doi:https://doi.org/10.1016/j.radonc.2021.11.027

Hong, C. R., Dickson, B. D., Jaiswal, J. K., Pruijn, F. B., Hunter, F. W., Hay, M. P., . . . Wilson, W. R. (2018). Cellular pharmacology of evofosfamide (TH-302): A critical re-evaluation of its bystander effects. *Biochemical Pharmacology, 156*, 265-280.

Hong, C. R., Mehta, S. Y., Liyanage, H., McManaway, S. P., Lee, H. H., Jaiswal, J. K., . . . Wilson, W. R. (2021). Spatially-resolved pharmacokinetic/pharmacodynamic modelling of bystander effects of a nitrochloromethylbenzindoline hypoxia-activated prodrug. *Cancer Chemotherapy and Pharmacology, 88*(4), 673-687.

Hong, D. S., Bowles, D. W., Falchook, G. S., Messersmith, W. A., George, G. C., O'Bryant, C. L., . . . Eckhardt, S. G. (2012). A multicenter phase I trial of PX-866, an oral irreversible phosphatidylinositol 3-kinase inhibitor, in patients with advanced solid tumors. *Clinical Cancer Research, 18*(15), 4173-4182.

Huang, B., Shang, Z.-F., Li, B., Wang, Y., Liu, X.-D., Zhang, S.-M., . . . Zhou, P.-K. (2014). DNA-PKcs associates with PLK1 and is involved in proper chromosome segregation and cytokinesis. *Journal of Cellular Biochemistry, 115*(6), 1077-1088. doi:10.1002/jcb.24703

Huang, R.-X., & Zhou, P.-K. (2020). DNA damage response signaling pathways and targets for radiotherapy sensitization in cancer. *Signal Transduction and Targeted Therapy, 5*(1). doi:10.1038/s41392-020-0150-x

Hughes, J., Rees, S., Kalindjian, S., & Philpott, K. (2011). Principles of early drug discovery. *British Journal of Pharmacology, 162*(6), 1239-1249. doi:10.1111/j.1476-5381.2010.01127.x

Hunter, F. W., Jaiswal, J. K., Hurley, D. G., Liyanage, H. S., McManaway, S. P., Gu, Y., . . . Print, C. G. (2014). The flavoprotein FOXRED2 reductively activates nitro-chloromethylbenzindolines and other hypoxia-targeting prodrugs. *Biochemical Pharmacology, 89*(2), 224-235.

Hunter, F. W., Wouters, B. G., & Wilson, W. R. (2016). Hypoxia-activated prodrugs: paths forward in the era of personalised medicine. *British Journal of Cancer, 114*(10), 1071-1077. doi:10.1038/bjc.2016.79

Hunter, F. W., Young, R. J., Shalev, Z., Vellanki, R. N., Wang, J., Gu, Y., . . . Wouters, B. G. (2015). Identification of P450 oxidoreductase as a major determinant of sensitivity to hypoxia-activated prodrugs. *Cancer Research, 75*(19), 4211-4223. doi:10.1158/0008-5472.can-15-1107

Hunter, T. (1995). When is a lipid kinase not a lipid kinase? When it is a protein kinase. *Cell, 83*(1), 1-4.

Ihle, N. T., Williams, R., Chow, S., Chew, W., Berggren, M. I., Paine-Murrieta, G., . . . Abraham, R. (2004). Molecular pharmacology and antitumor activity of PX-866, a novel inhibitor of phosphoinositide-3-kinase signaling. *Molecular Cancer Therapeutics, 3*(7), 763-772.

Ikushima, H. (2010). Radiation therapy: state of the art and the future. *The Journal of Medical Investigation, 57*(1,2), 1-11. doi:10.2152/jmi.57.1

Ishna N. Mistry, P., Matthew Thomas, Ewen D.D. Calder, Stuart J. Conway and Ester M. Hammond (2017). Clinical advances of hypoxia-activated prodrugs in combination with radiation therapy. *International Journal of Radiation Oncology.* 98.5 1183-1196

Ismail, I. H., Mårtensson, S., Moshinsky, D., Rice, A., Tang, C., Howlett, A., . . . Hammarsten, O. (2004). SU11752 inhibits the DNA-dependent protein kinase and DNA double-strand break repair resulting in ionizing radiation sensitization. *Oncogene, 23*(4), 873-882. doi:10.1038/sj.onc.1207303

Jackson, R. K., Liew, L. P., & Hay, M. P. (2019). Overcoming radioresistance: small molecule radiosensitisers and hypoxia-activated prodrugs. *Clinical Oncology, 31*(5), 290-302. doi:10.1016/j.clon.2019.02.004

Jackson, S. P., & Bartek, J. (2009). The DNA-damage response in human biology and disease. *Nature, 461*(7267), 1071-1078. doi:10.1038/nature08467

Jackson-Patel, V. J., Liu, E., Bull, M. R., Ashoorzadeh, A., Bogle, G., Hicks, K. O., . . . Patterson, A. V. (2022). Tissue pharmacokinetic properties and bystander potential of hypoxia-activated prodrug CP-506 by agent-based modelling. *Frontiers in Pharmacology*, 38.

Jameson, M. B., Rischin, D., Pegram, M., Gutheil, J., Patterson, A. V., Denny, W. A., & Wilson, W. R. (2010). A phase I trial of PR-104, a nitrogen mustard prodrug activated by both hypoxia and aldo-keto reductase 1C3, in patients with solid tumors. *Cancer Chemotherapy and Pharmacology, 65*(4), 791-801. doi:10.1007/s00280-009-1188-1

Janssens, G. O., Rademakers, S. E., Terhaard, C. H., Doornaert, P. A., Bijl, H. P., Van Den Ende, P., . . . Kaanders, J. H. (2012). Accelerated radiotherapy with carbogen and nicotinamide for laryngeal cancer: results of a phase III randomized trial. *Journal of Clinical Oncology, 30*(15), 1777-1783. doi:10.1200/jco.2011.35.9315

Jarosz-Biej, M., Smolarczyk, R., Cichoń, T., & Kułach, N. (2019). Tumor microenvironment as a "game changer" in cancer radiotherapy. *International Journal of Molecular Sciences, 20*(13), 3212. doi:10.3390/ijms20133212

Jimeno, A., Bauman, J. E., Weissman, C., Adkins, D., Schnadig, I., Beauregard, P., . . . Shirai, K. (2015). A randomized, phase 2 trial of docetaxel with or without PX-866, an irreversible oral phosphatidylinositol 3-kinase inhibitor, in patients with relapsed or metastatic head and neck squamous cell cancer. *Oral Oncology, 51*(4), 383-388. doi:10.1016/j.oraloncology.2014.12.013

Johnson, C. A., Kilpatrick, D., von Roemeling, R., Langer, C., Graham, M., Greenslade, D., . . . O'Dwyer, P. J. (1997). Phase I trial of tirapazamine in combination with cisplatin in a single dose every 3 weeks in patients with solid tumors. *Journal of Clinical Oncology, 15*(2), 773-780.

Joiner, M. C., & van der Kogel, A. J. (2018). Basic clinical radiobiology: CRC press.

Juan, C. A., Pérez De La Lastra, J. M., Plou, F. J., & Pérez-Lebeña, E. (2021). The chemistry of reactive oxygen species (ROS) revisited: outlining their role in biological macromolecules (DNA, lipids and proteins) and induced pathologies. *International Journal of Molecular Sciences, 22*(9), 4642. doi:10.3390/ijms22094642

Kamili, C., Kandoti, H. S., Radhakrishnan, S., Konde, A., & Vattikutti, U. M. R. (2020). Anti-angiogenic activity of chloride and potassium channel modulators: repurposing ion channel modulators. *Future Journal of Pharmaceutical Sciences, 6*(1). doi:10.1186/s43094-020-00041-1

Karve, S., Werner, M. E., Sukumar, R., Cummings, N. D., Copp, J. A., Wang, E. C., . . . Wang, A. Z. (2012). Revival of the abandoned therapeutic Wortmannin by nanoparticle drug delivery. *Proceedings of the National Academy of Sciences USA, 109*(21), 8230-8235. doi:10.1073/pnas.1120508109

Kashishian, A., Douangpanya, H., Clark, D., Schlachter, S. T., Eary, C. T., Schiro, J. G., . . . Halbrook, J. (2003). DNA-dependent protein kinase inhibitors as drug candidates for the treatment of cancer. *Molecular Cancer Therapeutics, 2*(12), 1257-1264.

Keepers, Y. P., Pizao, P. E., Peters, G. J., van Ark-Otte, J., Winograd, B., & Pinedo, H. M. (1991). Comparison of the sulforhodamine B protein and tetrazolium (MTT) assays for in vitro chemosensitivity testing. *European Journal of Cancer and Clinical Oncology, 27*(7), 897-900.

Kim, B., Hong, Y., Lee, S., Liu, P., Lim, J., Lee, Y., . . . Hong, Y. (2015). Therapeutic implications for overcoming radiation resistance in cancer therapy. *International Journal of Molecular Sciences, 16*(11), 26880-26913. doi:10.3390/ijms161125991

Knight, Z., & Shokat, K. (2007). Chemically targeting the PI3K family. Portland Press Ltd. 245-249.

Kolesnick, R., & Fuks, Z. (2003). Radiation and ceramide-induced apoptosis. *Oncogene, 22*(37), 5897-5906. doi:10.1038/sj.onc.1206702

Koukourakis, M. I., Bentzen, S. M., Giatromanolaki, A., Wilson, G. D., Daley, F. M., Saunders, M. I., . . . Harris, A. L. (2006). Endogenous markers of two separate hypoxia response pathways (hypoxia inducible factor 2 alpha and carbonic anhydrase 9) are associated with radiotherapy failure in head and neck cancer patients recruited in the CHART randomized trial. *Journal of Clinical Oncology, 24*(5), 727-735.

Kovacs, M. S., Hocking, D. J., Evans, J. W., Siim, B. G., Wouters, B. G., & Brown, J. M. (1999). Cisplatin anti-tumour potentiation by Tirapazamine results from a hypoxia-dependent cellular sensitization to cisplatin. *British Journal of Cancer, 80*(8), 1245-1251. doi:10.1038/sj.bjc.6690492

Le, P. N., Maranon, D. G., Altina, N. H., Battaglia, C. L., & Bailey, S. M. (2013). TERRA, hnRNP A1, and DNA-PKcs interactions at human telomeres. *Frontiers in Oncology, 3*, 91.

Leach, R., Rees, P., & Wilmshurst, P. (1998). Hyperbaric oxygen therapy. *BMJ, 317*(7166), 1140-1143.

Leahy, J. J., Golding, B. T., Griffin, R. J., Hardcastle, I. R., Richardson, C., Rigoreau, L., & Smith, G. C. (2004). Identification of a highly potent and selective DNA-dependent protein kinase (DNA-PK) inhibitor (NU7441) by screening of chromenone libraries. *Bioorganic & Medicinal Chemistry Letters, 14*(24), 6083-6087.

Lee, D.-J., Cosmatos, D., Marcial, V. A., Fu, K. K., Rotman, M., Cooper, J. S., . . . Wasserman, T. H. (1995). Results of an RTOG phase III trial (RTOG 85-27) comparing radiotherapy plus Etanidazole with radiotherapy alone for locally advanced head and neck carcinomas. *International Journal of Radiation Oncology*Biology*Physics, 32*(3), 567-576. doi:10.1016/0360-3016(95)00150-w

Lee, J. H., Jeon, B., Park, M., Ha, J., Kim, S. J., Son, M. K., . . . Jeong, Y. K. (2021). Synergistic radiosensitizing effect of BR101801, a specific DNA-dependent protein kinase inhibitor, in various human solid cancer cells and xenografts. *American Journal of Cancer Research, 11*(11), 5440-5451.

Lempiäinen, H., & Halazonetis, T. D. (2009). Emerging common themes in regulation of PIKKs and PI3Ks. *The EMBO Journal, 28*(20), 3067-3073. doi:10.1038/emboj.2009.281

Li, Y., Zhao, L., & Li, X.-F. (2021). Targeting hypoxia: hypoxia-activated prodrugs in cancer therapy. *Frontiers in Oncology*, 2920.

Liang, S., Thomas, S. E., Chaplin, A. K., Hardwick, S. W., Chirgadze, D. Y., & Blundell, T. L. (2022). Structural insights into inhibitor regulation of the DNA repair protein DNA-PKcs. *Nature, 601*(7894), 643-648. doi:10.1038/s41586-021-04274-9

Liang, Y., Lin, S.-Y., Brunicardi, F. C., Goss, J., & Li, K. (2009). DNA damage response pathways in tumor suppression and cancer treatment. *World Journal of Surgery, 33*(4), 661-666. doi:10.1007/s00268-008-9840-1

Linda Spiegelberg, R. Houben, Raymon, Niemans, Dirk de Ruysscher, Ala Yaromina, Jan Theys, Christopher P. Guise, Jeffrey B. Smaill, Adam V. Patterson, Philippe Lambin, Ludwig J. Dubois. (2019). Hypoxia-activated prodrugs and (lack of) clinical progress: The need for hypoxia-based biomarker patient selection in phase III clinical trials. *Elsevier, 15*. 62-69.

Liu, S., Opiyo, S. O., Manthey, K., Glanzer, J. G., Ashley, A. K., Amerin, C., . . . Oakley, G. G. (2012). Distinct roles for DNA-PK, ATM and ATR in RPA phosphorylation and

checkpoint activation in response to replication stress. *Nucleic Acids Research, 40*(21), 10780-10794. doi:10.1093/nar/gks849

Liu, S. V., Villaruz, L. C., Lee, V. H. F., Zhu, V. W., Baik, C. S., Sacher, A., . . . Camidge, D. R. (2020). LBA61 First analysis of RAIN-701: Study of Tarloxotinib in patients with non-small cell lung cancer (NSCLC) EGFR exon 20 insertion, HER2-activating mutations & other solid tumours with NRG1/ERBB gene fusions. *Annals of Oncology, 31*, S1189. doi:10.1016/j.annonc.2020.08.2294

Lomax, M. E., Folkes, L. K., & O'Neill, P. (2013). Biological consequences of radiation-induced DNA damage: Relevance to radiotherapy. *Clinical Oncology, 25*(10), 578-585. doi:10.1016/j.clon.2013.06.007

Mah, L.-J., El-Osta, A., & Karagiannis, T. C. (2010). γH2AX: a sensitive molecular marker of DNA damage and repair. *Leukemia, 24*(4), 679-686. doi:10.1038/leu.2010.6

Maluf, F., Leiser, A., Aghajanian, C., Sabbatini, P., Pezzulli, S., Chi, D., . . . Spriggs, D. (2006). Phase II study of tirapazamine plus cisplatin in patients with advanced or recurrent cervical cancer. *International Journal of Gynecologic Cancer, 16*(3).

Marechal, A., & Zou, L. (2013). DNA damage sensing by the ATM and ATR Kinases. *Cold Spring Harbor Perspectives in Biology, 5*(9), a012716-a012716. doi:10.1101/cshperspect.a012716

Martin Brown, J., & Lemmon, M. J. (1991). SR 4233: A tumor specific radiosensitizer active in fractionated radiation regimes. *Radiotherapy and Oncology, 20*, 151-156. doi:10.1016/0167-8140(91)90203-s

Matter, W. F., Brown, R. F., & Vlahos, C. J. (1992). The inhibition of phosphatidylinositol 3-kinase by quercetin and analogs. *Biochemical and Biophysical Research Communications, 186*(2), 624-631.

Mattiuzzi, C., & Lippi, G. (2019). Current Cancer Epidemiology. *Journal of Epidemiology and Global Health, 9*(4), 217-222. doi:10.2991/jegh.k.191008.001

McKeage, M. J., Gu, Y., Wilson, W. R., Hill, A., Amies, K., Melink, T. J., & Jameson, M. B. (2011). A phase I trial of PR-104, a pre-prodrug of the bioreductive prodrug PR-104A, given weekly to solid tumour patients. *BMC Cancer, 11*(1), 432. doi:10.1186/1471-2407-11-432

McKeage, M. J., Jameson, M. B., Ramanathan, R. K., Rajendran, J., Gu, Y., Wilson, W. R., . . . Tchekmedyian, N. S. (2012). PR-104 a bioreductive pre-prodrug combined with gemcitabine or docetaxel in a phase Ib study of patients with advanced solid tumours. *BMC Cancer, 12*(1), 496. doi:10.1186/1471-2407-12-496

Meng, F., Evans, J. W., Bhupathi, D., Banica, M., Lan, L., Lorente, G., . . . Hart, C. P. (2012). Molecular and cellular pharmacology of the hypoxia-activated prodrug TH-302. *Molecular Cancer Therapeutics, 11*(3), 740-751. doi:10.1158/1535-7163.mct-11-0634

Menolfi, D., & Zha, S. (2020). ATM, ATR and DNA-PKcs kinases—the lessons from the mouse models: inhibition ≠ deletion. *Cell & Bioscience, 10*(1). doi:10.1186/s13578-020-0376-x

Mikusová, V., Tichý, A., Rezáčová, M., & Vávrová, J. (2011). Mitoxantrone in combination with a DNA-PK inhibitor: possible therapy of promyelocytic leukaemia resistant forms. *Folia Biologica.(Praha), 57*(5), 200-205.

Minniti, G., Goldsmith, C., & Brada, M. (2012). Radiotherapy. In *Handbook of Clinical Neurology* (pp. 215-228): Elsevier.

Mohan, R., & Grosshans, D. (2017). Proton therapy – present and future. *Advanced Drug Delivery Reviews, 109*, 26-44. doi:10.1016/j.addr.2016.11.006

Mohiuddin, I. S., & Kang, M. H. (2019). DNA-PK as an emerging therapeutic target in cancer. *Frontiers in Oncology, 9*, 635.

Mortensen, D. S., Perrin-Ninkovic, S. M., Shevlin, G., Elsner, J., Zhao, J., Whitefield, B., . . . Sankar, S. (2015). Optimization of a series of triazole containing mammalian target of rapamycin (mTOR) kinase inhibitors and the discovery of CC-115. *Journal of Medicinal Chemistry, 58*(14), 5599-5608. doi:10.1021/acs.jmedchem.5b00627

Munck, J. M., Batey, M. A., Zhao, Y., Jenkins, H., Richardson, C. J., Cano, C., . . . Curtin, N. J. (2012). Chemosensitization of cancer cells by KU-0060648, a dual inhibitor of DNA-PK and PI-3K. *Molecular Cancer Therapeutics, 11*(8), 1789-1798. doi:10.1158/1535-7163.mct-11-0535

Munster, P., Mita, M., Mahipal, A., Nemunaitis, J., Massard, C., Mikkelsen, T., . . . Bendell, J. C. (2019). First-in-human phase I study of a dual mTOR Kinase and DNA-PK inhibitor (CC-115) in advanced malignancy. *Cancer Management and Research, Volume 11*, 10463-10476. doi:10.2147/cmar.s208720

Murr, R., Vaissière, T., Sawan, C., Shukla, V., & Herceg, Z. (2007). Orchestration of chromatin-based processes: mind the TRRAP. *Oncogene, 26*(37), 5358-5372. doi:10.1038/sj.onc.1210605

Muz, B., De La Puente, P., Azab, F., & Azab, A. K. (2015). The role of hypoxia in cancer progression, angiogenesis, metastasis, and resistance to therapy. *Hypoxia*, 83. doi:10.2147/hp.s93413

Nakada, S. (2016). Opposing roles of RNF8/RNF168 and deubiquitinating enzymes in ubiquitination-dependent DNA double-strand break response signaling and DNA-repair pathway choice. *Journal of Radiation Research, 57*(S1), i33-i40. doi:10.1093/jrr/rrw027

Niemantsverdriet, M., Van Goethem, M.-J., Bron, R., Hogewerf, W., Brandenburg, S., Langendijk, J. A., . . . Coppes, R. P. (2012). High and low LET radiation differentially induce normal tissue damage signals. *International Journal of Radiation Oncology*Biology*Physics, 83*(4), 1291-1297. doi:10.1016/j.ijrobp.2011.09.057

Nordsmark, M., Bentzen, S. M., Rudat, V., Brizel, D., Lartigau, E., Stadler, P., . . . Dunst, J. (2005). Prognostic value of tumor oxygenation in 397 head and neck tumors after primary radiation therapy. An international multi-center study. *Radiotherapy and Oncology, 77*(1), 18-24.

Nutley, B. P., Smith, N. F., Hayes, A., Kelland, L. R., Brunton, L., Golding, B. T., . . . Raynaud, F. I. (2005). Preclinical pharmacokinetics and metabolism of a novel prototype DNA-PK inhibitor NU7026. *British Journal of Cancer, 93*(9), 1011-1018. doi:10.1038/sj.bjc.6602823

Nyman, J., Hallqvist, A., Lund, J.-Å., Brustugun, O.-T., Bergman, B., Bergström, P., . . . Lax, I. (2016). SPACE – A randomized study of SBRT vs conventional fractionated radiotherapy in medically inoperable stage I NSCLC. *Radiotherapy and Oncology, 121*(1), 1-8. doi:10.1016/j.radonc.2016.08.015

O'Connor, M. J. (2015). Targeting the DNA damage response in cancer. *Molecular Cell, 60*(4), 547-560.

Overgaard, J. (2007). Hypoxic radiosensitization: adored and ignored. *Journal of Clinical Oncology, 25*(26), 4066-4074. doi:10.1200/jco.2007.12.7878

Overgaard, J., Hansen, H. S., Overgaard, M., Bastholt, L., Berthelsen, A., Specht, L., . . . Jørgensen, K. (1998). A randomized double-blind phase III study of Nimorazole as a hypoxic radiosensitizer of primary radiotherapy in supraglottic larynx and pharynx

carcinoma. Results of the Danish Head And Neck Cancer study (DAHANCA) protocol 5-85. *Radiotherapy and Oncology, 46*(2), 135-146.

Overgaard, J., Overgaard, M., & Timothy, A. R. (1983). Studies of the pharmacokinetic properties of Nimorazole. *British Journal of Cancer, 48*(1), 27-34. doi:10.1038/bjc.1983.153

Overgaard, J., Sand Hansen, H., Andersen, A. P., Hjelm-Hansen, M., Jørgensen, K., Sandberg, E., . . . Pedersen, M. (1989). Misonidazole combined with split-course radiotherapy in the treatment of invasive carcinoma of larynx and pharynx: Report from the DAHANCA 2 study. *International Journal of Radiation Oncology*Biology*Physics, 16*(4), 1065-1068. doi:10.1016/0360-3016(89)90917-6

Patterson, A. V., Ferry, D. M., Edmunds, S. J., Gu, Y., Singleton, R. S., Patel, K., . . . Wilson, W. R. (2007). Mechanism of action and preclinical antitumor activity of the novel hypoxia-activated DNA cross-linking agent PR-104. *Clinical Cancer Research, 13*(13), 3922-3932. doi:10.1158/1078-0432.ccr-07-0478

Pauwels, B., Korst, A. E. C., De Pooter, C. M. J., Pattyn, G. G. O., Lambrechts, H. A. J., Baay, M. F. D., . . . Vermorken, J. B. (2003). Comparison of the sulforhodamine B assay and the clonogenic assay for in vitro chemoradiation studies. *Cancer Chemotherapy and Pharmacology, 51*(3), 221-226. doi:10.1007/s00280-002-0557-9

Pawlik, T. M., & Keyomarsi, K. (2004). Role of cell cycle in mediating sensitivity to radiotherapy. *International Journal of Radiation Oncology* Biology* Physics, 59*(4), 928-942.

Phillips, R. M. (2016). Targeting the hypoxic fraction of tumours using hypoxia-activated prodrugs. *Cancer Chemotherapy and Pharmacology, 77*(3), 441-457. doi:10.1007/s00280-015-2920-7

Pospisilova, M., Seifrtova, M., & Rezacova, M. (2017). Small molecule inhibitors of DNA-PK for tumor sensitization to anticancer therapy. *Journal of Physiology Pharmacology, 68*(3), 337-344.

Prise, K. M., Schettino, G., Folkard, M., & Held, K. D. (2005). New insights on cell death from radiation exposure. *The Lancet Oncology, 6*(7), 520-528.

Rahman, R., Trippa, L., Fell, G., Lee, E., Arrillaga-Romany, I., Touat, M., . . . Wen, P. (2020). CTNI-11. CC-115 in newly diagnosed mgmt unmethylated glioblastoma in the individualized screening trial of innovative glioblastoma therapy (insight): A phase II randomized Bayesian adaptive platform trial. *Neuro-Oncology, 22*(Supplement_2), ii43-ii44. doi:10.1093/neuonc/noaa215.178

Rahman, R., Trippa, L., Fell, G., Lee, E. Q., Arrillaga-Romany, I., Touat, M., . . . Colman, H. (2021). Evaluating the benefit of adaptive randomization in the CC-115 arm of the Individualized Screening trial of Innovative Glioblastoma Therapy (INSIGhT): A phase II randomized Bayesian adaptive platform trial in newly diagnosed MGMT unmethylated glioblastoma. *Wolters Kluwer Health*. 2006-2006

Reddy, S. B., & Williamson, S. K. (2009). Tirapazamine: a novel agent targeting hypoxic tumor cells. *Expert Opinion on Investigational Drugs, 18*(1), 77-87. doi:10.1517/13543780802567250

Rischin, D., Boyer, M. J., Brzezniak, C. E., Colevas, A. D., Doebele, R. C., Gilbert, J., . . . Seiwert, T. Y. (2016). A phase 2 study of tarloxotinib bromide (TRLX) in patients (Pts) with recurrent or metastatic (R/M) squamous cell carcinoma of the head and neck (SCCHN) or skin (SCCS). *American Society of Clinical Oncology*. TPS6105-TPS6105.

Rischin, D., Hicks, R. J., Fisher, R., Binns, D., Corry, J., Porceddu, S., & Peters, L. J. (2006). Prognostic significance of [18F]-misonidazole positron emission tomography–detected tumor hypoxia in patients with advanced head and neck cancer randomly assigned to chemoradiation with or without tirapazamine: A substudy of Trans-Tasman Radiation Oncology Group Study 98.02. *Journal of Clinical Oncology, 24*(13), 2098-2104.

Rischin, D., Peters, L., Fisher, R., Macann, A., Denham, J., Poulsen, M., . . . Corry, J. (2005). Tirapazamine, cisplatin, and radiation versus fluorouracil, cisplatin, and radiation in patients with locally advanced head and neck cancer: a randomized phase II trial of the Trans-Tasman Radiation Oncology Group (TROG 98.02). *Journal of Clinical Oncology, 23*(1), 79-87.

Rischin, D., Peters, L., Hicks, R., Hughes, P., Fisher, R., Hart, R., . . . Von Roemeling, R. (2001). Phase I Trial of Concurrent Tirapazamine, Cisplatin, and Radiotherapy in Patients With Advanced Head and Neck Cancer. *Journal of Clinical Oncology, 19*(2), 535-542. doi:10.1200/jco.2001.19.2.535

Rischin, D., Peters, L., O'Sullivan, B., Giralt, J., Yuen, K., Trotti, A., . . . Fisher, R. (2008). Phase III study of tirapazamine, cisplatin and radiation versus cisplatin and radiation for advanced squamous cell carcinoma of the head and neck. *Journal of Clinical Oncology, 26*(15_suppl), LBA6008-LBA6008.

Rischin, D., Peters, L. J., O'Sullivan, B., Giralt, J., Fisher, R., Yuen, K., . . . Ringash, J. (2008). Tirapazamine, Cisplatin, and radiation versus Cisplatin and radiation for advanced squamous cell carcinoma of the head and neck (TROG 02.02, HeadSTART): a phase III trial of the Trans-Tasman Radiation Oncology Group. 0732-183X

Rivera-Calzada, A., López-Perrote, A., Melero, R., Boskovic, J., Muñoz-Hernández, H., Martino, F., & Llorca, O. (2015). Structure and assembly of the PI3K-like protein kinases (PIKKs) revealed by electron microscopy. *Aims Biophysics, 2*(2), 36-57.

Robert Grimes, D., & Partridge, M. (2015). A mechanistic investigation of the oxygen fixation hypothesis and oxygen enhancement ratio. *Biomedical Physics & Engineering Express, 1*(4), 045209. doi:10.1088/2057-1976/1/4/045209

Rohwer, N., & Cramer, T. (2011). Hypoxia-mediated drug resistance: novel insights on the functional interaction of HIFs and cell death pathways. *Drug Resistance Updates, 14*(3), 191-201.

Sandler, A. B., Nemunaitis, J., Denham, C., Von Pawel, J., Cormier, Y., Gatzemeier, U., . . . Einhorn, L. H. (2000). Phase III trial of Gemcitabine plus Cisplatin versus Cisplatin alone in patients with locally advanced or metastatic non–small-cell lung cancer. *Journal of Clinical Oncology, 18*(1), 122-122. doi:10.1200/jco.2000.18.1.122

Schulz-Ertner, D., & Tsujii, H. (2007). Particle radiation therapy using proton and heavier ion beams. *Journal of Clinical Oncology, 25*(8), 953-964. doi:10.1200/jco.2006.09.7816

Scully, R., Panday, A., Elango, R., & Willis, N. A. (2019). DNA double-strand break repair-pathway choice in somatic mammalian cells. *Nature Reviews: Molecular Cell Biology, 20*(11), 698-714. doi:10.1038/s41580-019-0152-0

Senan, S., Rampling, R., Graham, M. A., Wilson, P., Robin, H., Eckardt, N., . . . Workman, P. (1997). Phase I and pharmacokinetic study of Tirapazamine (SR 4233) administered every three weeks. *Clinical Cancer Research, 3*(1), 31-38.

Seol, J.-H., Shim, E. Y., & Lee, S. E. (2018). Microhomology-mediated end joining: good, bad and ugly. *Mutation Research/Fundamental and Molecular Mechanisms of Mutagenesis, 809*, 81-87. doi:10.1016/j.mrfmmm.2017.07.002

Shangary, S., & Wang, S. (2008). Targeting the MDM2-p53 interaction for cancer therapy. *Clinical Cancer Research, 14*(17), 5318-5324. doi:10.1158/1078-0432.ccr-07-5136

Sharif, H., Li, Y., Dong, Y., Dong, L., Wang, W. L., Mao, Y., & Wu, H. (2017). Cryo-EM structure of the DNA-PK holoenzyme. *Proceedings of the National Academy of Sciences USA, 114*(28), 7367-7372. doi:10.1073/pnas.1707386114

Sharma, R., Lewis, S., & Wlodarski, M. W. (2020). DNA repair syndromes and cancer: insights into genetics and phenotype patterns. *Frontiers in Pediatrics, 8,* 570084.

Sharma, S., Javadekar, S. M., Pandey, M., Srivastava, M., Kumari, R., & Raghavan, S. C. (2015). Homology and enzymatic requirements of microhomology-dependent alternative end joining. *Cell Death & Disease, 6*(3), e1697-e1697. doi:10.1038/cddis.2015.58

Shepherd, F., Koschel, G., Von Pawel, J., Gatzmeier, U., Van Zandwiyk, N., Woll, P., . . . Nicolson, M. (2000). Comparison of Tirazone (Tirapazamine) and Cisplatin vs. Etoposide and Cisplatin in advanced non-small cell lung cancer (NSCLC): final results of the international phase III CATAPULT II trial. *Lung Cancer, 1*(29), 28.

Shepherd, F., Koschel, G., von Pawel, J., Gatzmeier, U., Van Zandwiyk, N., Woll, P., . . . Loh, E. (2000). Comparison of Tirazone (Tirapazamine) and Cisplatin vs. Etoposide and Cisplatin in advanced non-small cell lung cancer (NSCLC): final results of the international phase III CATAPULT II trial. *Lung Cancer, 29*(1, Supplement 1), 28. doi:https://doi.org/10.1016/S0169-5002(00)80087-2

Shinde, S. S., Hay, M. P., Patterson, A. V., Denny, W. A., & Anderson, R. F. (2009). Spin trapping of radicals other than the •OH radical upon reduction of the anticancer agent Tirapazamine by cytochrome P450 Reductase. *Journal of the American Chemical Society, 131*(40), 14220-14221. doi:10.1021/ja906860a

Shinohara, E. T., Geng, L., Tan, J., Chen, H., Shir, Y., Edwards, E., . . . Hallahan, D. E. (2005). DNA-dependent protein kinase Is a molecular target for the development of noncytotoxic radiation–sensitizing drugs. *Cancer Research, 65*(12), 4987-4992. doi:10.1158/0008-5472.can-04-4250

Sia, J., Szmyd, R., Hau, E., & Gee, H. E. (2020). Molecular mechanisms of radiation-induced cancer cell death: a primer. *Frontiers in Cell and Developmental Biology, 8*, 41.

Singleton, D. C., Macann, A., & Wilson, W. R. (2021). Therapeutic targeting of the hypoxic tumour microenvironment. *Nature Reviews: Clinical Oncology, 18*(12), 751-772.

Siva, S., MacManus, M., & Ball, D. (2010). Stereotactic radiotherapy for pulmonary oligometastases: a systematic review. *Journal of Thoracic Oncology, 5*(7), 1091-1099.

Sørensen, B. S., & Horsman, M. R. (2020). Tumor hypoxia: impact on radiation therapy and molecular pathways. *Frontiers in Oncology, 10*, 562.

Sotiriou, S. K., Kamileri, I., Lugli, N., Evangelou, K., Da-Ré, C., Huber, F., . . . Halazonetis, T. D. (2016). Mammalian RAD52 functions in break-induced replication repair of collapsed DNA replication forks. *Molecular Cell, 64*(6), 1127-1134. doi:10.1016/j.molcel.2016.10.038

Spagnolo, L., Rivera-Calzada, A., Pearl, L. H., & Llorca, O. (2006). Three-dimensional structure of the human DNA-PKcs/Ku70/Ku80 complex assembled on DNA and its implications for DNA DSB repair. *Molecular Cell, 22*(4), 511-519. doi:10.1016/j.molcel.2006.04.013

Su, J., Gu, Y., Pruijn, F. B., Smaill, J. B., Patterson, A. V., Guise, C. P., & Wilson, W. R. (2013). Zinc finger nuclease knock-out of NADPH:cytochrome P450 oxidoreductase (POR) in human tumor cell lines demonstrates that hypoxia-activated prodrugs differ in POR

dependence. *Journal of Biological Chemistry, 288*(52), 37138-37153. doi:10.1074/jbc.m113.505222

Sui, J., Zhang, S., & Chen, B. P. C. (2020). DNA–dependent protein kinase in telomere maintenance and protection. *Cellular & Molecular Biology Letters, 25*(1). doi:10.1186/s11658-020-0199-0

Sun, J. D., Liu, Q., Wang, J., Ahluwalia, D., Ferraro, D., Wang, Y., . . . Hart, C. P. (2012). Selective tumor hypoxia targeting by hypoxia-activated prodrug TH-302 inhibits tumor growth in preclinical models of cancer. *Clinical Cancer Research, 18*(3), 758-770. doi:10.1158/1078-0432.ccr-11-1980

Sun, L., Tran, N., Liang, C., Tang, F., Rice, A., Schreck, R., . . . Tang, C. (1999). Design, synthesis, and evaluations of substituted 3-[(3- or 4-Carboxyethylpyrrol-2-yl)methylidenyl]indolin-2-ones as inhibitors of VEGF, FGF, and PDGF receptor tyrosine kinases. *Journal of Medicinal Chemistry, 42*(25), 5120-5130. doi:10.1021/jm9904295

Taghdiri, M., Dastsooz, H., Fardaei, M., Mohammadi, S., Farazi Fard, M. A., & Faghihi, M. A. (2017). A novel mutation in ERCC8 gene causing Cockayne syndrome. *Frontiers in Pediatrics, 5*, 169.

Tam, S. Y., Wu, V. W. C., & Law, H. K. W. (2017). Influence of autophagy on the efficacy of radiotherapy. *Radiation Oncology, 12*(1). doi:10.1186/s13014-017-0795-y

Tannock, I., Hill, R. P., Bristow, R. G., Harrington, L., & Amir, E. (2013). *The Basic Science of Oncology* (Fifth edition.. ed.): New York : McGraw-Hill Education Medical. 2013. Chapters: 5 p93-103, 15 p333-342 and 16 p357-388.

Tap, W. D., Papai, Z., Van Tine, B. A., Attia, S., Ganjoo, K. N., Jones, R. L., . . . Riedel, R. F. (2017). Doxorubicin plus Evofosfamide versus Doxorubicin alone in locally advanced, unresectable or metastatic soft-tissue sarcoma (TH CR-406/SARC021): an international, multicentre, open-label, randomised phase 3 trial. *The Lancet Oncology, 18*(8), 1089-1103.

Telarovic, I., Wenger, R. H., & Pruschy, M. (2021). Interfering with tumor hypoxia for radiotherapy optimization. *Journal of Experimental & Clinical Cancer Research, 40*(1). doi:10.1186/s13046-021-02000-x

Thariat, J., Hannoun-Levi, J.-M., Sun Myint, A., Vuong, T., & Gérard, J.-P. (2013). Past, present, and future of radiotherapy for the benefit of patients. *Nature Reviews: Clinical Oncology, 10*(1), 52-60. doi:10.1038/nrclinonc.2012.203

Thomas, K. A. (2016). Angiogenesis. In R. A. Bradshaw & P. D. Stahl (Eds.), *Encyclopedia of Cell Biology* (pp. 102-116). Waltham: Academic Press.

Thomlinson, R. H., & Gray, L. (1955). The histological structure of some human lung cancers and the possible implications for radiotherapy. *British Journal of Cancer, 9*(4), 539.

Threshold Pharmaceuticals. (2016). Threshold Pharmaceuticals announces interim results from Tarloxotinib program and its plans to focus on Evofosfamide and earlier-stage opportunities. https://www.globenewswire.com/news-release/2016/09/29/875884/0/en/Threshold-Pharmaceuticals-Announces-Interim-Results-from-Tarloxotinib-Program-and-its-Plans-to-Focus-on-Evofosfamide-and-Earlier-Stage-Opportunities.html accessed 12/2021

Timme, C. R., Rath, B. H., O'Neill, J. W., Camphausen, K., & Tofilon, P. J. (2018). The DNA-PK inhibitor VX-984 enhances the radiosensitivity of glioblastoma cells grown in vitro and as orthotopic xenografts. *Molecular Cancer Therapeutics, 17*(6), 1207-1216. doi:10.1158/1535-7163.mct-17-1267

Ting, N. S. Y., Pohorelic, B., Yu, Y., Lees-Miller, S. P., & Beattie, T. L. (2009). The human telomerase RNA component, hTR, activates the DNA-dependent protein kinase to phosphorylate heterogeneous nuclear ribonucleoprotein A1. *Nucleic Acids Research, 37*(18), 6105-6115. doi:10.1093/nar/gkp636

Tinganelli, W., Ma, N.-Y., Von Neubeck, C., Maier, A., Schicker, C., Kraft-Weyrather, W., & Durante, M. (2013). Influence of acute hypoxia and radiation quality on cell survival. *Journal of Radiation Research, 54*(suppl 1), i23-i30. doi:10.1093/jrr/rrt065

Trenner, A., & Sartori, A. A. (2019). Harnessing DNA double-strand break repair for cancer treatment. *Frontiers in Oncology, 9*, 1388.

Trojanowicz, M., Bobrowski, K., Szreder, T., & Bojanowska-Czajka, A. (2018). Gamma-ray, X-ray and electron beam based processes. In *Advanced Oxidation Processes for Waste Water Treatment* (pp. 257-331): Elsevier. 257-331.

Tubbs, A., & Nussenzweig, A. (2017). Endogenous DNA damage as a source of genomic instability in cancer. *Cell, 168*(4), 644-656. doi:10.1016/j.cell.2017.01.002

Van Beek, K. M., Kaanders, J. H. A. M., Janssens, G. O., Takes, R. P., Span, P. N., & Verhoef, C. G. (2016). Effectiveness and toxicity of hypofractionated high-dose intensity-modulated radiotherapy versus 2- and 3-dimensional radiotherapy in incurable head and neck cancer. *Head & Neck, 38*(S1), E1264-E1270. doi:10.1002/hed.24203

Van Bussel, M. T. J., Awada, A., De Jonge, M. J. A., Mau-Sørensen, M., Nielsen, D., Schöffski, P., . . . Schellens, J. H. M. (2021). A first-in-man phase 1 study of the DNA-dependent protein kinase inhibitor Peposertib (formerly M3814) in patients with advanced solid tumours. *British Journal of Cancer, 124*(4), 728-735. doi:10.1038/s41416-020-01151-6

Van Cutsem, E., Lenz, H.-J., Furuse, J., Tabernero, J., Heinemann, V., Ioka, T., . . . Wasan, H. (2016). MAESTRO: A randomized, double-blind phase III study of Evofosfamide (Evo) in combination with Gemcitabine (Gem) in previously untreated patients (pts) with metastatic or locally advanced unresectable pancreatic ductal adenocarcinoma (PDAC). In: American Society of Clinical Oncology. 4007-4007.

Van Der Wiel, A. M. A., Jackson-Patel, V., Niemans, R., Yaromina, A., Liu, E., Marcus, D., . . . Lambin, P. (2021). Selectively Targeting Tumor Hypoxia With the Hypoxia-Activated Prodrug CP-506. *Molecular Cancer Therapeutics, 20*(12), 2372-2383. doi:10.1158/1535-7163.mct-21-0406

Van Triest, B., Damstrup, L., Falkenius, J., Budach, V., Troost, E., Samuels, M., . . . Strotman, R. (2018). A phase Ia/Ib trial of the DNA-PK inhibitor M3814 in combination with radiotherapy (RT) in patients (pts) with advanced solid tumors: dose-escalation results. *American Society of Clinical Oncology*. 2518-2518.

Varvara Petrova , M. A.-P., Gerry Melino and Ivano Amelio. (2018). The hypoxic tumour microenvironment. *Oncogenesis, 7*(1), 1-13.

Vaupel, P., & Mayer, A. (2007). Hypoxia in cancer: significance and impact on clinical outcome. *Cancer and Metastasis Reviews, 26*(2), 225-239. doi:10.1007/s10555-007-9055-1

Veuger, S. J., Curtin, N. J., Richardson, C. J., Smith, G. C., & Durkacz, B. W. (2003). Radiosensitization and DNA repair inhibition by the combined use of novel inhibitors of DNA-dependent protein kinase and poly (ADP-ribose) polymerase-1. *Cancer Research, 63*(18), 6008-6015.

Vichai, V., & Kirtikara, K. (2006). Sulforhodamine B colorimetric assay for cytotoxicity screening. *Nature Protocols, 1*(3), 1112-1116. doi:10.1038/nprot.2006.179

Vlahos, C. J., Matter, W. F., Hui, K. Y., & Brown, R. F. (1994). A specific inhibitor of phosphatidylinositol 3-kinase, 2-(4-morpholinyl)-8-phenyl-4H-1-benzopyran-4-one (LY294002). *Journal of Biological Chemistry, 269*(7), 5241-5248. doi:10.1016/s0021-9258(17)37680-9

Voigt, W. (2005). Sulforhodamine B assay and chemosensitivity. In *Chemosensitivity* (pp. 039-048): Humana Press.

Von Figura, G., Hartmann, D., Song, Z., & Rudolph, K. L. (2009). Role of telomere dysfunction in aging and its detection by biomarkers. *Journal of Molecular Medicine, 87*(12), 1165-1171. doi:10.1007/s00109-009-0509-5

Von Pawel, J., Von Roemeling, R., Gatzemeier, U., Boyer, M., Elisson, L. O., Clark, P., . . . Treat, J. (2000). Tirapazamine plus Cisplatin versus Cisplatin in advanced non–small-cell lung cancer: a report of the international CATAPULT I study group. *Journal of Clinical Oncology, 18*(6), 1351-1359. doi:10.1200/jco.2000.18.6.1351

Walker, E. H., Pacold, M. E., Perisic, O., Stephens, L., Hawkins, P. T., Wymann, M. P., & Williams, R. L. (2000). Structural determinants of phosphoinositide 3-kinase inhibition by Wortmannin, LY294002, Quercetin, Myricetin, and Staurosporine. *Molecular Cell, 6*(4), 909-919. doi:10.1016/s1097-2765(05)00089-4

Walton, M., Wolf, C., & Workman, P. (1992). The role of cytochrome P450 and cytochrome P450 reductase in the reductive bioactivation of the novel benzotriazine di-N-oxide hypoxic cytotoxin 3-amino-l, 2, 4-benzotriazine-l, 4-dioxide (SR 4233, WIN 59075) by mouse liver. *Biochemical Pharmacology, 44*(2), 251-259.

Wang, S., Yoon, Y. N., Son, M. K., Kim, S. J., Lee, B. R., Yang, E. H., . . . Lee, J. H. (2021). 600 BR101801 stimulates anti-tumor immunity and enhances the efficacy of radiation in a syngeneic model. *Journal for ImmunoTherapy of Cancer, 9*(Suppl 2), A630-A630. doi:10.1136/jitc-2021-sitc2021.600

Wardman, P. (2018). Nitroimidazoles as hypoxic cell radiosensitizers and hypoxia probes: misonidazole, myths and mistakes. *The British Journal of Radiology*, 20170915. doi:10.1259/bjr.20170915

Weidemann, A., & Johnson, R. S. (2008). Biology of HIF-1α. *Cell Death & Differentiation, 15*(4), 621-627. doi:10.1038/cdd.2008.12

Weiss, G. J., Infante, J. R., Chiorean, E. G., Borad, M. J., Bendell, J. C., Molina, J. R., . . . Burris, H. A. (2011). Phase 1 study of the safety, tolerability, and pharmacokinetics of TH-302, a hypoxia-activated prodrug, in patients with advanced solid malignancies. *Clinical Cancer Research, 17*(9), 2997-3004. doi:10.1158/1078-0432.ccr-10-3425

Williamson, S. K., Crowley, J. J., Lara, P. N., Mccoy, J., Lau, D. H. M., Tucker, R. W., . . . Gandara, D. R. (2005). Phase III trial of Paclitaxel plus Carboplatin with or without Tirapazamine in advanced non–small-cell lung cancer: Southwest Oncology Group trial S0003. *Journal of Clinical Oncology, 23*(36), 9097-9104. doi:10.1200/jco.2005.01.3771

Willmore, E., De Caux, S., Sunter, N. J., Tilby, M. J., Jackson, G. H., Austin, C. A., & Durkacz, B. W. (2004). A novel DNA-dependent protein kinase inhibitor, NU7026, potentiates the cytotoxicity of topoisomerase II poisons used in the treatment of leukemia. *Blood, 103*(12), 4659-4665. doi:10.1182/blood-2003-07-2527

Wilson, W. R., & Hay, M. P. (2011). Targeting hypoxia in cancer therapy. *Nature Reviews: Cancer, 11*(6), 393-410. doi:10.1038/nrc3064

Wipf, P., & Halter, R. J. (2005). Chemistry and biology of wortmannin. *Organic & Biomolecular Chemistry, 3*(11), 2053. doi:10.1039/b504418a

Withers, H. R. (1985). Biologic basis for altered fractionation schemes. *Cancer, 55*(S9), 2086-2095.

Wong, W. W., Jackson, R. K., Liew, L. P., Dickson, B. D., Cheng, G. J., Lipert, B., . . . Hay, M. P. (2019). Hypoxia-selective radiosensitisation by SN38023, a bioreductive prodrug of DNA-dependent protein kinase inhibitor IC87361. *Biochemical Pharmacology, 169*, 113641.

Woodard, R. L., Anderson, M. G., & Dynan, W. S. (1999). Nuclear extracts lacking DNA-dependent protein kinase are deficient in multiple round transcription. *Journal of Biological Chemistry, 274*(1), 478-485. doi:10.1074/jbc.274.1.478

Wouters, B., Wang, L.-H., & Brown, J. M. (1999). Tirapazamine: a new drug producing tumor specific enhancement of platinum-based chemotherapy in non-small-cell lung cancer. *Annals of Oncology, 10*, S29-S33.

Yap, T. A., Chen, Y., Butler, L. H., Lao-Sirieix, S.-h., Cadogan, E., O'Connor, L. O., . . . Dean, E. (2020). Abstract CT248: AZD7648: a phase I/IIa first-in-human trial of a novel, potent and selective DNA-PK inhibitor in patients with advanced malignancies. *Cancer Research*, 80(16_Supplement), CT248-CT248.

Yin, X., Liu, M., Tian, Y., Wang, J., & Xu, Y. (2017). Cryo-EM structure of human DNA-PK holoenzyme. *Cell Research, 27*(11), 1341-1350.

Yu, K., Lucas, J., Zhu, T., Zask, A., Gaydos, C., Toral-Barza, L., . . . Cai, P. (2005). PWT-458, a novel pegylated-17-hydroxywortmannin, inhibits phosphatidylinositol 3-kinase signaling and suppresses growth of solid tumors. *Cancer Biology & Therapy, 4*(5), 538-545.

Yue, X., Bai, C., Xie, D., Ma, T., & Zhou, P.-K. (2020). DNA-PKcs: A multi-faceted player in DNA damage response. *Frontiers in Genetics, 11*, 1692.

Zeman, E. M., Hirst, V. K., Lemmon, M. J., & Brown, J. M. (1988). Enhancement of radiation-induced tumor cell killing by the hypoxic cell toxin SR 4233. *Radiotherapy and Oncology, 12*(3), 209-218.

Zenke, F. T., Zimmermann, A., Sirrenberg, C., Dahmen, H., Kirkin, V., Pehl, U., . . . Amendt, C. (2020). Pharmacologic inhibitor of DNA-PK, M3814, potentiates radiotherapy and regresses human tumors in mouse models. *Molecular Cancer Therapeutics, 19*(5), 1091-1101.

Zenke, F. T., Zimmermann, A., Sirrenberg, C., Dahmen, H., Vassilev, L., Pehl, U., . . . Blaukat, A. (2016). M3814, a novel investigational DNA-PK inhibitor: enhancing the effect of fractionated radiotherapy leading to complete regression of tumors in mice. *Molecular Cancer Therapeutics*, *19*(5), 1091-1101.

Zhao, Y., Thomas, H. D., Batey, M. A., Cowell, I. G., Richardson, C. J., Griffin, R. J., . . . Curtin, N. J. (2006). Preclinical evaluation of a potent novel DNA-dependent protein kinase inhibitor NU7441. *Cancer Research, 66*(10), 5354-5362.

Zhu, J., Hou, T., & Mao, X. (2015). Discovery of selective phosphatidylinositol 3-kinase inhibitors to treat hematological malignancies. *Drug Discovery Today, 20*(8), 988-994.

Zou, Z., Tao, T., Li, H., & Zhu, X. (2020). mTOR signaling pathway and mTOR inhibitors in cancer: progress and challenges. *Cell & Bioscience, 10*(1). doi:10.1186/s13578-020-00396-1

Hanahan, D., & Weinberg, R. A. (2011). Hallmarks of Cancer: The Next Generation. *Cell, 144*(5), 646-674. doi:10.1016/j.cell.2011.02.013

Mistry, I. N., Thomas, M., Calder, E. D. D., Conway, S. J., & Hammond, E. M. (2017). Clinical Advances of Hypoxia-Activated Prodrugs in Combination With Radiation Therapy. *International Journal of Radiation Oncology*Biology*Physics, 98*(5), 1183-1196. doi:10.1016/j.ijrobp.2017.03.024